



# Operational chemical weather forecasting with the ECCC online Regional Air Quality Deterministic Prediction System version 023 (RAQDPS023) - Part 1: System description

Michael D. Moran<sup>1\*</sup>, Verica Savic-Jovicic<sup>1</sup>, Craig A. Stroud<sup>1</sup>, Sylvain Ménard<sup>2</sup>, Wanmin Gong<sup>1</sup>, Junhua Zhang<sup>1</sup>, Qiong Zheng<sup>1</sup>, Jack Chen<sup>1</sup>, Ayodeji Akingunola<sup>1</sup>, Alexandru Lupu<sup>1</sup>, Konstantinos Menelaou<sup>2</sup>, and Rodrigo Munoz-Alpizar<sup>2</sup>

<sup>1</sup>Air Quality Research Division, Environment and Climate Change Canada (ECCC), Toronto, Ontario, Canada

<sup>2</sup>Canadian Centre for Meteorological and Environmental Prediction, ECC, Montreal, Quebec, Canada

\*Retired

10 Correspondence to: Michael Moran ([mike.moran@ec.gc.ca](mailto:mike.moran@ec.gc.ca)), Verica Savic-Jovicic ([verica.savic-jovicic@ec.gc.ca](mailto:verica.savic-jovicic@ec.gc.ca)), or Craig Stroud ([craig.stroud@ec.gc.ca](mailto:craig.stroud@ec.gc.ca))

## Abstract

The online version of the Regional Air Quality Deterministic Prediction System (RAQDPS) is a chemical weather forecast system that has been employed operationally by Environment and Climate Change Canada (ECCC) since 15 2009. It is run twice per day to produce 72-hour forecasts of hourly 10 km abundance fields of three key predictands, NO<sub>2</sub>, O<sub>3</sub>, and PM<sub>2.5</sub> total mass, as well as other gas-phase chemical species, PM<sub>2.5</sub> chemical components, and dry and wet deposition for Canada, the contiguous U.S., and northern Mexico. The forecasts of NO<sub>2</sub>, O<sub>3</sub>, and PM<sub>2.5</sub> are needed to calculate the Air Quality Health Index (AQHI), which is used to communicate current and forecasted pollutant levels to the Canadian public. Version 023 of the RAQDPS (RAQDPS023) went into service at ECC in December 2021 20 and was replaced by the RAQDPS025 in June 2024. This paper provides the first full description of any version of the online RAQDPS. After giving a brief history of the ECC operational air quality forecasting program, we provide a comprehensive description of the RAQDPS023 forecast system as well as shorter descriptions of several upstream and downstream forecast and analysis systems. The latter include two upstream operational meteorological forecast systems that were based on version 5.1.0 of the ECC Global Environmental Multiscale (GEM) numerical weather 25 prediction model, one which used a global configuration, the Global Deterministic Prediction System (GDPS 8.0.0), and the other which used a regional configuration, the Regional Deterministic Prediction System (RDPS 8.0.0). An emissions processing system, an Updateable Model Output Statistics-based system for bias-corrected station-specific pollutant concentration forecasts (UMOS-AQ), and a regional objective analysis system for surface pollutant concentration fields, the Regional Deterministic Air Quality Analysis system (RDAQA 2.0.0), are also described.

30 The RAQDPS023 itself consisted of version 3.1.0.0 of the GEM-Modelling Air quality and CHemistry (GEM-MACH) chemistry module, which was embedded with one-way coupling within GEM 5.1.0, its meteorological host model. The meteorological configuration of the RAQDPS023 closely followed that of the RDPS 8.0.0. Details covered in this paper include a summary of the dynamical representations and physical parameterizations used in the three GEM-based forecast systems, which are closely harmonized, the chemical parameterizations used in the MACH chemistry 35 module, numerical solvers, system inputs, including both anthropogenic and natural emissions of chemical species,



system outputs, and run configuration, strategies, and timings. One simplification employed to reduce RAQDPS023 execution time for operational deployment was to represent the particulate matter (PM) size distribution with only two aerosol particle size bins, one corresponding to particle diameters in the 0-2.5  $\mu\text{m}$  range (“fine particles” or  $\text{PM}_{2.5}$ ) and the other to the 2.5-10  $\mu\text{m}$  range (“coarse fraction” or  $\text{PM}_{\text{cf}}$ ). A second simplification was to represent the chemical composition of  $\text{PM}_{2.5}$  with only nine chemical components, and a third simplification was to use a longer time step (900 s) for the time integration of atmospheric chemistry than the time step used for time integration of atmospheric dynamics and physics (300 s). Even so, activating the MACH module increased RAQDPS023 run time by a factor of 4.4 on average compared to meteorology only, partly due to the cost of the integration of chemistry but partly to the increased cost of integration of the GEM dynamical core due to the advection with imposed shape preservation and mass conservation of 57 additional chemical tracers. The role of the RAQDPS-FW023, a second chemical weather forecast system that was identical to the RAQDPS023 except for the addition of near-real-time biomass burning emissions, is also described. Biomass burning emissions for Canada and the U.S. estimated from satellite measurements were first calculated by the Canadian Forest Fire Emissions Prediction System (CFFEPS) version 4.1 before each RAQDPS-FW023 run was launched. Outputs from the two RAQDPS versions were then used to produce forecasts of wildfire smoke transport and diffusion. The paper closes by summarizing the key upgrades made to the RAQDPS025, the current version of the ECCC operational chemical weather forecast system, and then describing some possible future improvements and updates. A companion paper by Moran et al. (2025) presents the results of a comprehensive, five-year performance evaluation of prospective and retrospective annual air quality simulations made with the RAQDPS023.

## 55 1 Introduction

Forecasting tomorrow’s weather means being able to predict the short-term future dynamical and physical state of the atmosphere. Operational weather forecasting, also known as numerical weather prediction (NWP), began in the 1950s once electronic computers started to become available commercially (e.g., Lorenz, 2006; Bauer et al., 2015). The chemical state of the atmosphere, on the other hand, particularly the concentrations of air pollutants of concern for human health, is often referred to as air quality (AQ). Recent epidemiological studies have determined that air pollution is the fourth leading cause of early death globally (Boogaard et al., 2019; Murray et al., 2020; WHO, 2021). However, predicting tomorrow’s air quality, or chemical weather as it is also known, is even more difficult than predicting tomorrow’s weather. As a consequence, operational regional AQ forecasting did not become possible until about 2000 (McHenry et al., 2004; Kukkonen et al., 2012; Zhang et al., 2012a), roughly a half century after the start of operational weather forecasting.

Air quality was initially only a local concern in the vicinity of large sources of air pollutants, including major urban centres (Pasquill and Smith, 1983). In the 1970s, however, emerging recognition of human health impacts caused by regional photochemical smog and the environmental harm caused by regional acidic deposition (or “acid rain”) spurred many laboratory and field studies to better understand these larger-scale AQ issues (e.g., Hecht et al., 1974; Likens and



70 Bormann, 1974; Eliassen and Saltbones, 1975; Barrie and Georgii, 1976; Calvert et al., 1978; Harrison et al., 1978; Schiermeir, 1978). The development of the first prognostic, three-dimensional, regional AQ models capable of simulating photochemical smog, especially ozone, and acidic deposition then followed in the 1980s, building on the steady increase in our scientific understanding of these issues (e.g., Chang et al., 1987; Seinfeld, 1988; Venkatram et al., 1988; Russell and Dennis, 2000). At first these regional AQ models, which are also known as chemical transport  
75 models (CTMs) and atmospheric chemistry models (Kukkonen et al., 2012), were only applied to retrospective case studies for research and policy applications (e.g., Clark et al., 1989; Fung et al., 1991; Roselle and Schere, 1995; Dunker et al., 1996; Middleton, 1997). Routine regional AQ forecasting was held back by two factors – the order-of-magnitude larger computational burden of AQ models relative to NWP models and the run-time constraints imposed by the need to disseminate forecasts in a timely fashion (McHenry et al., 2004) – but continuing improvements in computer  
80 capabilities have facilitated the introduction and rapid expansion of the use of operational AQ forecast systems in North America, Europe, and Asia over the past two decades (e.g., Grell and Baklanov, 2011; Kukkonen et al., 2012; Zhang et al., 2012a,b; Brasseur et al., 2019; WMO, 2020; Brasseur and Kumar, 2021).

The majority of AQ forecast systems employ a so-called “offline” model architecture, where an NWP model is run first and then a CTM is run using forecast meteorological fields from the NWP model as inputs. More recently,  
85 however, some AQ forecast systems have adopted an “online” architecture where meteorological and chemical variables are predicted simultaneously, in effect a merged NWP-CTM system (e.g., Grell et al., 2005; Zhang, 2008; Grell and Baklanov, 2011; Baklanov and Zhang, 2020).

Canada was one of the first countries to implement an operational regional AQ forecast system (e.g., Zhang et al., 2012a). Environment and Climate Change Canada (ECCC), Canada’s federal environment ministry, has run an  
90 operational, continental-scale Regional Air Quality Deterministic Prediction System (RAQDPS) for North America since 2001. The earliest version of the RAQDPS employed an offline CTM called CHRONOS (Canadian Hemispheric Regional Ozone and NO<sub>x</sub> System). This system was run once per day on a 21 km horizontal grid over North America with 25 vertical levels from the surface to 6 km to make 48 hour forecasts of surface ozone (O<sub>3</sub>) volume mixing ratio (Pudykiewicz et al., 1997; Pudykiewicz and Koziol, 2001; McHenry et al., 2004; McKeen et al., 2005; Ménard and  
95 Robichard, 2005; Moran et al., 2013; Robichaud and Ménard, 2014). The meteorological “driver” (i.e., NWP model) used with CHRONOS was the limited-area ECCC Regional Deterministic Prediction System (RDPS), the operational, nested, regional configuration of the ECCC Global Environmental Multi-scale (GEM) NWP model (Côté et al., 1998a,b; Fillion et al., 2010; Caron et al., 2015). The surface concentration of particulate matter (PM) with aerodynamic diameter smaller than 2.5 μm (PM<sub>2.5</sub>) was added as a predictand to CHRONOS in 2003 (Pudykiewicz et  
100 al., 2003; McKeen et al., 2007).

In 2009 the offline CHRONOS CTM in the RAQDPS was replaced by the online, one-way-coupled GEM-MACH (GEM–Modeling Air quality and CHemistry) chemical weather model, which included improved representations of gas-phase, aqueous-phase, and aerosol chemistry in the new MACH chemistry module that was added to the GEM model. This new generation of the RAQDPS used a new, continental-scale 15 km horizontal grid with 58 vertical



105 levels extending from the surface to 0.1 hPa (Anselmo et al., 2010; Moran et al., 2010, 2011). One design goal for the development of this next generation was to align its meteorological component and configuration with the operational RDPS as closely as possible to ensure equivalent meteorological forecasts from these two closely related systems.

From 2009 to 2025 there have been 24 upgrades of varying magnitude made to the GEM-MACH-based version of the RAQDPS to improve forecast skill and to adjust to new versions of the operational RDPS weather forecast model and  
110 upgrades to ECCC's computer system hardware and software. For example, version 023 of the RAQDPS (RAQDPS023), the subject of this paper, employed a continental forecast grid with 10 km horizontal grid spacing and 84 hybrid vertical levels from the surface to 0.1 hPa. As a second example, a key input to any AQ forecast model is a detailed representation of current anthropogenic and natural emissions of air pollutants and their precursors: the input emissions files used by the RAQDPS have been updated eight times since 2009. Other significant changes have  
115 included numerous improvements and some bug fixes to the chemistry module code, several modifications to the vertical discretization, the introduction of a duplicate version of the RAQDPS that considers near-real-time (NRT) wildfire emissions, and an extension of the forecast period from two days to three days. **Table A3** lists all of these upgrades and indicates the biggest ones, four of which involved major updates to the input anthropogenic emissions files resulting from the availability of newer national emission inventories.

120 The RAQDPS023 was implemented operationally on 1 December 2021 (Moran et al., 2021b). It was run routinely twice daily until 10 June 2024 to produce 72-hour forecasts of hourly surface abundance fields of O<sub>3</sub>, nitrogen dioxide (NO<sub>2</sub>), PM<sub>2.5</sub>, and other chemical species over North America. These first three species were needed to calculate Canada's national Air Quality Health Index (AQHI), a health-based, multi-pollutant, additive, no-threshold AQ index (Sect. 5.1). The RAQDPS-FW023, a duplicate version of the RAQDPS023 that also includes NRT wildfire emissions  
125 but is otherwise identical, was also implemented operationally on 1 Dec. 2021 (Chen and Menelaou, 2021). Forecasts made by this second system allowed the location and evolution of wildfire plumes to be calculated as the difference between forecasts from the two model versions (Pavlovic et al., 2016; Munoz-Alpizar et al., 2017; Chen et al., 2019b).

The goal of this paper is to describe and document all components of the RAQDPS023 and RAQDPS-FW023 forecast systems. As such it is the first publication to provide a comprehensive and detailed description of any version of the  
130 online, GEM-MACH-based RAQDPS. A companion paper (Moran et al., 2025) presents a detailed performance evaluation of five years of RAQDPS023 simulations consisting of the first year of RAQDPS023 forecasts and four years of retrospective annual simulations for the 2013-2016 period that used year-specific emissions. It should be noted that the RAQDPS023 was replaced in June 2022 by the RAQDPS024, a new but equivalent version that was necessary due to the migration of all ECCC forecast systems to a new computer system. The operational GEM-MACH  
135 code and the input emissions were unchanged between these two versions. Another release, the RAQDPS025, was implemented operationally on 11 June 2024 (see Table A3), but despite a number of upgrades introduced for the RAQDPS025 that are described near the end of this paper, almost all of the details related to the RAQDPS023 that are presented in this paper also apply to the RAQDPS025.



The rest of the paper is organized as follows. Section 2 provides a brief overview of the meteorological aspects of the RAQDPS023 operational chemical weather forecast system and the two upstream operational NWP forecast systems that provide the RAQDPS023 with meteorological initial conditions and boundary conditions. These two upstream systems are global and regional configurations of the GEM NWP model. Section 3 provides a detailed description of the MACH component of the RAQDPS023, including its chemical parameterizations and input anthropogenic and modelled natural emissions. Section 4 describes computational aspects of the RAQDPS023, including time integration and process splitting, chemical initial conditions and boundary conditions, advection scheme and tracer shape preservation and mass conservation, computer hardware and code parallelization, and forecast run strategies. Section 5 describes RAQDPS023 outputs, post-processing and downstream systems, and routine operational performance evaluation. Finally, Section 6 describes updates made for the current RAQDPS025 operational forecast system and some possible future improvements, and Section 7 summarizes the paper.

## 2 Meteorological forecast systems

The meteorological forecast component of the RAQDPS023 is the GEM NWP model (Côté et al., 1998a,b; Girard et al., 2014; McTaggart-Cowan et al., 2019a; Ritchie et al., 2022). As the GEM model has been described in more detail in many other publications, only its main characteristics are summarized here with an emphasis on those parameterizations that are also important for chemical weather forecasting. These include the treatment of vertical fluxes from land and water surfaces, turbulent mixing in the surface layer and the planetary boundary layer (PBL), shortwave and longwave radiation, and clouds and precipitation.

The GEM model can be configured for either a global domain or a regional domain (Côté et al., 1998a,b). The ECCC operational medium-range global forecast system based on GEM is named the Global Deterministic Prediction System (GDPS) while the operational short-range regional forecast system for the North American region is named the Regional Deterministic Prediction System (RDPS) (Buehner et al., 2015; Caron et al., 2015; McTaggart-Cowan et al., 2019a; Ritchie et al., 2022). The RDPS is also referred to as a limited-area model (LAM). These two meteorological forecast systems are very similar in terms of their dynamical cores (see Sect. S1.1 of the Supplement to this paper), but additional efforts were also made in recent years to harmonize them further in terms of numerics and physical parameterizations both for consistency and to reduce development and maintenance burdens. For example, both the GDPS and RDPS now employ the same number of vertical levels, the same model lid height, and the same set of atmospheric physics parameterizations (Mailhot et al., 1998; McTaggart-Cowan et al., 2019a).

New operational versions of the GDPS and RDPS, GDPS 8.0.0 and RDPS 8.0.0, were introduced on 1 December 2021 at the same time as the RAQDPS023 (CMC-GDPS-8.0.0, 2021a,b; CMC-RDPS-8.0.0, 2021a,b; Moran et al., 2021b; CMC-RAQDPS-023, 2021). Given that the focus of this paper is a regional chemical weather forecast system, the main reason that the GDPS 8.0.0 global system was included here is that the RDPS 8.0.0 regional system was one-way coupled with GDPS 8.0.0 forecasts so that the regional NWP system was dependent on the global NWP system. In addition, the meteorological aspects of the RAQDPS023 chemical weather forecast system were identical to the RDPS



8.0.0 configuration, and the RAQDPS023 was one-way coupled to the RDPS8.0.0 for meteorology since the RAQDPS023 horizontal domain was embedded within the RDPS8.0.0 horizontal domain (Sect. 4.2). Figure 1 shows the data-flow relationships between the GDPS 8.0.0, the RDPS 8.0.0, and the RAQDPS023, namely a sequence of three linked operational forecast systems where the GDPS 8.0.0 and RDPS 8.0.0 are “upstream” dependencies of the RAQDPS023.

All three systems were based on GEM version 5.1.0. Most of the following description of GEM 5.1.0 thus applies to all three systems, but differences are noted where they occur. The main differences between the global and the two regional GEM-based systems were related to run configurations, namely domain size, horizontal grid spacing, integration time step, initialization, and boundary conditions.

## 2.1 Grids, coordinate systems, and nesting

The GDPS 8.0.0 employed an overset Yin–Yang global horizontal grid system that combines two perpendicular and overlapping, rotated latitude-longitude limited-area horizontal grids referred to as the Yin grid and the Yang grid. The globe is thus divided into two regions that look somewhat reminiscent of the covering and seams of a baseball (Qaddouri and Lee, 2011). This global grid system has two major benefits: it avoids pole-related singularities and convergence issues and it is suitable for use with massively parallel computers (Kageyama and Sato, 2004). Forecasts were made independently at each time step on the two regional LAM grids and were then reconciled across the overlap region (Qaddouri and Lee, 2011). The horizontal grid spacing for both the Yin and Yang grids used by the GDPS 8.0.0 was quasi-uniform  $0.135^\circ$  ( $\sim 15$  km).

The rotated latitude-longitude LAM horizontal grid of the RDPS 8.0.0 covered the North American continent and adjacent oceans but was entirely a subdomain of the GDPS’s Yin grid (Fig. 2). Horizontal grid spacing was quasi-uniform  $0.09^\circ$  ( $\sim 10$  km). The RAQDPS023 horizontal grid, also shown in Fig. 2, was an embedded subgrid of the RDPS 8.0.0 grid with  $0.09^\circ$  grid spacing and grid-point superposition (i.e., co-location). The RDPS 8.0.0 horizontal grid was  $1108 \times 1082$  in size vs.  $772 \times 642$  for the RAQDPS023 horizontal grid. The smaller domain of the chemical weather model was necessary to balance the additional computational burden of the MACH chemistry module (see Sect. 4.1).

In terms of finite differencing, the horizontal discretization used for all three model grids was an Arakawa C grid, which Côté et al. (1998a) argued is more suitable for massively parallel computer architectures and for mesoscale applications. The vertical discretization for all three model grids was a staggered Charney–Phillips grid that was used with a log-hydrostatic-pressure-type  $\zeta$  (or hybrid) vertical coordinate (Holdaway et al., 2013a,b; Girard et al., 2014). The GDPS 8.0.0, RDPS 8.0.0, and RAQDPS023 also all used the same 84 hybrid vertical levels stretching from the Earth’s surface to 0.1 hPa. The lowest momentum “full” hybrid levels were located at approximately 20, 61, 114, 181, and 263 m AGL and the lowest thermodynamic “half” hybrid levels were located at approximately 10, 40, 87, 147, and 222 m AGL. Vertical layer thickness was monotonic increasing with distance from the Earth’s surface to the upper



troposphere (where it then decreased to better resolve the tropopause region), and there were 11 thermodynamic hybrid levels located within the first kilometer above the surface.

GDPS 8.0.0 forecasts started before RDPS 8.0.0 forecasts so that one-way nesting could be used to supply meteorological lateral boundary conditions (LBCs) from the global weather forecasts to the LAM regional weather forecasts (Benoit et al., 1997; Ritchie et al., 2022; see also Sect. 4.2). Similarly, RDPS 8.0.0 forecasts started before RAQDPS023 forecasts so that one-way nesting could again be used to supply meteorological LBCs from the RDPS 8.0.0 LAM forecasts to the RAQDPS023 LAM forecasts (see Figs. 1 and 2 and Sect. 4.2). This one-way nesting technique is sometimes referred to as “piloting”. In fact, successive versions of the RAQDPS have been “piloted” or “driven” by successive versions of the RDPS since 2009 (Table A3).

## 215 **2.2 RAQDPS023 meteorological configuration**

Table 1 provides a concise summary of the meteorological components and attributes of the RAQDPS023, including the dynamical core and various physical parameterizations. References are also provided for each component. These components and attributes were identical to those used by the RDPS 8.0.0 with two exceptions: horizontal grid size and LBC source (cf. CMC-RDPS-8.0.0, 2021b). For further information about Table 1, McTaggart-Cowan et al. (2021a) provide an excellent recent summary of ECCC implementations of the physical parameterizations listed in Table 1, Sect. S1 also provides some information about many of these components and attributes, and Sect. 4 covers some computational aspects.

## **3 Chemical forecast module**

The MACH (Modelling Air quality and CHemistry) module is an online chemistry module embedded in the GEM NWP model code to produce the GEM-MACH chemical weather model. It predicts the evolution in time of concentrations and removal rates of a number of gas-phase chemical species, including O<sub>3</sub> and NO<sub>2</sub>, as well as size- and composition-resolved PM. Many of the chemistry parameterizations used by the MACH module were adapted from two earlier ECCC atmospheric chemistry codes, the Canadian Aerosol Module (CAM), which was designed to represent aerosol processes in climate models (e.g., Gong et al., 1997a,b, 2002, 2003), and A Unified Regional Air Quality Modelling System (AURAMS) CTM, which was an offline AQ model with a size- and composition-resolved representation of PM developed by ECCC for research and policy applications (e.g., Moran et al., 1998; Zhang et al., 2002a; Gong et al., 2006; Stroud et al., 2008; Makar et al., 2009; Levy et al., 2010). Furthermore, as noted below several chemistry parameterizations used by AURAMS were adapted from an earlier regional CTM used by ECCC, the Acid Deposition and Oxidant Model (ADOM: Venkatram et al., 1988, 1992; Misra et al., 1989; Fung et al., 1991, Karamchandani and Venkatram, 1992; Macdonald et al., 1993; Li et al., 1994).



### 3.1 Alignment with weather forecast models

For the RAQDPS023 the GEM-MACH code version was updated from version 3.0.2 to version 3.1.0.0 (see Table A3 and Moran et al., 2021b). This updated version incorporates the GEM v5.1.0 code that was also used by the GDPS 8.0.0 and RDPS 8.0.0 (CMC-GDPS-8.0.0, 2021a; CMC-RDPS-8.0.0, 2021a).

240 As noted in Sect. 2.1 the RAQDPS023 meteorological configuration was also very closely aligned with that of the RDPS 8.0.0 regional weather forecast model. First, the RAQDPS023 employed (i) the same set of dynamics options and physics parameterizations as the RDPS 8.0.0, including those for advection, vertical turbulent diffusion, radiation, grid-scale and subgrid-scale (SGS) clouds and precipitation, and gravity wave drag and orographic blocking (Table 1), (ii) the same vertical grid and a closely related horizontal grid (the RDPS horizontal grid domain is larger; see Sect. 2.1  
245 and Fig. 2), and (iii) the same dynamics/physics integration time step (Table 1). As a consequence, weather forecasts made by the two systems are nearly identical over the RAQDPS horizontal domain.

Second, the chemistry parameterizations used by the RAQDPS023 made use of many meteorological fields predicted by GEM. For example, the treatment of non-chemical cloud processes resides in the GEM physics module, which provides a number of meteorological fields to the MACH chemistry module, including cloud water mixing ratio (liquid  
250 and solid), precipitation production rate (auto-conversion and coalescence), precipitation evaporation rate, and precipitation vertical fluxes (both liquid and solid) (Mailhot et al., 1998; Gong et al., 2006, 2015; McTaggart-Cowan et al., 2019a). Table 2 summarizes the meteorological fields predicted by GEM that are needed by various MACH parameterizations in the RAQDPS023.

Third, as noted in Table 1 the GEM dynamical core used by the RAQDPS023 included a small number of  
255 meteorological tracers. MACH considers a much larger number of chemical tracers, but these additional tracers are implemented in the GEM-MACH code in the same way as the meteorological tracers. In fact, MACH chemistry is essentially a run-time option of GEM that can either be activated to run GEM-MACH for chemical weather forecasts or not activated so that just GEM is run to make meteorological forecasts. Moreover, because GEM-MACH is an online system, it makes use of GEM schemes and Fortran2003 computer code for those dynamical and physical  
260 processes that are common to both meteorological and chemical tracers, including advection and vertical diffusion. One exception, however, is SGS convection, where SGS vertical transport of chemical tracers mirroring that of meteorological tracers has not yet been implemented.

Fourth, the same *a posteriori* treatments for shape preservation and mass conservation applied in the RDPS 8.0.0 for the advection of meteorological tracers (Table 1) are also applied in the RAQDPS023 for the advection of both  
265 meteorological chemical tracers. Shape preservation and mass conservation are very relevant for a regional AQ model since there can be many sharp chemical concentration gradients in the vicinity of strong local emissions sources, and the resulting loss of shape preservation after advection can introduce negative concentrations (e.g., Flemming et al., 2015).



And fifth, in order to use the treatment of vertical turbulent diffusion from GEM for chemical tracers, area emissions  
270 and dry deposition of gases and particles are treated as flux boundary conditions at the bottom boundary. Note that  
two small differences in the parameterization of vertical diffusion for meteorological tracers vs. chemical tracers used  
by the RAQDPS023 were introduced in 2019 when the RAQDPS021 became operational (Moran and Ménard, 2019).  
In the RAQDPS021 the height of the lowest model half-level (i.e., first thermodynamic level) was reduced from 20 m  
to 10 m and the scheme used to diagnose PBL height was also changed to a  $Ri_b$ -based scheme (Sect. S1.4), which  
275 resulted in PBL heights as small as 2 m being predicted under some stable conditions (Moran and Ménard, 2019). To  
avoid the occurrence of unrealistically high surface concentrations, two ad hoc modifications were introduced. One  
modification was to impose a minimum PBL height value of 100 m (other groups have imposed similar minimum  
values: e.g., Li and Rappenglueck, 2018). The second modification was to inject surface emissions equally into the  
two lowest model layers rather than just in the lowest layer as before 2019, which was equivalent to maintaining the  
280 40 m lowest full-layer thickness considered before the RAQDPS021. Both modifications were carried over to the  
RAQDPS023.

### 3.2 Representation of particulate matter

The term “particulate matter” (or aerosol particles) refers to the mixture of solid particles and liquid droplets found  
suspended in air. The size of these particles can range from the “ultrafine” (aerodynamic diameters less than 0.1  $\mu\text{m}$ )  
285 to the “giant” (aerodynamic diameters greater than 10  $\mu\text{m}$ ) (e.g., Wang et al., 2014a). PM is of interest for many  
reasons: for example, aerosol particles can interact with radiation via scattering and absorption (aerosol direct effect);  
they can act as condensation and ice nuclei in clouds and interact with cloud microphysics (aerosol indirect effect); and  
they can enter the human body via respiration, where they may impact human health. In fact, so-called “fine” particles  
( $\text{PM}_{2.5}$ ) are a major cause of human mortality and morbidity (e.g., Lelieveld and Pöschl, 2017; Murray et al., 2020).  
290 As a consequence, many countries have legislated ambient air quality standards for  $\text{PM}_{2.5}$ , including Canada  
(<https://ccme.ca/en/air-quality-report>) and the U.S. (<https://www.epa.gov/criteria-air-pollutants/naaqs-table>), and the  
World Health Organization has issued health-based guidelines for  $\text{PM}_{2.5}$  and  $\text{PM}_{10}$  ambient concentrations (WHO,  
2021).

PM is a complex pollutant: (i) it is typically composed of particles with a wide size range spanning orders of magnitude;  
295 (ii) it can contain many different elements and compounds, both inorganic and organic; (iii) it is subject to many  
different physical and chemical processes (see below); and (iv) it has many different types of sources, including both  
particle-phase primary sources and gas-phase secondary sources (e.g., Fuzzi et al., 2015). Representing size- and  
composition-resolved PM in an AQ model with an affordable number of tracer species is thus a significant challenge  
both scientifically and computationally.

300 Two conceptual approaches have been used in AQ models to represent the PM size distribution: a sectional  
representation, in which the PM size distribution is divided in  $n$  contiguous, nonoverlapping, discrete size sections or  
size bins (e.g., Gelbard and Seinfeld, 1980; Seigneur et al., 1986; Jacobson, 1997; Zhang et al., 1999); and a modal



representation, in which the PM size distribution is assumed to be composed of  $n$  distinct populations of particles, each of whose size distribution can be described by an analytical modal distribution function (e.g., Binkowski and Shankar, 1995; Whitby and McMurry, 1997). Many AQ models with a size-resolved treatment of PM have employed a sectional representation, (e.g., Jacobson, 1997; Kukkonen et al., 2012; Zhang et al., 2012a,b; WMO, 2020). For each model, though, the number of sections ( $n$ ) that are considered must be chosen.

For GEM-MACH two different values of  $n$  have been used, depending upon the application. For operational AQ forecasting with the RAQDPS, only two size bins have been used in order to reduce model execution times: PM<sub>2.5</sub> or “fine PM”, which corresponds to particle diameters in the 0-2.5  $\mu\text{m}$  range; and PM<sub>cf</sub> or “coarse fraction”, which corresponds to particle diameters in the 2.5-10  $\mu\text{m}$  range. Taken together these two size bins constitute PM<sub>10</sub> (“coarse PM”). These two size bins were chosen to enable prediction of PM<sub>2.5</sub> and PM<sub>10</sub>, the two PM size ranges of concern for AQ standards in North America, following the approach of an earlier size-resolved PM model (Middleton, 1997). These two size bins are also consistent with measurement studies, which have found that atmospheric aerosol volume and mass size distributions generally have only two distinct modes, an accumulation mode (0.1 to 2  $\mu\text{m}$  diameter range) and a coarse mode (diameter > 2  $\mu\text{m}$ ), except for very clean conditions or close to sources of hot gases where a distinct (and smaller) nucleation or Aitken mode is evident (e.g., Whitby, 1978; Morawska et al., 1999). Whitby (1978) also argued that there is little interaction between particles in the accumulation and coarse modes. Note too that PM<sub>2.5</sub> and PM<sub>10</sub> are the two PM size ranges that are considered by the Canadian, U.S., and Mexican national emissions inventories (see Sect. 3.11.1) and by a number of North American surface measurement networks (e.g., Brook et al., 1999b; NSTC, 2013; Moran et al., 2025). However, as discussed below in Sects. 3.3.4 and 3.8 it was necessary to introduce an additional subdivision of the PM<sub>2.5</sub> and PM<sub>cf</sub> size bins in order to reduce errors in the numerical solution of several aerosol process parameterizations. It should be noted that some model applications do need the PM size distribution to be resolved in more detail, such as calculations of atmospheric visibility and aerosol optical depth or studies of meteorology–aerosol interactions through aerosol direct and indirect effects. For such applications GEM-MACH is typically run with 12 size bins (e.g., Gong et al., 2015; Makar et al., 2015a,b; Ghahreman et al., 2021; Majdzadeh et al., 2022).

Another complication related to the PM size distribution is that there are multiple definitions of aerosol particle diameter. The most common definition is aerodynamic diameter, which is defined as the diameter of a spherical particle with a density of 1 g cm<sup>-3</sup> that behaves similarly to the particle of interest. This is the definition used for PM<sub>2.5</sub> and PM<sub>10</sub> for AQ standards, for reporting most ambient measurements, and for preparing emissions inventories. However, CTMs like GEM-MACH consider Stokes diameter, which is the diameter of a spherical particle that behaves similarly to the particle of interest and has the same density. Stokes diameter is equal to the aerodynamic diameter divided by the square root of the particle density (e.g., Seigneur and Moran, 2004), and this difference should be considered when comparing model-predicted PM values with observed PM values (see Moran et al., 2025).

While it is important for the RAQDPS to predict PM<sub>2.5</sub> “bulk” mass or total mass since PM<sub>2.5</sub> total mass is one of the three species considered by the AQHI, it is also important for the RAQDPS to resolve the chemical composition of



PM<sub>2.5</sub> and PM<sub>10</sub> since many PM properties and processes depend on a particle's chemical composition. In order to achieve this representation with only a modest number of chemical components so as to reduce computational costs, just nine components were considered by the RAQDPS023: sulfate (SU); nitrate (NI); ammonium (AM); elemental carbon (EC); primary organic matter (POM); secondary organic matter (SOM); crustal material (CM); sea salt (SS); and aerosol water (WA). This set of chemical components is consistent with the approach of three North American PM<sub>2.5</sub> speciation measurement networks (CSN, IMPROVE, NAPS) to report PM<sub>2.5</sub> chemical composition (see Dabek-Zlotorzynska et al., 2011; Chow et al., 2015) and with other AQ models that resolve PM composition (e.g., Table 6 of Kukkonen et al., 2012). Note, however, that all of these chemical components must be considered to be “lumped” species. In the case of particle SU, NI, and AM, they do not account for the molecular or stoichiometric form of these three inorganic constituents, which controls particle acidity. For example, particle SU may be present as sulfuric acid (H<sub>2</sub>SO<sub>4</sub>(aq)), ammonium sulfate ((NH<sub>4</sub>)<sub>2</sub>SO<sub>4</sub>(s)), ammonium bisulfate ((NH<sub>4</sub>HSO<sub>4</sub>(s)), or letovicite ((NH<sub>4</sub>)<sub>2</sub>H(SO<sub>4</sub>)<sub>2</sub>(s)) (e.g., Saxena et al., 1983; Makar et al., 2003b). Particle EC, which is often referred to as black carbon (BC), is implicitly defined by the source-testing and ambient measurement methods used to measure it (e.g., Chow, 1995; Chow et al., 2015, 2018). Particle organic matter (POM and SOM) is composed of other elements such as hydrogen, oxygen, sulfur, and nitrogen, in addition to carbon (e.g., Turpin and Lim, 2001; Pang et al., 2006; Malm and Hand, 2007; Philip et al., 2014). Particle CM (or soil dust) is composed of oxides of silicon, various metals (e.g., iron, aluminum, titanium), base cations (sodium, calcium, magnesium, and potassium), and carbonate (e.g., Malm et al., 2004; Dabek-Zlotorzynska et al., 2011; Hand et al., 2017). And particle SS is a complex mixture of multiple salts and organics in addition to NaCl (e.g., White, 2008; Ault et al., 2013).

One additional aspect of PM composition is its mixing state, which refers to the variation of PM chemical composition with particle size (e.g., Heintzenberg, 1989; Jacobson, 2001; Zhu et al., 2015). At one extreme, referred to as an internal mixture, all aerosol particles of a given size at a given point in space and time are assumed to have the same chemical composition. At the other extreme, referred to as an external mixture, each aerosol particle of the same size may be composed of any one of many pure chemical species. And between these two extremes lies a very wide range of transitional mixing states. Mixing state affects a particle's hygroscopicity, organic absorptivity, and radiative properties (Stevens et al., 2022). MACH assumes that each PM size bin is internally mixed (Gong et al., 2003; Park et al., 2011; Stevens et al., 2022). This assumption has the advantage of minimizing the number of PM chemical components that must be considered since no special considerations must be made for mixing state. It is least good close to emission sources of primary PM but becomes more realistic as aerosol particles age and undergo condensation and coagulation processes (e.g., Winkler, 1973).

Size- and composition-resolved atmospheric PM was thus represented in the RAQDPS023 with two internally-mixed size bins and nine chemical components for a total of 18 size bin-chemical component tracers (e.g., PM<sub>2.5</sub>-EC, PM<sub>c</sub>-NI). Sixteen of these PM tracers were prognostic fields and were advected while the two size bin-aerosol water tracers were diagnostic fields that were estimated by the Hänel (1976) scheme or the HETV code (Sects. 3.3.5 and 3.6). Although each size bin was assumed to be internally mixed, the chemical composition of the two size bins could be



different. Mass mixing ratio (MMR) with units of  $\mu\text{g}$  size bin-component / kg dry air was used in the PM conservation-of-mass equations in MACH to describe aerosol particle abundances. Mixing ratios have the advantage of being independent of pressure and temperature. While molar (or volume) mixing ratio is an official SI unit for species abundance in air (Schwartz and Warneck, 1995), MMR is a more appropriate choice when the chemical composition of a constituent is not known or is not well-defined as is the case for “lumped” chemical species such as the above nine PM chemical components. MMR units were also used for gaseous species in the RAQDPS023 for consistency, although unit conversions may be performed before and after some process operators (e.g., gas-phase chemistry).

### 380 3.3 Aerosol microphysical schemes

A number of physico-chemical processes affect the PM population and its size distribution and chemical composition: (i) emission of primary particles of different sizes and composition; (ii) nucleation of new ultrafine particles from gas-phase precursors; (iii) growth of existing particles via condensation of non-water vapours and the shrinkage of particles via volatilization of particulate species to the gas phase (i.e., gas-particle partitioning); (iv) collision and coagulation of particles; (v) swelling and activation of particles due to water-vapour sorption processes; and (vi) size-dependent removal of particles via dry and wet deposition processes. CTMs that resolve the PM size distribution should in principle simulate all of these processes. However, urban-scale CTMs often neglect nucleation (by assuming that condensation prevails under conditions with moderate to high PM concentrations) and coagulation (which is typically slow compared to other processes), but regional-scale CTMs with their larger domains and longer transport times may consider these two processes. As described in this section and in Sects. 3.10 and 3.11.1, MACH represents all of the above physical processes as well as several aerosol chemical processes that are described in Sects. 3.5 to 3.7.

#### 3.3.1 Nucleation scheme

Nucleation refers to the creation of new particles by the formation of molecular clusters by low-volatility gases such as sulfuric acid vapour  $\text{H}_2\text{SO}_4(\text{g})$  and some organic species. Such nucleation-mode particles are tiny, with diameters less than 3 nm (Semeniuk and Dastoor, 2018). MACH uses a parameterization of the nucleation process based on classical nucleation theory for sulfuric acid and water binary homogeneous nucleation as proposed by Kulmala et al. (1998) and adopted in CAM (Gong et al., 2003). The expression for particle nucleation rate is dependent on sulfuric acid vapour abundance, temperature, and relative humidity (RH), and the particle mass that is created is assigned to the smallest PM size bin, which for the RAQDPS023 is the  $\text{PM}_{2.5}$  size bin.

#### 400 3.3.2 Condensation/evaporation scheme

Aerosol particles will grow in size due to the condensation of gas-phase species onto these particles but will shrink in size due to the evaporation of semi-volatile gases from these particles. A modified Fuchs-Sutugin equation is used to calculate the condensation rate for  $\text{H}_2\text{SO}_4(\text{g})$  onto aerosol particles (Fuchs and Sutugin, 1971; Hegg, 1990; see eq. A14 of Gong et al., 2003). The expression for the condensation rate to a single particle is linearly dependent on particle diameter and  $\text{H}_2\text{SO}_4(\text{g})$  ambient vapour pressure, where the surface vapour pressure of  $\text{H}_2\text{SO}_4$  at the particle surface is very small and is assumed to be zero so that  $\text{H}_2\text{SO}_4$  mass transfer is one-way from the gas phase to the particle phase



(Russell et al., 1994). The overall condensation rate to a given particle size bin also depends on the particle number concentration for that bin, and condensation to multiple size bins will occur simultaneously. The condensation process does not change the total particle number density, but it does increase the mass of individual particles. As a  
410 consequence, some particles in size bin  $i$  may grow in size enough to move to a larger size bin. The treatment of such particles by size “rebinning” is described in Sect. 3.8.

One additional complication is that nucleation and condensation processes compete for  $\text{H}_2\text{SO}_4(\text{g})$ . Following the procedure used in CAM (Gong et al., 2003), the division of  $\text{H}_2\text{SO}_4(\text{g})$  between these two processes for each time step is calculated by solving the time rate of change equation of  $\text{H}_2\text{SO}_4(\text{g})$  accounting for both production of  $\text{H}_2\text{SO}_4(\text{g})$  and  
415 removal by nucleation and condensation. As noted by Morawska et al. (1999), however, most of the time removal by condensation will dominate removal by nucleation.

The condensation of those organic gases that partition to the particle phase to form SOM (Sect. 3.7) is treated very similarly to the condensation of  $\text{H}_2\text{SO}_4(\text{g})$ . The relative condensation rate of  $\text{H}_2\text{SO}_4(\text{g})$  to each PM size bin is used as a proxy for the relative condensation rates of these organic gases to each PM size bin.

### 420 3.3.3 Coagulation scheme

Coagulation is the process by which two or more aerosol particles can combine through collision. Coagulation acts to reduce the number concentration of aerosol particles, especially small particles, and hence serves as a control on the evolution of the number concentration of nucleation-mode and directly-emitted accumulation-mode particles. Four distinct physical processes may result in coagulation of particles: Brownian motion; gravitational collection; turbulent  
425 inertial motion; and turbulent shear (e.g., Jacobson, 1999; Seinfeld and Pandis, 2016).

MACH follows CAM by using a semi-implicit numerical solution of the general coagulation equation (Jacobson et al., 1994) to compute the coagulation rate and intersectional transfer of aerosol particles (Gong et al., 2003). This scheme conserves bulk particle volume for any time step but results in the transfer of particle volume from smaller to larger  
430 size bins. Since MACH assumes that each PM size bin is internally mixed, the mass concentration change of each chemical component can be computed from the calculated volume change of any size bin due to coagulation. Note that the coagulation coefficient is dependent on the “wet”, or real, size of aerosol particles, not the dry size (see Sect. 3.3.5).

### 3.3.4 Gravitational settling and dry deposition schemes

Particles in the atmosphere undergo gravitational settling (or sedimentation) towards the Earth’s surface under the influence of gravity. The downward vertical speed is called the terminal settling velocity and depends on a particle’s  
435 density and the square of its wet diameter (e.g., Seinfeld and Pandis, 2016). Particles close to the Earth’s surface can then be removed from the atmosphere by dry deposition, a complicated process that depends on near-surface meteorological conditions, the nature of the underlying surface, and particle density and size.



Size-resolved particle dry deposition in MACH is represented using a scheme proposed by Zhang et al. (2001), which accounts for a number of relevant processes: turbulent transfer; Brownian diffusion; impaction; interception; 440 gravitational settling; and particle rebound. Calculated particle dry deposition velocities have a strong dependence on particle size with a minimum at particle diameters of about 1  $\mu\text{m}$  and larger values for both smaller and larger particle sizes (Gong et al., 2003). Surface characteristics for 15 different land-use categories are considered for this calculation (e.g., Zhang et al., 2001; Table S7 of Makar et al., 2018b). Particle dry deposition is only applied at the lowest model level, where the sum of dry deposition velocity and terminal settling velocity is used, whereas gravitational settling 445 occurs throughout the vertical column.

A revised numerical solution for the gravitational settling process was introduced in the RAQDPS023 based on a semi-Lagrangian advection approach. Vertical back trajectories were calculated from the settling and deposition velocities, and then mass-conservative interpolation was used to determine the new vertical concentration profile and deposition flux to the surface (Makar et al., 2018a). This new scheme replaced a previous numerical scheme based on an analytical 450 exponential decay rate and better accounts for the model's decreasing vertical grid spacing close to the Earth's surface (Sect. 2.2), which results in a reduction of the rate of removal by downward particle advection. As a consequence, near-surface PM concentrations increased by as much as 0.5  $\mu\text{g m}^{-3}$  compared to those predicted using the old solution scheme (Moran et al., 2021b).

Lastly, to address the strong dependence of particle dry deposition and sedimentation on particle size (e.g., Zhang et al., 2001; Gong et al., 2003), the numerical solution of these processes was modified for the simplified two-bin 455 description of the PM size distribution used by the RAQDPS023 to reduce numerical errors. The two PM size bins were each subdivided into six sub-bins. Settling velocities were then estimated for each sub-bin based on a third-order polynomial fit to a typical  $\log_{10}(\text{settling velocity})$  as a function of  $\log_{10}(\text{radius})$  that was determined using a stand-alone version of the code. Dry deposition velocities were also calculated for each sub-bin based on a weighted average 460 of third-order polynomial fits to a typical  $\log_{10}(\text{dry deposition velocity})$  as a function of  $\log_{10}(\text{radius})$  for non-urban land surfaces and urban land surfaces (which has higher values). Revised values of settling velocity and dry deposition velocity for the two size bins were then calculated as logarithms of the sum of the exponentials of the sub-bin values. The revised values of the settling velocities for  $\text{PM}_{2.5}$  and  $\text{PM}_{\text{cf}}$  based on the sub-bin division were roughly 30% smaller and 100% larger, respectively. The revised values of the dry deposition velocities for  $\text{PM}_{2.5}$  and  $\text{PM}_{\text{cf}}$ , on the other 465 hand, were roughly 100% larger and 50% smaller. Analogous modifications to the numerical solution of three other aerosol processes to address intersectional mass transfer in the two-bin configuration are described in Sect. 3.8.

### 3.3.5 Hygroscopic growth and aerosol activation schemes

The hygroscopic growth of mixed aerosol particles at subsaturation conditions (i.e.,  $\text{RH} < 1$ ), which is sometimes referred to as swelling, can result in substantial aerosol water component WA values. For example, Tsyro (2005) has 470 suggested that for  $T=20^\circ\text{C}$  and  $\text{RH}=50\%$  aerosol water may contribute 20–35% of annual mean  $\text{PM}_{2.5}$  concentrations in Europe. Nguyen et al. (2016) have shown based on field study measurements from around the world that aerosol



water is ubiquitous and at rural locations contributed on average  $3 \mu\text{g}\cdot\text{m}^{-3}$  and 35% of  $\text{PM}_{10}$  total mass. In fact, at high RH values the aerosol water component can dominate aerosol particle composition and mass (e.g., Tang and Munkelwitz, 1994; Nguyen et al., 2016; Widziewicz-Rzońca and Tytła, 2020).

475 The RAQDPS23 calculates aerosol water using a mixing rule for soluble components (SU, NI, AM, POM, SOM, SS), where EC and CM are assumed to be hydrophobic (Gong *et al.*, 2003, App. A1). This approach follows that of Hänel (1976). Note that the aerosol water component WA is also diagnosed independently by the HETV scheme (Sect. 3.6).

Under supersaturated conditions (i.e.,  $\text{RH} > 1$ ) hygroscopic aerosol particles can grow rapidly by water-vapour condensation to form cloud droplets, whose diameters typically fall in the  $10\text{--}200 \mu\text{m}$  range vs.  $500\text{--}8000 \mu\text{m}$  for  
480 raindrops (e.g., Jacobson, 1999). This process is called aerosol activation but may also be referred to as nucleation scavenging or droplet nucleation, and aerosol particles that can be activated are referred to as cloud condensation nuclei (CCN). Aerosol particle activation is important because it may result in modification of the PM mass and size distributions within and below clouds by aqueous-phase chemistry and wet removal (Sects. 3.5 and 3.10). This trio of processes is referred to collectively as cloud processing. However, whether a CCN particle is activated depends on the  
485 level of supersaturation and the particle's size and physical and chemical properties (e.g., Gong et al., 2011).

Two different parameterizations of aerosol particle activation are available in MACH (Gong et al., 2015). For the RAQDPS023, MACH uses the empirical aerosol activation scheme of Jones et al. (1994) to determine the cloud droplet number concentration  $N_d$  in a cloud as a function of the particle number concentration  $N_p$ . This scheme permits the calculation of a critical particle radius above which all aerosol particles are assumed to be activated (Gong et al., 2006).  
490 The portion of aerosol particles incorporated in these cloud droplets is then determined by adding particles from the largest size bin in descending order of size until  $N_d$  is reached (Gong et al., 2006, 2015). Next, the bulk cloud liquid water content from GEM (Table 2) is distributed evenly to all activated aerosol particles, after which the cloud droplet size associated with each PM size bin can be determined (Gong et al. 2006). Information about the activated aerosol particles, including their wet diameter, is then available for use by other aerosol process parameterizations, including  
495 aqueous-phase chemistry and in-cloud scavenging. Note that for the RAQDPS023 with only two size bins, the  $\text{PM}_{10}$  size bin must be fully activated for the fine size bin to be even partially activated.

### 3.4 Gas-phase chemistry scheme

Numerous gas-phase chemical reactions occur in the atmosphere (e.g., Jenkin et al., 2015), and some important gas-phase species such as  $\text{O}_3$  and hydrogen peroxide ( $\text{H}_2\text{O}_2$ ) are reaction products only and are not directly emitted to the  
500 atmosphere. It is thus necessary to represent these reactions in a CTM (e.g., Dodge, 2000), but it is also challenging. In particular, volatile organic compounds (VOCs) play a key role in determining the oxidative state of the atmosphere because they may react with three important oxidants: hydroxyl radical (OH); nitrate radical ( $\text{NO}_3$ ); and  $\text{O}_3$  (e.g., Atkinson, 1990; Seinfeld and Pandis, 2016). As a consequence VOCs influence photochemistry, PM formation, and acid deposition. However, thousands of VOC species with varying chemical and physical properties, including OH  
505 reactivity, vapour pressure, and solubility, are emitted to the atmosphere (e.g., Makar et al., 2003b), and it is not



computationally feasible for three-dimensional AQ models to consider the chemical reactions of all of these individual species. Instead, a number of parameterized gas-phase chemistry mechanisms have been developed that consider reduced-form or condensed representations of the full atmospheric chemical system by "lumping" or aggregating groups of VOC species with similar chemical properties together in order to reduce the number of species and chemical reactions that must be considered (e.g., Carter, 1990; Middleton et al., 1990; Kuhn et al., 1998; Dodge, 2000).

The RAQDPS023 used a modified version of the ADOM-2 gas-phase chemistry mechanism to parameterize tropospheric chemistry (Stockwell and Lurmann, 1989; Pudykiewicz et al., 1997; Moran et al., 1998). The ADOM-2 mechanism, which itself was an update of the ADOM-1 mechanism (Lurmann et al., 1986; Fung et al., 1991), was designed to give an accurate representation of hydrocarbon gas-phase reactivity using a modest number of model VOC species. It employs a "lumped molecule" approach (Dodge, 2000) to define 16 lumped VOC species and eight organic radicals in addition to CH<sub>4</sub> and C<sub>2</sub>H<sub>6</sub> plus 21 inorganic species. Table 3 lists these 46 ADOM-2 chemical species and some of their properties, and Table 4 lists the ADOM-2 mechanism's 114 associated chemical reactions, including 16 photolytic reactions that depend on sunlight.

Note from Table 3 that the abundances of 41 of these gas-phase species were forecast and advected while the abundances of five species (CH<sub>4</sub>, C<sub>2</sub>H<sub>6</sub>, H<sub>2</sub>O, O<sub>2</sub>, M) had specified, time-invariant vertical profiles and were not advected. Eighteen of the advected species were organic species, of which 11 were emitted along with eight inorganic species (Table 3). Only two of the ADOM-2 VOC species that were emitted were individual or unlumped species, namely formaldehyde (HCHO) and isoprene (ISOP; C<sub>5</sub>H<sub>8</sub>). The other nine were lumped species, and this high degree of lumping imposes a limitation for evaluating model predictions of VOC species (e.g., Stroud et al., 2008; Moran et al., 2025).

The calculation of lumped ADOM-2 VOC emissions begins with the assignment of individual emitted VOC species to one of the 32 VOC categories proposed by Middleton et al. (1990) to aggregate the 1980 National Acid Precipitation Assessment Program (NAPAP) anthropogenic VOC emissions inventory or to three additional biogenic categories (Isoprene, Alpha- and Beta-Pinene, and Other Monoterpenes) suggested by Makar et al. (2003b). These 35 VOC categories are then further lumped to the 11 emitted ADOM-2 VOC species using mole-based reactivity weights (see Table 5). Most of the ADOM-2 VOC species represent tens, hundreds, or even thousands of individual VOC species. For example, the ADOM-2 C<sub>3</sub>H<sub>8</sub> lumped VOC species includes propane (C<sub>3</sub>H<sub>8</sub>) as would be expected, but it also includes benzene, acetylene, and some other lower-reactivity species (e.g., alcohols, ethers, and esters) that are assigned to NAPAP category 27 (e.g., Plummer et al., 2001; Makar et al., 2003b). The ETHE lumped VOC species includes ethene (C<sub>2</sub>H<sub>4</sub>), but it also includes isoprene oxidation products such as methacrolein and methyl vinyl ketone in order to implement a condensed isoprene chemistry mechanism used by the Carbon Bond-IV chemistry mechanism (Gery et al., 1988, 1989; Stockwell and Lurmann, 1989; Stroud et al., 2008). Note that emissions of acetone, organic acids, haloalkenes, and three other NAPAP VOC categories (26, 31, 32) are not included in emissions for the ADOM-2 mechanism due to their low or unknown reactivities (referred to collectively in Table 9 as EOTH).



540 Rate constants for the inorganic reactions considered by the ADOM-2 mechanism were based largely on the  
recommendations of DeMore et al. (1987) while those for the organic reactions were based largely on Atkinson et al.  
(1992). The rates of the 16 photolytic reactions in Table 4 are expressed as the abundance of photoactive species  
multiplied by the photodissociation rate coefficient (i.e., J value). The ADOM-2 photodissociation rate coefficients  
were calculated from lookup tables of clear-sky actinic flux from Peterson (1976), which were based on the radiative  
545 transfer model of Dave (1972) and absorption cross-sections and photodissociation quantum yields from DeMore et  
al. (1987) (Stockwell and Lurmann, 1989). The photodissociation rate coefficients for  $J_{\text{NO}_2}$  and  $J_{\text{O}_3 \rightarrow \text{O}^1\text{D}}$  depend on  
both altitude and solar zenith angle whereas the other photodissociation rate coefficients depend only on solar zenith  
angle and species-dependent scale factors (Kelly et al., 2012). Lastly, to account for the effect of clouds on clear-sky  
photolysis rate constants, the total cloud fraction field  $f_{\text{cl,d}}$  (ftot in Table 2), which accounts for both resolved and SGS  
550 clouds in a model layer, and cloud liquid water content field (lwc in Table 2) predicted by GEM were used to scale the  
precalculated clear-sky J values following an algorithm from Chang et al. (1987). More details are given in Majdzadeh  
et al. (2022). Note that the performance of the ADOM-2 gas-phase mechanism was compared to a number of other  
gas-phase chemistry mechanisms by Kuhn et al. (1998), and its predictions were found to be close to the median for  
the nine mechanisms tested.

555 To integrate the chemistry tracer conservation-of-mass equations in time, the Young and Boris (1977) predictor-  
corrector method was used to solve the gas-phase chemistry step of the process operator splitting sequence (see  
Sect. 4.1). This asymptotic algorithm, which typically must use much smaller integration time steps than the overall  
MACH chemistry time step of 900 s due to the stiffness of the ADOM-2 chemical system, is integrated over the MACH  
chemistry time step.

560 The treatment of stratospheric chemistry in the RAQDPS023 was much simpler than that for tropospheric chemistry.  
The LINOZ scheme for ozone stratospheric chemistry (McLinden et al., 2000) was used to forecast ozone  
concentrations while concentrations of other species were only affected by dynamics and physics. The definition of  
the stratosphere used to apply the LINOZ scheme in each grid column was either those vertical levels located above  
100 hPa or with specific humidity less than 10 ppmv. The ADOM-2 scheme was used below these levels. The LINOZ  
565 scheme was also implemented in the GDPS 8.0.0 to support the data assimilation of satellite-based ozone  
measurements (CMC-GDPS-8.0.0, 2021a).

### 3.5 Aqueous-phase chemistry scheme

Cloud chemistry, that is, aqueous-phase chemistry in cloud water, is an important pathway for the conversion of  $\text{SO}_2$   
to  $\text{SO}_4^-$  (e.g., Barth et al., 2000; Gong et al., 2011). As well as referring to chemical reactions amongst various species  
570 in dilute aqueous solution in the cloud droplets, the term aqueous-phase chemistry usually encompasses two related  
processes: mass transfer of species between the gas phase and aqueous phase (absorption/condensation) inside clouds  
and the dissociation/ionisation in cloud water of certain dissolved species. Note that consideration of these processes  
is necessarily restricted to activated aerosol particles (Sect. 3.3.5).



MACH employs a slightly adapted version of the ADOM aqueous-phase chemistry mechanism, which considers 12  
575 gas-phase and 13 aqueous-phase species together with 25 reactions, to represent these processes (Young and Lurmann,  
1984; Fung et al., 1991). Note from Table 4 that one ADOM-2 mechanism species, NH<sub>3</sub>, does not participate in any  
gas-phase reactions, but NH<sub>3</sub> participates in aqueous-phase and inorganic heterogeneous reactions (see also Sect. 3.6).  
Table 6 lists the 25 gas and aqueous species and Table 7 lists the 25 reactions that are considered by this condensed  
mechanism. Reactions 19-22 describe the four pathways for SO<sub>2</sub> oxidation (i.e., S(IV) → S(VI)) included in the  
580 mechanism: these reactions involve three aqueous-phase oxidants (H<sub>2</sub>O<sub>2</sub>, O<sub>3</sub>, ROOH) and oxygen catalyzed by iron  
and manganese (e.g., Seinfeld and Pandis, 2016). Fourteen of the mechanism reactions in Table 7 describe the mass  
transfer of soluble gases as a reversible diffusion process constrained by chemical equilibrium (i.e., forward-backward  
reaction pairs 2-3, 4-5, 6-7, 8-9, 10-11, 12-13, and 15-16 for gas-phase SO<sub>2</sub>, O<sub>3</sub>, H<sub>2</sub>O<sub>2</sub>, HNO<sub>3</sub>, ROOH, NH<sub>3</sub>, and CO<sub>2</sub>,  
respectively). Moreover, reaction pairs 2-3, 8-9, and 12-13 describe both mass transfer from the gas- to the aqueous  
585 phase and subsequent dissociation in cloud water. Aerosol particle scavenging, which is represented by reactions 1  
and 23-25, is an irreversible process that can occur by nucleation, Brownian motion, phoretic attachment, or inertial  
impaction (e.g., Wang et al., 2010), but only nucleation (i.e., aerosol activation) is currently considered for in-cloud  
scavenging. Inorganic particle components SU, NI, and AM enter cloud droplets through this process. The diffusion  
coefficients needed to describe the mass transfer process are determined using the Fuchs and Sutugin (1971)  
590 formulation (Young and Lurmann, 1984).

To reduce computer time, following Gong et al. (2006) this chemistry mechanism is implemented in MACH as a “bulk”  
(i.e., non-size-resolved) process that occurs in a generic cloud droplet whose size is determined from the bulk or total  
cloud liquid water content (LWC) supplied from GEM (Table 2) and cloud droplet number concentration  $N_d$   
(Sect. 3.3.5). In addition, the GEM total cloud fraction field  $f_{\text{clid}}$  is used to convert grid-average values to “in-cloud”  
595 values before the cloud chemistry operator is applied.

Like the gas-phase mechanism the aqueous-phase mechanism is solved for a MACH chemistry time step using the  
computationally efficient Young and Boris (1977) predictor–corrector algorithm with a number of smaller integration  
time steps. At the end of the aqueous-phase chemistry integration step, the gridded gas-phase concentrations of SO<sub>2</sub>,  
O<sub>3</sub>, H<sub>2</sub>O<sub>2</sub>, HNO<sub>3</sub>, ROOH, and NH<sub>3</sub> are updated to account for their in-cloud depletion and the resulting bulk mass  
600 increments of three dissolved inorganic aerosol components (SU, NI, AM) are redistributed across activated PM size  
bins in air, effectively returning particle concentrations to clear air conditions. This redistribution is done by using the  
ratios of LWC in each activated (or partially activated) size bin to the total LWC, which implies that aqueous-phase  
chemistry is a volume-controlled process (Gong et al., 2006). The LWC in each bin depends on the number of activated  
aerosol particles in each bin and is obtained by distributing bulk LWC to all activated aerosol particles evenly (Gong  
605 et al., 2006, 2011). This mass redistribution step at the end of the aqueous-phase chemistry operator is then followed  
by a “rebinning” step that is needed to maintain the fixed size bin structure (Sect. 3.8). Note, however, that the resulting  
ambient concentrations of inorganic particle components NI and AM may not be in equilibrium with the gas phase so  
the inorganic heterogeneous chemistry operator is called next.



### 3.6 Inorganic heterogeneous chemistry scheme

610 Ambient sulfuric and nitric acid vapours and ammonia gas can partition to atmospheric particles to form one or more inorganic salts, and the resulting SU, NI, and AM aerosol components can make up a significant fraction of  $PM_{2.5}$  mass (e.g., Brook and Dann, 1999; Malm et al., 2004). Depending on the relative fractions of these three gas-phase species, four different salts may be formed (e.g., Ansari and Pandis, 1998): ammonium sulfate  $((NH_4)_2SO_4)$ , ammonium bisulfate  $(NH_4HSO_4)$ , letovicite  $((NH_4)_3H(SO_4)_2)$ , or ammonium nitrate  $(NH_4NO_3)$ . Because  $H_2SO_4(g)$  has a very low  
615 vapour pressure (Sect. 3.3.2), it is a reasonable approximation to assume that it resides completely in the aerosol phase (Nenes et al., 1998), whereas nitric acid vapour  $(HNO_3(g))$  and ammonia gas  $(NH_3(g))$  exist in a reversible equilibrium between the gas and particle phases. Knowledge of inorganic heterogeneous chemistry thus allows the secondary inorganic component of PM to be determined.

Inorganic heterogeneous chemistry was parameterized in the RAQDPS023 version of MACH with the computationally  
620 efficient HETV (HETerogeneous Vectorized) scheme (Makar et al., 2003a), which is based on a subset of the ISORROPIA thermodynamic equilibrium algorithms (Nenes et al., 1998, 1999). In ISORROPIA the full system of inorganic equilibrium equations is broken up into subsystems, each corresponding to fixed ranges of RH and the ratio of total ammonia to total sulfate, where total ammonia includes both gas and particle forms in molar units. These ranges constrain which inorganic species (gases, ions and salts) may be present in aerosol particles. HETV considers  
625 12 such range-based subsystems or “cases”. The multicomponent activity coefficient calculations that are required for non-ideal, high-concentration solutions use the formula of Kusik and Meissner (1978) as described by Kim et al. (1993) but are approximated using higher-order Taylor series to reduce calculation time (Makar et al., 2003a). The metastable state assumption, namely that some particle liquid water is always present even at low RH, was also made to reduce the number of cases that must be considered (e.g., Rood et al., 1989; Miller et al., 2024).

630 Similar to the implementation of the aqueous-phase chemistry parameterization (Sect. 3.5), HETV assumes a bulk equilibrium in the particulate phase over all particle sizes to save computer time. At the end of the inorganic-heterogeneous-chemistry integration step, gridded concentrations of  $HNO_3(g)$  and  $NH_3(g)$  are updated to account for inorganic gas-particle partitioning during the time step, where the updated values may have either increased or decreased. If the bulk mass increments of the three inorganic aerosol components (SU, NI, AM) are positive, then  
635 these increments are redistributed across the PM size bins. This redistribution is carried out by using the ratios of gas-phase condensation rates to all particles in a size bin based on the modified Fuchs-Sutugin equation (Hegg, 1990; Makar et al., 1998; Gong et al., 2003) and the total condensation rate summed over all size bins. If the bulk mass increments are negative, though, then mass is removed from each size bin starting with the largest based on the same condensation rate ratios. Note that it is possible that for some bins the mass that is available to be removed may be  
640 less than the pro-rated increment, in which case a second removal iteration may be required. This redistribution step is then followed by a mass-conserving “rebinning” step that is needed to maintain the fixed size bin structure (Sect. 3.8).



### 3.7 Secondary organic aerosol formation scheme

The term “secondary organic aerosol” (SOA; equivalent to SOM) refers to organic PM that results from the oxidation of gas-phase VOC precursor species followed by condensation to the particle phase (e.g., Hallquist et al., 2009; Jimenez et al., 2009). The RAQDPS023 used the Instantaneous secondary organic Aerosol Yield (IAY) scheme described by Jiang (2003, 2004, 2005) to represent SOA formation from five model VOC species. Four of these are lumped VOC species: ALKA (long-chain anthropogenic and biogenic alkanes); ALKE (long-chain anthropogenic and biogenic alkenes); AROM (multi-substituted aromatics); and TOLU (toluene and mono-substituted aromatics) (Stroud et al., 2008). The fifth model VOC species is ISOP (isoprene), which is not lumped and is dominated by biogenic emission sources (although there are also minor anthropogenic sources). The total SOA contribution from ALKE oxidation is further divided into contributions from anthropogenic ALKE and from biogenic  $\alpha$ -pinene and  $\beta$ -pinene (derived from BEIS monoterpene emissions; see Sect. 3.11.3).

The Jiang scheme is based on a two-condensable-product fit to chamber data (Pankow, 1994; Griffin et al., 1999), where initial products are assumed to be converted rapidly to non-volatile organic PM. Values of the IAY parameters that were used by the RAQDPS023 are listed in Table 8, where  $\alpha_{1i}$  and  $\alpha_{2i}$  are the mass-based stoichiometric coefficients (unitless) and  $K_{om,1i}$  and  $K_{om,2i}$  are the partitioning coefficients ( $\text{m}^{-3}\cdot\mu\text{g}$ ) of the  $i$ -th condensable species  $\text{CS}_i$ , respectively (Odum et al., 1996; Jiang, 2003). The  $\alpha_i$  and  $K_{om,i}$  values for ALKA and anthropogenic ALKE are taken from Griffin et al. (1999), those for AROM,  $\alpha$ -pinene, and  $\beta$ -pinene are taken from Jiang (2003), the TOLU values come from Odum et al. (1997), and the ISOP values are taken from Barsanti et al. (2013).

The amount of SOA product available for condensation at each MACH chemistry time step is the sum of  $\text{IAY}_i \cdot \text{CS}_i$  over the seven VOC condensable species (CS) values listed in Table 8, where  $\text{IAY}_i$  is a dimensionless fraction and  $\text{CS}_i$  is the reduction due to oxidation of ALKA, ALKE, AROM, TOLU, and ISOP MMRs over a MACH time step as calculated by the gas-phase chemistry operator (Sect. 3.4). The condensation rate of SOA products to aerosol particles is described by a modified Fuchs-Sutugin equation (see eq. A14 of Gong et al., 2003), similar to the treatment for  $\text{H}_2\text{SO}_4$  condensation (Sect. 3.3.2), and the relative condensation rates of  $\text{H}_2\text{SO}_4(\text{g})$  to each PM size bin are used as a proxy for the relative condensation rates of these SOA organic gases. Lastly, like the  $\text{H}_2\text{SO}_4$  condensation step the SOA condensation step must be followed by a “rebinning” step to maintain the fixed PM size bin structure as described next.

### 3.8 Intersectional mass transfer schemes

As already noted, one complication of using a fixed sectional representation of the PM size distribution is that particles belonging to a particular size bin may grow too large for that bin due to the addition of mass from condensation or from aqueous-phase or heterogeneous chemistry (e.g., Jacobson, 1999; Gong et al., 2006). This problem can be addressed by applying a rebinning operator that partitions the enlarged particles between two adjacent size bins in a mass- and number-conserving manner in order to maintain the fixed bin structure. Jacobson (1999) refers to this rebinning approach as a quasi-stationary size structure for the PM size distribution. Interestingly, fixed modal



representations of the PM size distribution suffer from an analogous issue that has an analogous solution, referred to as mode merging (e.g., Binkowski and Shankar, 1995; Binkowski and Roselle, 2003).

MACH implements a mass-conservative rebinning procedure each time step after each of three processes: condensational growth (Sects. 3.3.2 and 3.7); aqueous-phase chemistry (Sect. 3.5); and inorganic heterogeneous chemistry (Sect. 3.6). A slightly different approach to rebinning is used for each of these three processes. For  
680 condensational growth the rebinning calculation is treated as mathematically equivalent to two-particle coagulation (Gong et al., 2003). The volume of a particle in the size bin that underwent condensation (the “donor” bin) is considered to be one colliding particle while the volume of the condensable species per particle is considered to be the other colliding particle. The same formulation used by Jacobson et al. (1994, Eq. 13) to partition the volume of an  
685 intermediate particle of two coagulating particles into two model size bins (the “receiver” bins) is then used (Gong et al., 2003). The two volume partitioning factors that are calculated depend on the particle volumes of the donor and receiver size bins before condensation occurred and the particle volume for the donor bin after condensation occurred. The sum of the two partitioning factors is unity (to conserve the allocated volume), and the smaller of the two adjacent receiver size bins may be the same as the donor size bin but may also be a larger size bin (if  $n > 2$ ). The choice of the  
690 receiver size bins depends on the mean particle diameter diagnosed for the new total mass for the donor size bin mass after condensation using the initial donor-bin particle number. The rebinning calculations are applied to each size bin beginning with the smallest one. Note that all PM chemical components are affected by rebinning due to the assumption of internal mixing even though condensational particle growth is due only to one or two chemical components (i.e., sulfuric acid vapour or condensable organic gases).

695 For activated particles that have grown due to the production of particle sulfate by aqueous-phase chemistry, rebinning is performed after the redistribution step at the end of the aqueous-phase chemistry operator. A similar equivalence to two-particle coagulation is invoked, with each activated particle size bin corresponding to a donor bin and the size-bin mass gain due to cloud chemistry corresponding to the second particle, but the partitioning-factor pairs for the receiver bins are calculated with the mass-based method described by Gong et al. (2006; Eq. 3), which also conserves particle  
700 number. Rebinning is restricted to size bins with activated particles, where the rebinning calculations are applied beginning with the smallest activated or partially activated bin and then moving to successively larger activated size bins but are based on non-activated particle properties.

The inorganic heterogeneous operator is called immediately after the aqueous-phase chemistry operator (see Sect. 4.1) because the updated PM composition resulting from the latter may not be in stable equilibrium with the gas phase  
705 However, once HETV determines a new gas-particle partitioning equilibrium, some particles may have gained mass or lost mass and hence may need to be assigned to a different size bin. The mass-based method of Gong et al. (2006) is also used for rebinning here but with two adjustments. First, activation is not relevant so in the case of mass gain rebinning is applied to all particle size bins beginning with the smallest size bin and moving to successively larger bins. Second, since particles may have lost mass as well as gained mass, the two-particle coagulation analogy is generalized



710 to account for a “donor” particle with a negative mass gain. For such negative mass increments the rebinning moves mass to a pair of smaller receiver size bins beginning with the largest size bin and moving to successively smaller bins.

The above descriptions are general and also apply to the 12-bin version of GEM-MACH. For the RAQDPS023, which only considers two PM size bins, the two adjacent receiver size bins can only be the  $PM_{2.5}$  and  $PM_{cf}$  size bins and the rebinning step can only transfer particle mass from the  $PM_{2.5}$  size bin to the  $PM_{cf}$  size bin. During development of the original GEM-MACH-based RAQDPS, it was found that the rebinning operator was transferring too much mass from  
715 the  $PM_{2.5}$  size bin to the  $PM_{cf}$  size bin. This problem was not apparent for the 12-bin version, suggesting that the very coarse representation of the PM size distribution was introducing numerical errors. Conceptually if we consider that it is those particles whose diameters are already close to the upper end of a size bin that are most likely to grow into the next larger size bin after mass is added by condensation or other processes, then an assumption that particles of any  
720 size from the ultrafine to 2.5  $\mu m$  might increase enough in size in one time step to join the  $PM_{cf}$  size bin is unrealistic.

The solution adopted for the two-bin version to avoid this assumption was to subdivide each size bin into a number of sub-bins, allocate the mass increase for each size bin across the sub-bins, apply the rebinning operator to the individual sub-bins, and then aggregate the sub-bin particles back to the original size bins. In addition to the choice of the number of sub-bins, however, the subdivision and allocation steps could be performed in a number of ways, such as a linear  
725 vs. a logarithmic subdivision of size bins and allocation of the mass increment to a uniform distribution vs. an assumed log-normal distribution.

After some experimentation a linear subdivision of each size bin into six equal-sized sub-bins by radius was adopted with the mass of each chemical component for the size bin divided equally between the six sub-bins. For condensational growth the allocation of size-bin gained mass for a time step across the sub-bins was based on the  
730 relative fraction of total particle area by sub-bin for the size bin. For cloud chemistry the allocation step was done in three steps. First, aerosol number concentration was allocated to sub-bins based on the equal distribution of particle mass to the sub-bins. Next, cloud liquid water was allocated to each sub-bin based on the relative fraction of total particle number by sub-bin for the size bin. And third, the relative fraction of cloud liquid water by sub-bin for the size bin was used to allocate the mass increment to each sub-bin. Finally, for inorganic heterogeneous chemistry the  
735 allocation step for aerosol particle mass changes followed the approach for condensational growth: the size-bin mass increment for a time step was divided equally between the six sub-bins, but with the additional possibility that the size-bin mass increment could be negative, that is, a mass decrement, due to volatilization of the nitrate and ammonium aerosol components. The net result of introducing these modifications was to reduce the intersectional transfer of mass after these process operators from the  $PM_{2.5}$  bin to the  $PM_{cf}$  bin.

### 740 3.9 Gas-phase dry deposition scheme

Many atmospheric gases, like aerosol particles (Sect. 3.3.4), are removed at the Earth's surface by dry deposition after downward transport by air motions (though gravitational settling plays no role, unlike the particle case). The rate of removal by dry deposition is determined in part by the chemical and physical properties of each individual gas,



including its reactivity, solubility, and molecular diffusivity. The rate of removal is also affected by surface properties,  
745 including vegetation characteristics in the case of removal through plant stomata and by other vegetative surfaces,  
including wetted surfaces (e.g., Wesely and Hicks, 2000; Zhang et al., 2002b; Clifton et al., 2020, 2023; Galmarini et  
al., 2021).

To represent the dry deposition of gas-phase species MACH uses a variant of Wesely's resistance-analogy  
parameterization (Wesely, 1989), which is based on the product of the concentration of a gas-phase species at the  
750 Earth's surface and its dry deposition velocity. Following an analogy to electrical circuits, the dry-deposition velocity  
of a species is given by the inverse of total "resistance", which consists of the sum of three components: aerodynamic  
resistance, quasi-laminar sublayer resistance, and surface resistance. Aerodynamic resistance  $R_a$  is a function of only  
near-surface micrometeorological conditions and the roughness characteristics of the underlying surface, so it is  
independent of the chemical species. Quasi-laminar sublayer resistance  $R_b$  is a function of friction velocity and the  
755 molecular diffusivity of each chemical species. The surface resistance  $R_c$  is the most important and complex resistance  
for most gas-phase chemical species, and it effectively determines whether a particular species is dry deposited or not.  
Soil resistance, soil wetness, and snow cover must be considered for all land surfaces in calculating  $R_c$ , with additional  
resistances (stomatal, mesophyll, cuticle, in-canopy, leaf-litter) required in the case of vegetated surfaces.

To account for the different dry deposition rates of gas-phase species, MACH considers two master species,  $\text{SO}_2$  and  
760  $\text{O}_3$ , which behave quite differently for wet surfaces (Zhang et al., 2002a,b). Weighted averages of the dry deposition  
velocities for these two master species are then used to scale dry deposition velocities for other dry depositing species  
(Zhang et al., 2002; Makar et al., 2018b). Table 3 lists the 17 ADOM-2 gas-phase species that are dry deposited and  
the master-species dry deposition scaling factors (DDF) that are assumed for each. Stomatal resistance is parameterized  
using a single-layer, two-big-leaf approach that treats sunlit and shaded leaf surfaces separately (Zhang et al., 2002a,b).  
765 One limitation of the Zhang et al. (2002a) scheme, however, is its simplistic treatment of vegetation phenology and  
seasons in both time and space: only five phenologically-based seasons are considered, which vary by month and  $5^\circ$   
latitude bands without any dependence on longitude or elevation (Brook et al., 1999a). For some months this can result  
in zonal bands being visible in surface concentration fields due to seasonal differences between latitude bands. Two  
removal processes for  $\text{SO}_2$  were also recently identified as missing from the RAQDPS023: the soil-wetness and cuticle-  
770 wetness gas-phase dry deposition pathways (e.g., Wesely, 1989; Galmarini et al., 2021; Clifton et al., 2023). Further  
details about the scheme used by MACH to model the dry deposition of gases may be found in Makar et al. (2018b),  
and evaluation results for  $\text{O}_3$  deposition for this scheme and for comparable schemes used by other CTMs can be found  
in three recent papers (Clifton et al., 2023; Hogrefe et al., 2025; Kioutsioukis et al., 2025).

### 3.10 Wet deposition schemes

775 Wet deposition, which is also referred to as wet removal or precipitation scavenging, consists of multiple processes  
related to tracer scavenging and transport by hydrometeors, which may have the form of raindrops, snowflakes, ice  
pellets, graupel, or hail (e.g., Slinn, 1984; Seinfeld and Pandis, 2016). Some wet deposition processes act within clouds



while other wet deposition processes act below clouds. The former are referred to as in-cloud scavenging or “rain-out” while the latter are referred to as below-cloud scavenging or “wash-out”. “Snow-out” must also be considered, and, unlike raindrops, solid hydrometeors can have many shapes or habits, including plates, needles, dendrites, and columns (e.g., Slinn, 1984; Zhang et al., 2013). As well, the processes responsible for the removal of soluble gases vs. aerosol particles are not identical. But regardless of these complexities, a number of modelling studies have suggested that wet deposition can be the dominant removal pathway for aerosol particles, though not for soluble gas-phase species (e.g., Barrie et al., 2001; Iversen and Seland, 2002; Textor et al., 2006).

As described in Sect. 3.3.5 aerosol particles that are activated in the supersaturated conditions within clouds act as CCN and become cloud droplets. Soluble gases inside clouds may also enter cloud droplets through gas-particle partitioning (Sect. 3.5). The majority of clouds are non-precipitating, but if cloud droplets do form raindrops that then fall from the cloud, both dissolved particle mass and dissolved gases from the cloud layer are also carried downwards by the raindrops. This “rain-out” process is parameterized in MACH using both bulk autoconversion (or precipitation production or cloud-to-rain conversion) rate  $f_{ctr}$  obtained from GEM (ppro in Table 2; see Eq. 5 of Gong et al., 2006) and SGS convective precipitation production from the middle and deep convection implementations of the Kain-Fritsch scheme (Sect. S1.7). The GEM total cloud fraction field  $f_{cld}$  (ftot in Table 2) is then used to convert grid-averaged parameters (e.g., cloud liquid water content, precipitation rates/fluxes) for each model layer to “in-cloud” values (Gong et al., 2006). The contribution of mid-level SGS convective precipitation to precipitation scavenging was added in MACH for the RAQDPS023 (Moran et al., 2021b). Note that the “snow-out” process within cold clouds consisting of ice crystals is not considered explicitly by MACH (Gong et al., 2006).

Falling hydrometeors can also scavenge aerosol particles and soluble gases located below cloud base (e.g., Slinn, 1984; Gong et al., 2006; Wang et al., 2010; Zhang et al., 2013). To calculate the below-cloud scavenging of aerosol particles by liquid or solid precipitation, MACH follows CAM (Gong et al., 1997a, 2003; Gong et al., 2011; Ghahreman et al., 2024) and employs a simplified treatment of the particle-size-dependent precipitation scavenging rate coefficient  $A(d)$  proposed by Slinn (1977, 1984), where  $d$  is the particle diameter. This includes a semi-empirical expression for the collection efficiency  $E(d,D)$ , where  $D$  is a characteristic size of the hydrometeor, that accounts for the three dominant particle collection mechanisms (Brownian diffusion, interception, inertial impaction) and assumes that the retention efficiency is unity (Slinn, 1977, Eq. 10). In the case of rain,  $D$  corresponds to the diameter of a spherical raindrop, the particle settling velocity is neglected relative to the raindrop terminal fall speed  $V_{rt}$ , and the precipitation number distribution is assumed to be monodisperse and characterized by a mean raindrop diameter  $D_m$  that can be calculated from the precipitation rate  $p$  (Slinn, 1977, Eq. 14).  $V_{rt}$  is calculated using a formula from Beard (1976).  $D_m$  and  $V_{rt}$  are then used with Eq. 10 of Slinn (1977) to calculate the mean collection efficiency  $\bar{E}(d,D_m)$ , which is used in turn to calculate  $A_r(d)$ , the particle-size-dependent rate coefficient for rain scavenging.  $A_r(d)$  depends directly on  $p$  and  $\bar{E}(d,D_m)$  and inversely on  $D_m$  (Slinn, 1977, Eq. 13).

A similar formulation is used by MACH to parameterize below-cloud scavenging of particles by snow, but the precipitation rate  $p$  corresponds to a rainwater equivalent (snow density is assumed to be a factor of 10 less than rain)



and the mean collection efficiency  $\bar{E}(d,l)$  depends on  $l$ , a characteristic dimension of the solid hydrometeors for particle collection that may be different from  $D$ , the size of the hydrometeors. The resulting snow scavenging rate coefficient  
815  $A_s(d)$  depends directly on  $p$  and  $\bar{E}(d,l)$  and inversely on  $D_m$  (Slinn, 1984, Eq. 11.36). The frozen hydrometeor terminal fall speed  $V_{st}$  needed to calculate  $\bar{E}(d,l)$  is obtained using the parameterization of Slinn (1984) (see also Gong et al., 1997a). Slinn (1984) suggested  $D_m$  values for five different snow habits, of which MACH considers snow scavenging for three different temperature ranges by needle snow ( $-8^\circ\text{C}$  to  $0^\circ\text{C}$ ), stellar snow ( $-25^\circ\text{C}$  to  $-8^\circ\text{C}$ ), and graupel ( $< -25^\circ\text{C}$ ) (Gong et al., 2011).

820 Below-cloud scavenging is assumed to be due to a single precipitation phase, either rain or snow. A threshold of the ambient dry-bulb temperature  $T$  is used to determine the phase: rain for  $T > 0^\circ\text{C}$  and snow for  $T < 0^\circ\text{C}$  (Ghahreman et al., 2024). To account for wet removal of particles in the partial vertical column below cloud base, a two-dimensional cloud cover field is first calculated from the three-dimensional total cloud fraction field  $f_{\text{clid}}$  using a random overlapping algorithm (Mailhot et al., 1998). This two-dimensional cloud cover field is then used to convert grid-averaged  
825 parameters (e.g., precipitation rate) into separate below-cloud and clear-sky values and then to recalculate grid-averaged values (Gong et al., 2006).

Six soluble gases ( $\text{SO}_2$ ,  $\text{HNO}_3$ ,  $\text{NH}_3$ ,  $\text{H}_2\text{O}_2$ ,  $\text{ROOH}$ ,  $\text{CO}_2$ ) are also removed in MACH by below-cloud precipitation scavenging. The removal of  $\text{HNO}_3$ ,  $\text{NH}_3$ ,  $\text{H}_2\text{O}_2$ , and  $\text{ROOH}$  is treated as an irreversible process similar to particle scavenging. This is a reasonable assumption when the ambient concentration of the gas-phase species is much greater  
830 than its equilibrium concentration at the surface of the raindrop or if the effective Henry's law coefficient for the species is very large (e.g., Seinfeld and Pandis, 2016).  $A_i$ , the scavenging rate coefficient for rain for the  $i$ -th gas species, is calculated using Eqs. 6 and 7 of Gong et al. (2006), where the four key parameters are  $p$ ,  $D_m$ ,  $V_r$ , and  $D_i$ , the gas-phase diffusivity of the  $i$ -th species. Wet scavenging of  $\text{SO}_2$  and  $\text{CO}_2$ , on the other hand, is treated as a reversible process since their gas-phase and gas-droplet equilibrium concentrations may be closer in magnitude or their effective Henry's  
835 law coefficient is not large. The two equilibrium equations given by Eq. 8 of Gong et al. (2006) are used for these two species, where the key parameter is  $H'$ , the effective equilibrium constant that combines absorption and dissociation equilibria. Lastly, scavenging of soluble gases by snow and ice is only considered for  $\text{HNO}_3$  and  $\text{NH}_3$ . This process is assumed to be irreversible and is based on scaling the  $\text{H}_2\text{SO}_4$  scavenging rate (Karamchandani et al., 1985; Gong et al., 2006).

840 While wet deposition results from hydrometeors transporting pollutants downwards to the Earth's surface where they are removed, some hydrometeors may evaporate before they reach the ground, in which case the pollutants are released back to the ambient air, though at a lower elevation. This vertical transport process is explicitly included in MACH (see Gong et al., 2006) by using the precipitation evaporation rate predicted by GEM ( $\text{pevp}$  in Table 2). Pollutants are assumed to be released from evaporating hydrometeors at the same rate as water vapour.



### 845 3.11 Chemical emissions inputs

Files of gridded chemical emission fluxes are a key input to CTMs, and they have a direct and large impact on model performance. In effect these emission fluxes constitute a chemical forcing term that transforms the chemical-species mass conservation equations of a CTM from an initial-value problem into an initial-boundary value problem. However, the preparation of these emission fluxes into a model-ready form is a challenging task. For one thing, all sources of emission fluxes must be considered, including both anthropogenic and natural emissions. In addition, extensive pre-processing is required to prepare files of anthropogenic emission fluxes before a CTM simulation can be performed whereas natural emissions are typically not known in advance and must be modelled and predicted during a CTM simulation.

A new set of gridded, hourly anthropogenic emissions flux input files for each month of the year for a typical seven-day week was generated for use by the RAQDPS023 and RAQDPS-FW023 (Moran et al., 2021b; see also Table A3). This emissions data set is referred to as SET4.0.0. This section describes the data sources and the preparation of the SET4.0.0 data set along with the modelling of biomass burning emissions, biogenic emissions, and sea-salt emissions.

#### 3.11.1 Anthropogenic emissions

Information about year-specific anthropogenic emissions for North America for use by CTMs is usually obtained from available annual national emissions inventories (e.g., Miller et al., 2006; Moran et al., 2013; Day et al., 2019; Foley et al., 2023). Such inventories are most often compiled by government agencies. The following three annual national anthropogenic emission inventories were used as the basis for generating the SET4.0.0 emissions input files:

- Projected 2020 Canadian Air Pollutant Emissions Inventory (APEI) based on the 2015 APEI (ECCC, 2016; Sassi et al., 2021);
- 865 • Projected 2023 U.S. National Emissions Inventory (NEI) based on version 1 of the U.S. Environmental Protection Agency (EPA) 2016 Emissions Modeling Platform for policy development applications (U.S. EPA, 2019); and
- Projected 2023 Mexican NEI based on 2008 Mexican NEI (U.S. EPA, 2019, page 168).

Each of these inventories contains annual or monthly emissions of seven criteria air contaminants (CACs), namely SO<sub>2</sub>, NO<sub>x</sub>, CO, VOC, NH<sub>3</sub>, PM<sub>2.5</sub>, and PM<sub>10</sub>, reported for different emission source sectors (e.g., heavy-duty diesel vehicles, residential wood combustion, solvent use, agricultural tillage, etc.) by subnational jurisdiction. Emission source sectors corresponding to 417 Source Classification Codes (SCCs) were contained in the 2020 Canadian inventory vs. 5,473 SCCs for the 2023 U.S. inventory and 791 SCCs for the 2023 Mexican inventory, while Canadian emissions were reported for 13 provinces and territories vs. 3,249 counties for the U.S. and 2,457 counties for Mexico (CMC-RAQDPS-023, 2021). It should be noted that the level of detail or granularity of emissions reporting in each inventory affects the level of detail that can be employed for subsequent emissions processing (see Sect. S2). For example, the county-level reporting of emissions for the U.S. and Mexico vs. province-level reporting for Canada meant in effect that some spatial allocation had already been performed for the U.S. and Mexico. Note too that not all



U.S. and Mexican counties were located within the RAQDPS023 model domain, which meant that these emissions were not included in the SET4.0.0 files.

880 Most emissions inventories are retrospective (i.e., historical) because their preparation requires the use of year-specific annual activity data such as the amount of fuel combusted or vehicle kilometers travelled in the inventory base year, and such activity data will only be available sometime after the end of the base year. Projected (or future-year) emissions inventories, on the other hand, are prospective (i.e., forecasts) because they are generated by “projecting” the emissions from a retrospective base inventory forward in time to a future year based on a set of assumptions about  
885 expected future changes to the economy, population and housing, on-road and off-road vehicle fleets, etc. along with information about any emissions changes that are expected to result from the phased implementation of existing emissions control legislation. When annual emissions levels are changing rapidly, the use of a retrospective inventory may not represent current emission levels as well as a projected inventory despite the greater uncertainties associated with a projected inventory due to the additional assumptions involved in its generation (e.g., Pan et al., 2014; Moran et al., 2020a). This was the reasoning used to choose each of the three projected future-year emission inventories listed  
890 above (in addition, importantly, to their availability): the RAQDPS023 became operational in 2021 at a time when the most recent available retrospective national emissions inventories were for base years 2015 or 2016 whereas overall North American emissions had been trending downwards for more than two decades (e.g., ECCC, 2022b; <https://gispub.epa.gov/air/trendsreport/2021>).

895 After special, emissions-processing-ready versions of the three projected annual national anthropogenic emissions inventories had been generated by ECCC for Canada and acquired for the U.S. and Mexico (U.S. EPA, 2019), they underwent extensive processing to prepare the SET4.0.0 emissions input files. A first step was to make some adjustments to the Canadian and U.S. inventories to account for additional information. The inventories were then read by the SMOKE (Sparse Matrix Operation Kernel Estimation) emissions processing system (see  
900 <https://www.cmascenter.org/smoke/>) to prepare the model-ready SET4.0.0 input emissions files. More details about this demanding and time-consuming task can be found in Sect. S2.

Table 9 compares the annual totals of model-ready anthropogenic emissions of the seven CAC species by country. These values were obtained from the full set of SET4.0.0 emissions files. It is clear from Table 9 that total U.S. emissions are larger than either Canadian or Mexican total emissions, but the relative size of the national emissions for  
905 the three countries depends on the pollutant species. For example, U.S. SO<sub>2</sub> emissions are twice as large as Canadian SO<sub>2</sub> emissions and U.S. NO<sub>x</sub> emissions are four times larger than Canadian NO<sub>x</sub> emissions, but U.S. emissions for the other five CAC species are all larger than the corresponding Canadian emissions by a factor of six or more. Interestingly, NO<sub>x</sub> emissions from ocean shipping are comparable to land-based Canadian and Mexican NO<sub>x</sub> emissions. Note too that this summary is based on SMOKE outputs and hence does not agree exactly with inventory totals (cf.  
910 Table 1 of Moran et al., 2025). One source of these differences is that the model domain does not contain all inventory emissions. This is especially true for Mexico, for which only 340 of Mexico’s 2,457 counties are completely or partially included in the model domain, but also applies to the U.S., for which 105 counties, including the state of



Hawaii, and overseas territories such as Puerto Rico, the U.S. Virgin Islands, Guam, and American Samoa, are located outside of the model domain although their emissions are included in the U.S. NEI. Another source of these differences is the VOC definition: VOC in Table 9 is the sum of the emissions of the 11 model reactive VOC species (i.e., post-SMOKE) whereas VOC in Table 1 of Moran et al. (2025) corresponds to the bulk VOC emissions reported in the inventories, including unreactive species (i.e., pre-SMOKE). Third, the PM emission values in Table 9 are much lower than in the inventory totals in the other table because they have been reduced by scaling with the transportable-fraction (TF) factor to account for SGS removal processes after emission (Pace, 2005).

Figure 3 shows the spatial distribution across the RAQDPS023 domain of mean July SET4.0.0 anthropogenic emissions of four chemical species: NO, VOC, NH<sub>3</sub>, and PM<sub>2.5</sub>. These spatial distributions are quite different due to variations in the relative contributions of different emissions source types for each species. For example, the contribution of ocean-going vessels to NO and PM<sub>2.5</sub> emissions is obvious in Figs. 3a and 3d. NO emissions are also associated with urban areas, highways, power plants, and agriculture. The spatial distribution of NH<sub>3</sub> emissions, on the other hand, is dominated by the agricultural sector, including fertilizer application for field crops and animal husbandry, which includes farm-level emissions but also concentrated animal feeding operations located in rural areas.

### 3.11.2 Biomass burning emissions

Wildfires and other biomass burning (BB) sources such as prescribed burns can emit large quantities of atmospheric pollutants, including PM<sub>2.5</sub>, NO<sub>x</sub>, CO, VOC, and NH<sub>3</sub>, and sometimes occur over many days in the case of long-lived fires (e.g., Akagi et al., 2011; Urbanski, 2014). In addition to their significant local impacts, smoke from wildfires can also be transported hundreds or even thousands of kilometres downwind (e.g., Jaffe et al., 2004; Pavlovic et al., 2016; Teakles et al., 2017). About 39% of Canada and 34% of the U.S. are covered by forest (<https://data.worldbank.org/indicator/AG.LND.FRST.ZS>), so wildfires started by lightning strikes or human activity are common in both countries (e.g., <https://ciffc.ca/publications/canada-reports>; <https://www.ncei.noaa.gov/access/monitoring/monthly-report/fire/>). Wildfires occur sporadically, however, and their initiation and evolution are difficult to predict. Moreover, wildfire emissions depend on many factors, including fire location, availability and condition of fuel, and past and current weather. Thus, in order to quantify and incorporate wildfire emissions into a CTM, wildfires occurring even in remote locations must be detected in near real time and their future hourly emissions predicted by the modelling system.

In 2013 ECCC, in collaboration with the Canadian Forest Service (CFS) and with contributions from the U.S. Forest Service (USFS), began to run an experimental version of the RAQDPS named FireWork, which was identical to the operational RAQDPS except for the addition of hourly BB emissions to the usual hourly anthropogenic emissions (Pavlovic et al., 2016). The BB emissions were calculated by combining NRT satellite-derived “hotspot” locations with estimates of fuel moisture, total fuel consumption, and fraction of smoldering vs. flaming combustion at these locations. This information was provided by the CFS Canadian Wildland Fire Information System (CWFIS), with hourly BB emission estimates produced using the Fire Emission Production Simulator (FEPS), a component of the



USFS's BlueSky Modeling Framework (Lee et al., 2002; Anderson et al., 2004; Larkin et al., 2009; Pavlovic et al., 2016; Munoz-Alpizar et al., 2017). The CWFIS tracks current fire danger conditions and fire activity and characteristics across Canada and the U.S. (<https://cwfis.cfs.nrcan.gc.ca/>), while FEPS manages data concerning fuel  
950 type, pollutant emission factors, and heat release characteristics of individual BB events (<https://www.fs.usda.gov/pnw/fera/feeps/>). Note that we refer here to BB emissions rather than wildfire emissions because of the possibility that large grass fires and prescribed burns may also be detected by satellite.

FireWork was then introduced operationally by ECCC in 2016 as a nearly identical copy of the RAQDPS, that is, identical except for the inclusion of NRT satellite-derived BB emissions (Munoz-Alpizar et al., 2017). Running these  
955 two very similar forecast systems allowed wildfire plumes to be identified by their  $PM_{2.5}$  concentration (referred to as "fire- $PM_{2.5}$ "), which were calculated by "brute force" as the difference between the FireWork and RAQDPS  $PM_{2.5}$  fields. The hourly evolution of these smoke plumes could then be predicted and displayed (Pavlovic et al., 2016; [https://weather.gc.ca/firework/index\\_e.html](https://weather.gc.ca/firework/index_e.html)). FireWork then underwent a number of upgrades after 2016 (see Table A3), including the implementation of the Canadian Forest Fire Emissions Prediction System (CFFEPS). CFFEPS  
960 incorporates the code for the CWFIS while introducing a more flexible and updateable alternative to the FEPS module along with a new fire plume-rise scheme (Chen et al., 2019a,b). Section S3 describes CFFEPS version 4.1 and the calculation of NRT BB emissions by the RAQDPS-FW023, the formal name of FireWork v023, which was implemented operationally at the same time as the RAQDPS023 (Chen and Menelaou, 2021).

### 3.11.3 Other natural emissions

965 Two other important sources of natural emissions are vegetation (i.e., biogenic emissions) and the oceans (i.e., sea-salt emissions). Both of these sources of emissions were represented in the RAQDPS023 by emissions models as described below. Note, however, that some other sources of natural emissions, including lightning emissions, volcanic emissions, pollen and other biological emissions, and aeolian dust emissions, were not considered by the RAQDPS023.

Vegetation naturally releases numerous VOCs to the atmosphere as a byproduct of photosynthesis and other plant  
970 physiological processes (e.g., Fehsenfeld et al., 1992; Monson et al., 1995; Fuentes et al., 2000; Guenther et al., 2000). Many of these compounds, such as isoprene, monoterpenes, sesquiterpenes, and aldehydes and other oxygenated VOCs, are reactive and thus can influence atmospheric chemistry (e.g., Guenther et al., 2000; Duhl et al., 2008). Moreover, globally and in many regions, including eastern North America, these biogenic VOC emissions are larger in magnitude in total than anthropogenic VOC emissions (Roselle et al., 1991; Guenther et al., 1995, 2000; Pierce et al., 1998). Emissions of NO from microbial processes in certain soil types is a second type of biogenic emission  
975 (Williams et al., 1992a,b; Yienger and Levy II, 1995; Stohl et al., 1996; Guenther et al., 2000). Soil NO emissions tend to occur in rural regions, where other anthropogenic sources of NO are small, and especially in agricultural areas where nitrogen fertilizer is applied since soil nitrogen availability is a controlling factor (Sha et al., 2021).

To calculate biogenic emissions at each chemistry time step the RAQDPS023 employed in-line code based on a  
980 modified version of the Biogenic Emission Inventory System (BEIS) version 3.09, which was developed by the U.S.



EPA (Vukovich and Pierce, 2002), together with a modified version of the Biogenic Emissions Landuse Database version 3 (BELD3), a North American vegetation database (Pierce et al., 2000; Zhang et al., 2018), and meteorological fields predicted by GEM. BEIS v3.09 calculates the emissions of four chemical species or groups of species – isoprene; monoterpenes; “other VOCs” (OVOC); and soil NO – using formulas from Geron et al. (1994). To save computer  
985 time, gridded summer and winter standard emissions fluxes (unit:  $\text{g s}^{-1} \text{grid cell}^{-1}$ ) were pre-calculated for standard mid-day meteorological conditions (ambient temperature of  $30^\circ\text{C}$ , photosynthetic active radiation (PAR) photon flux density of  $1000 \mu\text{mol m}^{-2} \text{s}^{-1}$ ) by summing vegetation-species-specific emission fluxes weighted by the vegetation-species fraction for each model grid cell (Geron et al., 1994; Guenther et al., 1994; Pierce et al., 1998). Winter emission  
990 fluxes for deciduous species were assumed to be zero. These standard biogenic emission flux fields were then treated like other time-independent geophysical fields and were input at the start of a RAQDPS023 simulation. A season-specific standard emission flux for each grid cell was then calculated during a simulation as the weighted average of the summer and winter standard emission fluxes using one of the following pairs of weights for the five phenological seasons of Zhang et al. (2002a): 1.0/0.0, 0.66/0.34, 0.25/0.75, 0.0/1.0, and 0.5/0.5 for midsummer, autumn before  
995 harvest, autumn after harvest, winter, and spring seasons, respectively (cf. Sect. 3.9). The phenological season for each grid cell was determined based on the month and latitude (Brook et al., 1999a). GEM-predicted air temperature and solar angle fields were then used at each chemistry time step to calculate a light correction factor for isoprene and temperature correction factors for all three VOC species and soil NO. These correction factors accounted for the difference between the actual meteorological conditions and the standard meteorological conditions and were used to scale the season-specific standard biogenic emission fluxes. Lastly, emissions of the first two VOC species and soil  
1000 NO were mapped directly to three ADOM-2 model species (ISOP, ALKE, and NO) while emissions of OVOC were split equally between ALKA and ALKE.

Note that three major updates were made to the standard BEIS v3.09 system described by Vukovich and Pierce (2002). First, the v3.09 biogenic emission factors have been replaced by newer BEIS v3.13 emission factors (Schwede et al., 2005). Second, standard emission fluxes for monoterpenes and OVOC were reduced for all pine species by factors of  
1005 roughly five and two and for all spruce species by factors of roughly five and three as suggested by Stroud et al. (2010). And third, the original BELD3 vegetation database was updated over Canada to replace the three generic forest types (coniferous, deciduous, mixed) that had been specified for Canada with 30 BELD3 tree species based on the 2001 Canadian Forest Inventory (Beaudoin et al., 2014).

The generation of sea spray aerosol over the world’s oceans is an important PM source (e.g., de Leeuw et al., 2011).  
1010 These sea-salt particles have a major influence on marine cloud properties and the radiation balance over the oceans, as well as coastal areas. A number of semi-empirical schemes are available for estimating sea-salt emission fluxes, but their estimates of these emissions at the global scale can vary by nearly two orders of magnitude (Textor et al., 2006; de Leeuw et al., 2011). One reason for this large uncertainty is the need for commonality in terms of assumed RH, reporting height, and particle size range.



1015 Two schemes for sea-salt emission fluxes from the open ocean are available in MACH: the Smith et al. (1993) scheme,  
which is applicable to particles with wet diameters (RH=80%) in the 2 to 40  $\mu\text{m}$  range, and the Gong-Monahan scheme  
(Gong, 2003), which is applicable to particles with wet diameters (RH=80%) in the 0.14 to 40  $\mu\text{m}$  range. A third  
scheme for estimating sea-salt emission fluxes in the near-shore surf zone based on a single power law is also available  
in the model (de Leeuw et al., 2000, Eq. 4). This simple scheme is applicable to particles with wet diameters (RH=80%)  
1020 in the 1.6 to 20  $\mu\text{m}$  range. Note that sea-salt particles are assumed to equilibrate instantaneously with the ambient  
water vapour in all three schemes (Fitzgerald et al., 1998). As well, all three schemes are formulated in terms of 10 m  
wind speed and describe the dependence of particle number flux at 10 m height on wet particle size (RH=80%), which  
must then be used to calculate integrated dry particle mass flux estimates across each model size bin. Note that de  
Leeuw et al. (2011) suggest that sea-salt particle diameters at RH=80% are roughly double their diameters at RH=0%.  
1025 The RAQDPS023 used the latter two schemes, where the Gong-Monahan scheme was applied for any grid cell that  
includes at least some ocean while the surf zone scheme was used when the fraction of a grid cell covered by ocean  
was less than unity. For both schemes the resulting sea-salt emission flux estimates were scaled for each grid cell by  
the fraction of ocean coverage. Lastly, to calculate sea-salt emission fluxes for the two RAQDPS023 size bins, each  
bin was subdivided into 35 sub-bins in order to integrate the particle-size-dependent emission flux functions by particle  
1030 radius.

### 3.12 Meteorological modulation of fugitive PM emissions

Anthropogenic fugitive PM emissions are incidental soil dust emissions that originate from surface sources such as  
vehicles travelling on paved or unpaved roads and a number of industrial, construction, and agricultural activities like  
land-clearing, excavating, grading, demolition, tilling, and harvesting. The dominant chemical components of fugitive  
1035 PM emissions are CM and POM (e.g., Boutz et al., 2020). These emissions make up a major fraction of the  
anthropogenic primary PM emissions considered by regional AQ models. For example, in the 2020 Canadian APEI,  
fugitive dust emissions contributed 88% of total primary  $\text{PM}_{2.5}$  emissions and 94% of total primary  $\text{PM}_{10}$  emissions  
(ECCC, 2022a).

Unlike primary PM emissions from smokestacks and tailpipes (i.e., combustion processes), fugitive PM emissions can  
1040 be directly affected by meteorological conditions since soil wetness or snow cover may reduce fugitive PM emissions.  
To account for such meteorological “modulation”, hourly inventory-based fugitive PM emissions were reduced in the  
RAQDPS023 at each time step during a model simulation according to predicted meteorological conditions in a surface  
grid cell if one of the following two meteorological thresholds was exceeded:

- (i) grid-scale soil moisture (soil volumetric water content) greater than 10%; or
- 1045 (ii) grid-scale snow depth greater than 5 cm.

If either threshold was exceeded, then fugitive PM emissions from that grid cell for that time step were set to zero for  
all PM size bins and chemical components. This scheme was thus most active during rainy seasons and in winter.



Note that in order to apply this scheme, input PM surface emissions had to have been separated and saved as non-fugitive and fugitive components when they were generated (see **Sect. S2**).

1050 The choice of 10% for the grid-scale soil wetness threshold was made based on sensitivity tests for several trial values followed by comparison of predicted near-surface CM concentrations with CM values measured in one Canadian and two U.S. PM<sub>2.5</sub> speciation networks (NAPS, CSN, IMPROVE). The U.S. operational AQ forecast system, the National Air Quality Forecast Capability (NAQFC), also applies a similar reduction of fugitive dust emissions by scaling PM emission fluxes by snow-cover fraction (Lee et al., 2017).

1055 Note that this meteorological modulation scheme, which accounts for day-specific reductions of anthropogenic fugitive dust emissions by precipitation and snow cover, was independent of the land-cover-dependent TF scaling that was applied to anthropogenic fugitive dust emissions at the end of emissions processing (see **Sect. S2**). It should also be noted that natural aeolian (i.e., wind-blown) fugitive dust emissions, which were not considered by the RAQDPS023, can be important in arid or semi-arid parts of North America such as the desert southwest of the U.S. Such emissions are very episodic, however, and tend to occur in the spring and summer seasons under dry and very windy conditions (e.g., Orgill and Sehmel, 1976; Park et al., 2007; Foroutan et al., 2017; Kim et al., 2021). Nevertheless, these natural emissions may contribute over 50% of PM<sub>2.5</sub> mass in the spring season in the southwestern U.S. and 20-30% of PM<sub>2.5</sub> mass in the summer in the central and southeastern U.S. (e.g., Orgill and Sehmel, 1976; Hand et al., 2017; Tong et al., 2023), and the operational U.S. NAQFC does include an aeolian dust emissions scheme (Dong et al., 2016; Campbell et al., 2022).

### 3.13 Plume rise and vertical spread

Emissions from large smokestacks may disperse in the atmosphere quite differently from surface emissions. Such continuous pollutant plumes can rise well above the top of the emitting smokestack (plume rise) and then, depending on atmospheric vertical stability, display a number of types of dispersive behaviour, including coning, looping, fanning, 1070 lofting, and fumigating (e.g., Pasquill and Smith, 1983). Plume rise also exposes these pollutant plumes to different meteorological conditions at different elevations, including differing wind speeds and directions (referred to as vertical wind shear).

Pollutant point sources for which plume rise is modelled are often referred to as major point sources. In order to calculate plume rise, four major-point-source characteristics (known as stack parameters) are typically required: 1075 geometric stack height; geometric stack exit diameter; pollutant stack exit temperature; and pollutant stack exit flow speed (or stack volume flow rate). Major-point-source emissions were read by the RAQDPS023 from a separate file that also included stack-parameter values for each major point source (see **Sect. S2**). Information was also needed about atmospheric conditions at each stack location, including the vertical temperature profile, wind speed at the stack exit, PBL height, Monin-Obukhov length, and friction velocity. These values were all forecast by the GEM model 1080 (Table 2).



To calculate plume rise and vertical spread the RAQDPS023 employed a set of empirical formulations developed by Briggs (1984) that consider both buoyancy- and momentum-driven processes. Vertical spread represents the impact of SGS vertical diffusion associated with the mixing of the plume with its surrounding environment; it was expressed in the RAQDPS023 in terms of the vertical layers into which the emitted pollutant is injected. The implementation of the Briggs scheme in the RAQDPS023 has been described in detail by Akingunola et al. (2018). Note, though, that plume rise associated with wildfire plumes was treated differently (Sect. S3)

While the Briggs (1984) scheme provides estimates of mean injection height and plume vertical spread, one limitation of the treatment of major point source emissions by GEM-MACH (and other Eulerian CTMs) is that instantaneous horizontal and vertical mixing is assumed across the horizontal grid cell in which the point source is located and the vertical layers into which the pollutant is injected. This assumption usually has a minor impact on the far-field dispersion of the plume, but it does overestimate near-field plume diffusion and also changes plume chemistry by removing the distinction between SGS pollutant concentrations inside and outside of the plume. Note that a number of SGS plume-in-grid schemes have been proposed to address this limitation (e.g., Mathur et al., 1992; Kumar and Russell, 1996; Karamchandani et al., 2011), but the RAQDPS023 did not account for SGS plume chemistry.

## 1095 **4 Computational aspects**

### **4.1 Time integration**

For the time integration of a GDPS, RDPS, or RAQDPS simulation, time-stepping calculations start with the GEM dynamical core (Sect. S1.1). After the calculations for a dynamics time step have been completed, the GEM “physics” module (e.g., Mailhot et al., 1998; McTaggart-Cowan et al., 2019a) is then called to step through a set of parameterization schemes representing different atmospheric physical processes. Changes to GEM state variables that result from each physical process parameterization (i.e., tendencies) are treated by GEM as forcings that modify the dynamical equations using the sequential tendency-splitting technique for physics-dynamics coupling discussed by Gross et al. (2018). One exception, though, is the atmospheric radiative transfer scheme, which is computationally expensive and which, in both the RDPS 8.0.0 and RAQDPS023, was only called every fifth dynamic time step (i.e., every 1500 s).

In a GEM-MACH simulation the MACH module is called at the end of the GEM physics module. In order for the RAQDPS023 to fit within its operational forecast “window” of 30 minutes wall-clock time, however, computational cost and execution time was reduced by using a chemistry integration time step of 900 s, three times longer than its dynamics integration time step of 300 s. This was necessary because even with this simplification the computational cost of MACH chemistry for one 900 s time step was approximately four times greater than the computational cost of GEM meteorology for 900 s for three shorter 300 s time steps. When the start of an RAQDPS023 chemistry integration time step of 900 s coincided with a dynamics integration time step, the MACH chemistry module was triggered after the GEM physics module had been executed. If the time steps did not align, though, the chemistry module was not called. This difference between dynamic and chemistry time steps was possible because chemistry processes were not



1115 permitted to impact dynamics/physics fields; that is, the RAQDPS023 was run with no feedback from chemistry fields  
to dynamics/physics fields, an approach referred to as one-way coupling (e.g., Grell et al., 2005). This is an acceptable  
approximation most of the time for tropospheric chemistry (though not for stratospheric chemistry). It should be noted,  
though, that the GEM-MACH code does support two-way coupling with feedbacks from chemistry fields to  
dynamics/physics fields as an option (e.g., Gong et al., 2015; Makar et al., 2015a,b).

1120 As is common practice for CTMs, which must deal with a wide variation in time scales for different processes, process  
splitting is used in GEM-MACH to transform the coupled set of partial differential equations for tracer mass-  
conservation into a sequence of “smaller” problems where each process is described by a numerical operator (e.g.,  
McRae et al., 1982; Marchuk, 1990; Pudykiewicz et al., 1997; Oran and Boris, 2000; Dimov et al., 2008; Wan et al.,  
2013). This operator-splitting approach simplifies the numerical solution of this system of equations and allows  
1125 different specialized numerical solvers to be used for the chemistry time-step integration of different process operators.  
For example, as noted in Sects. 3.4 and 3.5, in order to integrate the gas-phase and aqueous-phase chemistry operators  
over a chemistry integration time step, each operator is treated using a specialized solver designed to handle a ‘stiff’  
set of ordinary differential equations, where much finer, variable “process-internal” time steps are employed. The  
solvers for each process are each applied once sequentially in a non-centered or non-symmetric manner, again to reduce  
1130 computational cost (Dimov et al., 2008).

The operator sequence applied for the RAQDPS023 for each chemistry time step consisted of three groups of process  
operators: (i) emissions, vertical diffusion, and dry deposition; (ii) gas-phase chemistry; and (iii) aerosol processes. In  
the first process group, hourly anthropogenic and BB emission fluxes were input hourly and allocated to each chemistry  
time step while biogenic and sea-salt emission fluxes were calculated for each chemistry time step. Also in the first  
1135 group, for each chemistry time step meteorological modulation was applied to fugitive PM emissions, plume rise was  
calculated for each point source and those elevated emissions were injected into the vertical column, dry deposition  
velocities were calculated, and then the GEM vertical diffusion scheme was applied with dry deposition fluxes used as  
bottom boundary conditions. Note that surface emission fluxes would normally be included in the specification of the  
bottom boundary fluxes, but as described at the end of Sect. 3.1, in the RAQDPS023 these emissions were instead  
1140 injected into the two lowest model layers. The second operator group consisted of the gas-chemistry chemistry operator  
alone, which was applied for each chemistry time step but integration of this operator is performed using many smaller  
time steps in order to address numerical stiffness (Sect. 3.4). The third operator group consisted of many PM-related  
operators: one sub-group consisted of the operators for particle nucleation, condensation, and intersectional mass  
transfer of sulfuric acid and SOA precursor condensate; a second (cloud processing) sub-group included particle  
1145 activation, gas-phase–aqueous-phase mass transfer and aqueous-phase chemistry, in-cloud scavenging and rainout,  
inorganic heterogeneous chemistry, and intersectional mass transfer; and the third sub-group consisted of particle  
coagulation followed by below-cloud precipitation scavenging of gases and particles by falling hydrometeors and  
hydrometeor evaporation.



In terms of computational cost, based on a number of timing tests for eight RAQDPS024 January and July hindcast cases (Moran et al., 2025) it was found that with chemistry turned off, GEM dynamics and physics each took about 45% of run time, with model initialization accounting for most of the rest. Turning chemistry on (i.e., activating MACH), however, increased total run time by a factor of 4.4 on average. Interestingly, the computational burden of the set of chemistry operators only increased total run time by 107%, even though these operators were only called every third meteorological time step. However, with chemistry activated the cost of the dynamics calculations increased by a factor of 6.0 and the cost of the physics calculations, which include chemistry, increased by a factor of 3.4. The large increase in the cost of dynamics was due to the large increase in the cost of advection due to the 58 extra chemical tracers that had to be advected every meteorological time step (Sects. 3.2, 3.4). Lastly, looking at the relative cost of the different chemistry operators we find that gas-phase chemistry operator took about 23% of the time and PM-related operators used about 73% of the time, with the calculation of plume rise, biogenic emissions, gas-phase dry deposition, and vertical diffusion accounting for the rest.

#### 4.2 Initial conditions and boundary conditions

The RAQDPS023 followed the same initialization procedure used to provide meteorological initial conditions (ICs) for the RDPS 8.0.0, including the use of the same meteorological analysis files. Both systems employed a continuous data assimilation cycle and a four-dimensional incremental analysis update (4D-IAU) approach (Bloom et al., 1996; Buehner et al., 2015; Lei and Whitaker, 2016; CMC-RDPS-8.0.0, 2021a; Lu and Wang, 2021; Ritchie et al., 2022). In this approach, hourly analysis increments were applied from T-3 to T+3 hours, where T=0 was the run start time, in order to maximize the dynamical balance between the mass and momentum fields through the application of relatively small but continuous forcing. The use of this scheme also allowed “recycling” of a number of unobserved model physics fields at T-3 hours that were obtained from the previous operational RDPS 8.0.0 run, namely turbulence kinetic energy (TKE), turbulence regime, mixing length, friction velocity, PBL height, total condensate (combined liquid and ice) and cloud fraction from the Sundqvist scheme (Sect. S1.6), PBL cloud water and cloud fraction, and the flux enhancement factor from the MoisTKE scheme (Buehner et al., 2015; CMC-RDPS-6.0.0, 2018; CMC-RDPS-8.0.0, 2021b). Recycling these selected forecast physics fields reduced the spin-up time required for these fields to reach equilibrium in the new simulation. For example, cloud-related fields normally require a number of hours to reach equilibrium if initialized to zero, and the PBL-parameterization-related fields also contain information about PBL history that cannot be reconstructed diagnostically (Buehner et al., 2015).

Dynamical downscaling with one-way nesting was used to specify the meteorological LBCs (e.g., Fillion et al., 2010; Ritchie et al., 2022). Piloting files of hourly meteorological LBCs were provided from a RDPS 8.0.0 forecast to the RAQDPS023 forecast for the same start time, where the RAQDPS023 forecast followed the RDPS 8.0.0 forecast in wall-clock time, and the RAQDPS023 grid was a co-located subset of the RDPS 8.0.0 grid (Sect. 2.1). Hourly RDPS 8.0.0 forecast fields from the piloting files were then linearly interpolated in time to each 300 s GEM-MACH dynamics time step. The RAQDPS023 horizontal grid consisted of a large, interior “free” zone and a narrow (eight-grid-cell-wide) outer “blending” zone. A 12-grid-cell piloting zone also surrounded the RAQDPS023 free zone, so that it



covered the blending zone but also extended another four grid cells outside of the RAQDPS023 grid domain. Following  
1185 the approach of Thomas et al. (1998), open or inflow/outflow meteorological LBCs were applied at the RAQDPS023  
horizontal grid boundary while a Davies-type boundary relaxation scheme (Davies, 1976) was applied across the  
blending zone after each dynamics time step to relax RAQDPS023 near-boundary values towards RDPS 8.0.0 piloting  
values using a cosine<sup>2</sup> cross-zone weighting function (see also Benoit et al., 1997). By smoothly blending RDPS 8.0.0  
1190 piloting values with interior values along the edges of the RAQDPS023 grid, the blending zone transmitted information  
about upstream atmospheric conditions external to the RAQDPS023 domain while also acting as a horizontal “sponge”  
zone to dampen spurious wave reflections from the lateral boundaries.

The meteorological upper boundary conditions, on the other hand, assumed a material surface with zero cross-boundary  
flow specified as a “truncated closed-top” boundary condition (Girard et al., 2014). Enhanced horizontal diffusion was  
also imposed at the top six model levels to reduce spurious wave reflections from the upper boundary by acting as a  
1195 damping vertical “sponge layer” (CMC-RDPS-8.0.0, 2021b).

Chemical tracer ICs and LBCs are also required. The RAQDPS023 did not employ chemical data assimilation (CDA).  
It was instead run in a “perpetual forecast” mode, in which chemical IC fields for the start time of interest are copied  
from forecast chemical fields corresponding to that same time from the previous RAQDPS023 forecast launched 12  
hours earlier. Chemical LBCs (CLBCs), on the other hand, were specified using “climatological” seasonal vertical  
1200 cross-sections of model species MMRs for each lateral boundary. These predetermined seasonal CLBCs were derived  
from a 2009 annual simulation of MOZART-4 (Model for OZone and Related chemical Tracers version 4), a global  
CTM that contains a detailed treatment of tropospheric inorganic chemistry and of some organic species (Emmons et  
al., 2010). The 2009 simulation was run on a 128 x 64 horizontal grid (approximately 2.8° × 2.8°) with 28 vertical  
levels reaching to 2 hPa. MOZART-4 does not have a complete stratospheric chemistry mechanism, so O<sub>3</sub>, NO<sub>x</sub>, and  
1205 CO mixing ratios were constrained to climatological values from 50 hPa to 2 hPa, and by relaxing to the climatology  
with a time scale of 10 days from 50 hPa to the tropopause. An annual set of six-hourly chemistry outputs from  
MOZART-4 was mapped to GEM-MACH model species, divided and averaged over each season, and horizontally  
and vertically interpolated to the RAQDPS023 grid to obtain four sets of seasonal CLBCs (Pendlebury et al., 2018).  
While this approach for providing CLBCs was an improvement over schemes used in earlier versions of the RAQDPS,  
1210 where constant values or static vertical profiles were used at the lateral boundaries, it was still computationally simple  
and efficient.

### 4.3 Tracer advection, shape preservation, and mass conservation

RAQDPS023 prognostic chemical tracers such as O<sub>3</sub>, NH<sub>3</sub>, and PM<sub>2.5</sub>-EC were treated by the GEM dynamical core in  
the same way as the two RDPS 8.0.0 and RAQDPS023 prognostic meteorological tracers (water vapour, cloud water)  
1215 described in Sect. S1.1. The GEM semi-Lagrangian advection scheme was thus also used to advect 58 GEM-MACH  
chemical tracers: 42 gas-phase tracers (Table 3) and 16 (= 2 x 8) PM size bin–chemical component tracers (Sect. 3.2),  
where the same two-step ILMC monotonicity correction used by GEM for meteorological tracers to impose shape



1220 preservation and avoid the creation of artificial local minima or maxima by the advection scheme (cf. Sect. S1.1) was also used for the chemical tracers. In addition, the Bermejo and Conde (2002) global mass fixer with LAM boundary-flux estimation (Diamantakis and Flemming, 2014; Aranami et al., 2015) that was applied to the meteorological tracers in the RDPS 8.0.0 and RAQDPS023 to impose mass conservation (Sect. S1.1) was also applied in the RAQDPS023 to the chemical tracers (de Grandpré et al., 2016).

1225 One concern with global mass adjustments made to tracer species fields to conserve mass is that they have the potential to introduce artificial numerical diffusion by being imposed at locations far from locations where mass-conservation violations occurred. Diamantakis and Flemming (2014) found, however, that global mass tracer conservation schemes could improve forecast accuracy, and de Grandpré et al. (2016) recommended the use of the ILMC scheme for shape preservation in part due to its good mass-conservation properties, which then result in smaller mass adjustments for mass conservation. Note that one additional complication with the advection of a suite of chemical tracers is that they are often chemically coupled, so that the imposition of shape preservation and mass conservation on individual 1230 chemical species as was done in the RAQDPS023 may result in the generation of chemical imbalances (e.g., Lauritzen and Thuburn, 2012; Diamantakis, 2013), which then require equilibration by the gas-phase chemistry operator (Sect. 3.4).

#### 4.4 Computer hardware and code parallelization

1235 When the RAQDPS023 was implemented operationally in late 2021, it was run on the ECCC high-performance computing (HPC) system then available. The heart of this system consisted of two Cray XC50 massively parallel supercomputers, each with 1,330 shared-memory compute nodes and 53,200 compute cores, where each compute node had 192 GB of random-access memory. Having two identical computers available for operational use provides redundancy and allows hardware maintenance, software upgrades, and various system diagnostics and tests to be performed on one computer while operational forecasts continue to be run on the other computer. As well the two 1240 supercomputers were located in separate halls to reduce physical risk. In June 2022 the two Cray supercomputers were replaced by two new IBM ThinkSystem SD650v2 direct-water-cooling supercomputers. Each of these new machines has 1,496 shared-memory compute nodes and 119,680 compute cores, where each compute node has 512 GB of random-access memory. The RAQDPS023 was migrated without any algorithmic upgrades to this new HPC system and was re-named RAQDPS024 in June 2022 (see Table A3).

1245 The GEM and GEM-MACH Fortran2003 codes support both the Message Passing Interface (MPI) and Open MultiProcessing (OpenMP) parallelization paradigms. This allows the RAQDPS023 to employ hybrid parallelization, that is, distributed-memory and shared-memory parallel programming techniques, respectively, to take advantage of the large number of available compute nodes and cores. Domain decomposition has been used to implement MPI parallelization, where the RAQDPS023 horizontal grid was divided into 30 subgrids or “tiles” in the x-direction 1250 (longitude) and 36 tiles in the y-direction (latitude) for a total of 1,080 tiles. Integration was then performed simultaneously on these tiles on 1,080 compute nodes, where for each tile, calculations were carried out sequentially



across each tile or subgrid from south to north on a set of XZ vertical “slices”. Two OpenMP threads were used to speed up the integration.

#### 4.5 Forecast run strategy

1255 The RAQDPS023 was run two times per day for 72-hour simulations starting (nominally) at 00 UTC and 12 UTC. These runs, which had to follow the 00 UTC and 12 UTC RDPS 8.0.0 (and GDPS 8.0.0) runs that were needed to provide piloting fields (Fig. 1), started at 03 UTC and 15 UTC wall-clock time. Each RAQDPS023 run, including pre- and post-processing tasks, took approximately 90 minutes of wall-clock time, including approximately 30 minutes for the 75-hour GEM-MACH simulation; the extra three hours included the  $T = -3$  hour start for the 4D-IAU initialization  
1260 procedure (Sect. 4.2). Forecast results were available for the 00 UTC and 12 UTC runs at approximately 04:30 UTC and 16:30 UTC, respectively, or close to local midnight and local noon in both Atlantic Standard Time and Eastern Standard Time. The independent runs of the RAQDPS-FW023 launched and finished at similar times, with the one extra complication that RDPS 8.0.0 72-hour forecasts were also needed by CFFEPS v4.1 (which must be run before the RAQDPS-FW023) for estimating BB emissions for the next 72 hours (see Sect. S3). Note that the start times and  
1265 run times for the RAQDPS024 and RAQDPS-FW024 systems were very similar to those for the RAQDPS023 and RAQDPS-FW023.

## 5 Outputs, post-processing, downstream systems, and performance evaluation

### 5.1 Outputs

Routine RAQDPS023 (and RAQDPS-FW023) hourly outputs included a large number of surface chemical fields, among them 41 gas-phase species MMR fields (first 41 species in Table 3), eight  $PM_{2.5}$  and eight  $PM_{cf}$  chemical  
1270 component MMR fields,  $PM_{2.5}$  and  $PM_{10}$  total mass concentration fields, 21 dry deposition flux fields ( $SO_2$ ,  $H_2SO_4$ , NO,  $NO_2$ ,  $O_3$ ,  $HNO_3$ , HONO, PAN,  $RNO_3$ ,  $NH_3$ ,  $H_2O_2$ , HCHO,  $NO_y$ , SU, NI, AM, CM, EC, POM, SOM, SS, where  $SU = SU_1 + SU_2$ , etc.), 12 wet deposition flux fields ( $HSO_3^-$ ,  $SO_4^{=}$ ,  $NO_3^-$ , EC, POM, SOM, CM, SS,  $NH_4^+$ ,  $H_2O_2$ , ROOH,  $H_2O$ ), and four biogenic emission flux fields (ISOP, ALKA, ALKE, NO). RAQDPS023 forecasts of  $NO_2$ ,  $O_3$ , and  
1275  $PM_{2.5}$  surface fields in particular were used as guidance by operational AQ forecasters at ECCC and elsewhere, were provided as inputs to several post-processing systems, and were made available to the public through ECCC’s public weather website (see [http://www.weather.gc.ca/aqfm/index\\_e.html](http://www.weather.gc.ca/aqfm/index_e.html)). It should be noted that the  $PM_{2.5}$  and  $PM_{10}$  total mass values were calculated as the sum of seven chemical components (SU, NI, AM, EC, POM, SOM, CM); they thus correspond to dry  $PM_{2.5}$  and dry  $PM_{10}$  total mass (i.e., without aerosol water) without a contribution from sea salt, thus  
1280 emphasizing values over land and without a dependence on RH.

For public outreach on the weather website, ECCC also provides forecasts of the AQHI as a key product to communicate the total health risk of a mixture of air pollutants and also to disseminate warnings during forecasted periods of poor air quality ([https://weather.gc.ca/mainmenu/airquality\\_menu\\_e.html](https://weather.gc.ca/mainmenu/airquality_menu_e.html)). The AQHI is a multi-pollutant, additive, no-threshold, health-based, hourly AQ index with a range (in whole numbers) from 0 to 10+. It was developed



1285 from daily time-series analysis of air pollutant concentrations and mortality data and is calculated as a weighted sum  
of NO<sub>2</sub>, O<sub>3</sub>, and PM<sub>2.5</sub> surface concentrations (Stieb et al., 2008; Trieu et al., 2020). Two interpretative health messages  
are provided with a 72 hour AQHI forecast, one for the general population and one for at-risk groups, including  
children, the elderly, and individuals with heart or breathing problems. While O<sub>3</sub> and PM<sub>2.5</sub> are known to have direct  
health effects (e.g., Murray et al., 2020), NO<sub>2</sub> is included in the index largely as a proxy for other, non-measured  
1290 pollutants with health impacts that are emitted by combustion processes (Stieb et al., 2008). It is worth noting that  
AQHI advisories and warnings in Canada in the warm season are increasingly being driven by elevated PM<sub>2.5</sub> levels  
associated with wildfire smoke forecasts.

## 5.2 Post-processing tasks and downstream systems

Figure 1 also shows the data flow between the RAQDPS023 and two operational downstream post-processing systems,  
1295 the Updateable Model Output Statistics for Air Quality (UMOS–AQ) system and version 2.0.0 of the Regional  
Deterministic Air Quality Analysis (RDAQA) system. UMOs–AQ is a statistical AQ post-processing package for bias  
correction that can compensate for systematic model errors, account for unresolved SGS phenomena, and be updated  
frequently. An operational UMOs post-processing package for meteorology has been used by EC since 1995 to  
forecast meteorological predictands such as surface temperature and probability of precipitation (Wilson and Vallée,  
1300 2002, 2003). UMOs–AQ uses the UMOs framework to combine multiple sources of AQ-related information: AQ  
forecasts; current AQ measurements; meteorological forecasts; and physical variables (e.g., solar flux, sine of scaled  
Julian day). AQ forecasts made by the RAQDPS023 provided the operational UMOs–AQ package with point-specific  
hourly surface forecasts of NO<sub>2</sub>, O<sub>3</sub>, and PM<sub>2.5</sub> concentrations at Canadian AQ measurement station locations . The  
UMOs–AQ package itself consists of a large set of multi-variate linear regression (MLR) equations, where one MLR  
1305 equation is generated per Canadian AQ station per pollutant per season per forecast hour per 00/12 UTC run  
(Antonopoulos et al., 2011; Moran et al., 2014). These equations are regenerated every week using the most recent  
four months of model AQ forecasts and station measurements, which permits ongoing adjustments to account for  
changes in model forecast skill due to many causes, such as forecast system upgrades, systematic seasonal variations,  
and unexpected emissions changes such as accompanied the COVID-19 pandemic in 2020 (e.g., Griffin et al., 2020;  
1310 Mashayekhi et al., 2021). UMOs–AQ-derived values of NO<sub>2</sub>, O<sub>3</sub>, and PM<sub>2.5</sub> are used to calculate the location-specific  
AQHI forecast values that are disseminated to the Canadian public (see  
[https://weather.gc.ca/mainmenu/airquality\\_menu\\_e.html](https://weather.gc.ca/mainmenu/airquality_menu_e.html)).

A second operational AQ post-processing system, the RDAQA system, provides objective analyses (OA) of hourly  
North American surface concentration fields for O<sub>3</sub>, NO<sub>2</sub>, NO, PM<sub>2.5</sub>, PM<sub>10</sub>, SO<sub>2</sub>, and the AQHI (Robichaud and  
1315 Ménard, 2014; Robichaud et al., 2016; Robichaud, 2017; Ménard, 2021). These surface OA fields are produced by  
combining recent hourly AQ surface measurements at station locations with hourly gridded model surface forecast  
fields in a kind of measurement–model fusion (e.g., Fu et al., 2022). AQ measurements are in general accurate and  
unbiased, but they have limited spatial coverage and may not always be spatially representative, especially in locations  
with complex topography or heterogeneous land cover. Model forecast fields, on the other hand, may have inaccuracies



1320 and biases, but they also provide complete spatial coverage and areal representativeness and should account for the  
meteorology, physics, and chemistry of air pollution. An objective analysis that is an optimal combination (known as  
optimal interpolation or OI) of both of these information sources will lead to a significant improvement of the coverage  
and accuracy of analyzed air pollution spatial patterns (Robichaud et al., 2016). Hourly analyses are prepared because  
many pollutants, including O<sub>3</sub> and NO<sub>2</sub>, have marked diurnal variations and also respond to synoptic meteorological  
1325 variations.

A new version of the RDAQA post-processing system, version 2.0.0, was introduced operationally at ECCC in  
December 2021 at the same time as the RAQDPS023 (Ménard, 2021). RDAQA 2.0.0 employed a new formulation of  
the error covariances with a slightly modified analysis solver. The error covariances were derived from ensembles of  
RAQDPS023 model simulations for each hour of the day and captured non-homogeneous, non-isotropic error  
1330 correlations related to terrain-dependent features such as mountains, valleys, water surfaces, and emissions (Ménard et  
al., 2020; Ménard, 2021). These simulation ensembles were “climatological” and were composed of about 60  
RAQDPS023 forecast runs from a previous two-month development period. It was assumed that error correlations for  
these ensembles would be sufficient to capture stationary and terrain-dependent structures associated with terrain  
features and surface emissions sources. RAQDPS023 hourly gridded forecast fields were used by the RDAQA 2.0.0  
1335 as first-guess fields. The resulting linear combinations of hourly AQ measurements and RAQDPS023 forecasts  
minimized the analysis (or combination) error variance. Figure 4 shows an example of hourly output fields from the  
RDAQA 2.0.0 for PM<sub>2.5</sub> at 16 UTC as a four-panel analysis.

The availability of hourly deposition flux forecast fields from the RAQDPS023 also allowed seasonal and annual dry  
and wet deposition fields to be accumulated on an ongoing basis. These fields could then be used to examine deposition  
1340 trends and ecosystem impacts (e.g., Vet and Ro, 2008; Makar et al., 2018a, 2025). These gridded multi-month  
deposition fields can also be used by the ECCC ADAGIO (Atmospheric Deposition Analysis Generated by optimal  
Interpolation from Observations) tool, which is being developed to produce OAs of dry, wet, and total deposition of  
acidifying pollutants over North America (Robichaud et al., 2020) in parallel to some similar U.S. efforts (Schwede et  
al., 2019; Fu et al., 2022).

1345 Wildfire smoke plume forecasts were also generated as a post-processing step. As described in Sect. 3.11.2 the  
RAQDPS023 served as the base platform for the ECCC RAQDPS-FW023 (“FireWork”) wildfire forecast system,  
which augmented the air pollutant emissions considered by the RAQDPS023 with NRT emissions from wildfires and  
other large BB events (Pavlovic et al., 2016; Munoz-Alpizar et al., 2017; Chen et al., 2019a; Chen and Menelaou,  
2021). Both RAQDPS023 versions were run twice daily at 00 and 12 UTC for 72-hour periods. Hourly forecasts of  
1350 the transport and evolution of wildfire smoke plumes were then calculated as the difference between the RAQDPS-  
FW023 and RAQDPS023 PM<sub>2.5</sub> forecast fields. Four post-processing products for wildfire smoke plumes were  
prepared and posted to an ECCC public website ([https://weather.gc.ca/firework/index\\_e.html](https://weather.gc.ca/firework/index_e.html)): (i) 72-hour animations  
of hourly ground-level smoke concentration fields ( $\mu\text{g m}^{-3}$ ); (ii) 72-hour animations of hourly, vertically-integrated  
total column smoke fields ( $\text{kg m}^{-2}$ ); (iii) 24 hour mean ground-level smoke concentration fields for Days 1, 2, and 3;



1355 and (iv) 24-hour maximum ground-level smoke concentration fields for Days 1, 2, and 3. Figure 5 shows examples of  
two of these products. RAQDPS-FW023 forecasts were also made available on the WMO North American Regional  
Vegetation Fire and Smoke Pollution Warning and Advisory Centre (RVFSP-WAC) website, which is operated by  
ECCC (<https://hpfx.collab.science.gc.ca/~svfs000/na-vfsp-was/public/dist/home/introduction>).

### 5.3 Performance evaluation

1360 The operational performance of the RAQDPS023 was routinely monitored and reported internally (e.g., Moran et al.,  
2021a), but only the small number of pollutants whose NRT measurements were routinely available from surface  
networks could be considered. These pollutants include the three AQHI component pollutants, NO<sub>2</sub>, O<sub>3</sub>, and PM<sub>2.5</sub>  
total mass, plus NO, SO<sub>2</sub>, and PM<sub>10</sub> total mass. These same six pollutants were considered by the RDAQA 2.0.0 system  
described above. Note that performance evaluation statistics are usually based on point measurements, but analysis  
1365 increments from the RDAQA 2.0.0 can be viewed as regional errors (e.g., Fig. 4). The companion paper by Moran et  
al. (2025) has examined RAQDPS023 performance for five years: the first year of RAQDPS023 operational forecasts  
and four years of retrospective annual simulations for the 2013-2016 period. For the 2021/22 forecasts of NO<sub>2</sub>, O<sub>3</sub>,  
and PM<sub>2.5</sub> total mass made by the RAQDPS023, the seasonal and annual evaluation scores for O<sub>3</sub> hourly forecasts were  
generally the highest, followed by NO<sub>2</sub> scores and then PM<sub>2.5</sub> scores. Another important finding was that predicted  
1370 monthly mean PM<sub>2.5</sub> total mass was biased low in all months in 2021/22.

Other pollutants are also monitored, but these measurements are only available after a lag of months or even years to  
allow time for laboratory analysis and quality assurance/quality control (QA/QC) measures and hence can only be used  
for retrospective performance evaluations. The companion paper by Moran et al. (2025) also examined RAQDPS023  
performance using this larger suite of species measurements, including other gas-phase species, PM<sub>2.5</sub> chemical  
1375 components, and concentrations in precipitation, for the 2013-2016 retrospective simulations, which used year-specific  
anthropogenic emissions in place of the SET4.0.0 emissions set. Access to the much more comprehensive  
measurement data set provided additional insights into model performance. One insight was that one PM<sub>2.5</sub> chemical  
component (SU) was consistently underpredicted for the four years while two others (EC, SS) were consistently  
overpredicted. O<sub>3</sub> predictions in the spring were also biased low while isoprene predictions were biased high. These  
1380 findings all suggest possible directions for model improvement. For more details see Moran et al. (2025).

ECCC has also been working with other agencies since 2017 to exchange, evaluate, and compare operational AQ  
forecasts for North America. ECCC has built an automated verification system to receive, ingest and compare these  
daily forecasts against surface measurements (Pavlovic et al., 2018; Moran et al., 2020b). Three regional AQ forecast  
models and three global AQ forecast models from five agencies are currently participating in this initiative. A  
1385 performance evaluation report containing North American monthly evaluation statistics for these six models is  
produced every quarter by ECCC and is then made available through the WMO Global Air Quality Forecasting and  
Information System (GAFIS) initiative website (<https://community.wmo.int/en/activity-areas/gaw/science-for->



[services/gafis](#)) on webpage <https://hpfx.collab.science.gc.ca/~svfs000/na-aq-mm-fe/dist/>. This effort is discussed in more detail in Moran et al. (2025).

## 1390 **6 Further development and future work**

The previous sections have described the RAQDPS023 and RAQDPS-FW023 operational AQ forecast systems that became operational on 1 Dec. 2021 (Table A3). Moran et al. (2025), the companion paper to this paper, documents both strengths and weaknesses of these two systems, including some model weaknesses that future system versions might address. During the preparation of these two papers, however, a major new version of the RAQDPS, 1395 RAQDPS025, which does at least partially address some of these weaknesses, including PM<sub>2.5</sub> total mass underpredictions, was implemented operationally on 11 June 2024 (Table A3). This section briefly summarizes the main updates and innovations introduced in the RAQDPS025 and then outlines some possible improvements for future system versions.

### **6.1 RAQDPS025 updates and innovations**

1400 The RAQPS025 system is documented in CMC-RAQPS025 (2024). As described below it includes two innovations related to meteorology, eight innovations related to chemistry, and one innovation related to input emissions. So-called “unit” tests were performed during the development of this new version to quantify the impact of each innovation, similar to the approach described by Foley et al. (2010). Five of these innovations were judged to have a “high” impact, five were judged to have a “medium” impact, and one was judged to have a “low” impact (CMC-RAQPS025, 2024).

1405 The key acceptance criterion for the adoption of a new operational forecast system at ECCC is that it should improve, or at least not degrade, overall system performance regardless of whether the proposed system is believed to deliver improvements to science representations or numerical schemes or system architecture. An ECCC internal management committee is responsible for approving parallel and operational implementations of new forecast system versions. If preliminary approval is given by the committee based on evaluation results from several retrospective evaluation 1410 periods, the new forecast system is run side-by-side (i.e., in parallel) with the existing forecast system for a minimum of two months before results of evaluations for the parallel period are presented to the committee and final approval for implementation is either given or withheld. The RAQDPS025 was run in parallel with the RAQDPS024 from 13 February to 10 June 2024.

#### **6.1.1 Updates to GEM and GEM-MACH computer codes**

1415 The RAQDPS023 was based on the GEM 5.1.0 and GEM-MACH v3.1.0.0 computer codes, and the RAQDPS024 was based on the GEM 5.1.2 and GEM-MACH v3.1.1.2 computer codes. The RAQDPS025 is based on the GEM 5.2.1 and GEM-MACH v3.2.1.1 computer codes (Table A3). Many of the following innovations were introduced with GEM-MACH v3.2.1.1.



### 6.1.2 Updates to meteorological piloting model

1420 One ongoing challenge for operational forecasting at the Canadian Meteorological Centre (CMC) is providing the  
computer and human resources required (i) to maintain the large number of complex weather and environmental  
forecast systems that are being run operationally and (ii) to implement a suite of system updates at regular intervals  
while addressing the complicated interdependencies of these systems. As noted in Sect. 2 the regional 10 km  
RAQDPS023 was dependent on both the global 15 km GDPS 8.0.0 and the regional 10 km RDPS 8.0.0. In June 2024  
1425 a new version of the GDPS, GDPS 9.0.0, with horizontal grid spacing reduced to 10 km was implemented  
operationally, and at the same time the RDPS 8.0.0 was retired as an independent forecast system without a replacement  
(CMC-RDPS-9.0.0, 2024). As a consequence it was necessary to replace the RDPS 8.0.0 as the meteorological piloting  
model for the RAQDPS025 with the GDPS 9.0.0, but there was no loss of horizontal resolution. In principle this  
change also has the added benefit of allowing access to the GDPS 9.0.0 ozone field, which is updated by satellite data  
1430 assimilation.

### 6.1.3 Merger of RAQDPS and RAQDPS-FW forecast systems

In order to identify and track BB smoke plumes by means of the “brute-force” method (Sect. 3.11.2) the ECCC AQ  
forecast system architecture required the same modelling system to be run twice at each forecast time, once with BB  
emissions (RAQDPS-FW023) and once without BB emissions (RAQDPS023). However, other approaches to track  
1435 BB smoke plumes with only a single run are possible. One dynamic approach is “tagging”, in which BB emissions are  
tracked separately during a model simulation as “tagged” species (e.g., Wagstrom et al., 2008; Wang et al., 2009;  
Samaali et al., 2011; Grewe, 2013). Another approach is to include BB emissions but identify the presence of BB  
smoke at the post-processing stage by using known chemical characteristics of BB smoke, including both speciated  
PM components and gas-phase species (e.g., Akagi et al., 2011; Urbanski, 2014; Andreae, 2019; Hayden et al., 2022),  
1440 to identify the locations of ambient concentrations of multiple species predicted by the model that match those chemical  
characteristics of BB smoke. Either approach would allow the existing system architecture to be streamlined by  
removing the need for two simulations with two versions of the same forecast system. However, two issues that must  
be considered are the different “signatures” of BB emissions associated with different ecosystems and the formation  
of secondary air pollutants such as O<sub>3</sub> and SOA in BB smoke plumes in addition to the primary pollutants emitted by  
1445 BB.

The second approach was adopted in the RAQDPS025 to track BB smoke plumes in a single RAQDPS025 simulation,  
where the ranges of two ratios of three primary PM<sub>2.5</sub> components (EC, POM, CM) were used together to identify BB-  
dominated smoke plumes (CMC-RAQPS025, 2024). The lower and upper thresholds of these two ratios that identify  
a BB-dominated PM<sub>2.5</sub> concentration were determined from an analysis of chemical speciation profiles of PM  
1450 emissions associated with different types of wood combustion, including wildfires. This tracer-ratio approach does  
represent a change in strategy since the previous brute-force approach yielded PM<sub>2.5</sub> concentration values due only to  
the contribution of BB emissions (i.e., fire-PM<sub>2.5</sub>) whereas the PM<sub>2.5</sub> concentration values produced by the new  
approach also include the contributions of emissions from other emission source types. This loss of source



differentiation will be less of an issue, however, when BB emissions are the dominant  $PM_{2.5}$  source. Note that in  
1455 contrast to the RAQDPS023 and RAQDPS-FW023, the RAQDPS025 is referred to at ECCC as a unified AQ forecast  
system.

#### 6.1.4 Updates to representation of vertical diffusion in the stable planetary boundary layer

The design philosophy for the development of the RAQDPS has been to employ GEM parameterizations without  
modification whenever possible. As noted in Sect. 3.1, however, the RAQDPS023 treated the vertical diffusion of  
1460 chemical tracers in stable PBLs slightly differently than the vertical diffusion of meteorological tracers. GEM did  
impose two limiting values related to its turbulence parameterizations: a minimum Obukhov length (Sect. S1.3) and a  
maximum eddy dissipation length scale (Sect. S1.4). Many CTMs, on the other hand, also specify a minimum threshold  
value for the vertical eddy diffusivity of pollutant tracers ( $K_z$ ) to avoid overpredictions of surface concentrations under  
stable conditions (e.g., McNider and Pour-Biazar, 2020), and a number of studies have examined CTM forecast  
1465 sensitivity to the choice of this minimum value (e.g., Pleim, 2007; Jin et al., 2010; Makar et al., 2014; Li and  
Rappenglueck, 2018; Jia and Zhang, 2021; Jiang et al., 2024). The RAQDPS023 employed a minimum  $K_z$  value of  
 $0.1 \text{ m}^2\text{-s}^{-1}$ . Another CTM, the CMAQ (Community Multiscale Air Quality) model extends this approach by  
considering land-surface-type-dependent minimum vertical eddy diffusivity values, which are specified to be  
higher over urban areas (Li and Rappenglueck, 2018). This approach is appealing since urban areas have large  
1470 surface roughness values and are typically also areas of high surface emissions in which surface concentrations  
are very sensitive to the exact balance between near-ground turbulent vertical mixing and surface emissions  
(Makar et al., 2014; Li and Rappenglueck, 2018). However, the specification of the allowable range of minimum  
eddy diffusivity values in the CMAQ scheme is still arbitrary.

Makar et al. (2021) tested a novel vertical diffusion parameterization in which the near-surface vertical diffusion  
1475 of on-road vehicle emissions is modulated by vehicle-induced turbulence (VIT), which is calculated from traffic  
density and vehicle speeds. Like the CMAQ scheme this VIT scheme can increase vertical mixing in urban areas  
for stable conditions, but it also offers a physical basis for this increase and it will affect non-urban areas with  
high levels of traffic as well (e.g., rural highways). The VIT scheme has been implemented in the RAQDPS025.  
As might be expected it has a greater impact in the winter months when stable conditions are more common. A  
1480 co-benefit of adding this new scheme was the elimination of the arbitrary lower limit on PBL height of 100 m and  
the imposed injection of area emissions into the two lowest model layers instead of the first layer alone that was  
used in the RAQDPS023 (Sect. 3.1).

#### 6.1.5 Updates to chemical lateral boundary conditions

CLBCs are important for regional AQ models and may even be controlling for those species whose lifetimes are greater  
1485 than a few days, which is often the time needed for an air parcel to traverse a regional model domain (e.g., Brost, 1988).  
Among these longer-lived species are (i) tropospheric  $O_3$ , which has a lifetime of a week to several months and a



globally averaged tropospheric lifetime of 22-23 days (e.g., Archibald et al., 2020), (ii)  $PM_{2.5}$ , which has a tropospheric lifetime on the order of days to a week (e.g., Heintzenberg, 1989; Pandis et al., 1995), and (iii) CO, whose lifetime is 30-90 days (e.g., Seinfeld and Pandis, 2016). The western, northern, and eastern lateral boundaries of the RAQDPS023 continental domain are located in low-emissions regions over the Pacific Ocean, Arctic Ocean, and Atlantic Ocean, respectively, while a portion of the southern boundary is located over Mexico roughly 2500 km from the Canada-U.S. border (Fig. 2). This combination of low emissions and distance will help to reduce the contribution of CLBCs to elevated pollutant levels over Canada. On the other hand,  $O_3$  and CO have high background levels, and those levels can vary significantly with time at the lateral boundaries. For  $O_3$  those variations may be due to processes such as stratospheric  $O_3$  intrusions and trans-Pacific transport of Siberian wildfire plumes (e.g., Heald et al., 2003; Flemming et al., 2017; Pendlebury et al., 2018).  $PM_{2.5}$  levels can also vary with time over the oceans due to trans-oceanic transport of wildfire plumes from Siberia and desert dust from the Sahara and from northern China, Mongolia, and Central Asia (e.g., McKendry et al., 2008; Teakles et al., 2017; Tang et al., 2021).

As described in Sect. 4.2, the RAQDPS023 used “climatological” seasonal CLBCs based on results from a 2009 annual simulation with the MOZART4 offline global CTM. For the RAQDPS025 new climatological monthly CLBC files were generated by calculating monthly averages from outputs for the 2012–2019 period extracted from a 20-year global simulation made with version 6 of the Community Atmosphere Model with chemistry (CAM-chem) (Emmons et al., 2020; Tilmes et al., 2022; CMC-RAQPS025, 2024).

#### 6.1.6 Updates to representation of below-cloud scavenging of size-resolved PM

As described in Sect. 3.10 the treatment of below-cloud scavenging of PM in the RAQDPS023 was based on Slinn (1984). More recent studies by Wang et al. (2014a,b) have proposed an updated and unified parameterization of below-cloud wet removal of size-resolved PM by different precipitation types in all seasons. This newer parameterization was tested in a research version of GEM-MACH (Ghahreman et al., 2024) and was then implemented operationally in the RAQDPS025.

As well the RAQDPS023 used a fixed threshold temperature of  $0^{\circ}C$  to define the transition between liquid cloud droplet scavenging and solid snow scavenging. In the RAQDPS025 the phase state for cloud droplets predicted by GEM cloud physics, which includes mixed-phase as well as liquid and solid hydrometeors, has been used instead (Ghahreman et al., 2024). This better aligns the treatment of below-cloud scavenging of pollutants in GEM-MACH with the treatment of cloud processes in GEM.

#### 6.1.7 Updates to representation of gas-phase dry deposition

Three minor updates were implemented to the gas-phase dry deposition code in the RAQDPS025 (CMC-RAQPS025, 2024): (i) a correction was made to the value of the Schmidt number (changed from 0.84 to 0.62); (ii) the algorithm for calculating the ratio of the molecular diffusion coefficient for water vapour to that of a depositing pollutant species was updated; and (iii) a correction was made to the calculation of aerodynamic resistance  $R_a$ . In addition, the monthly



1520 climatology of satellite-derived, gridded leaf area index (LAI) described by Zhang et al. (2021), which provides high-resolution (500 m), latitude-longitude-dependent descriptions of variations in this important vegetation phenological attribute, was adopted in the calculation of the surface resistance term  $R_c$ .

### 6.1.8 Inclusion of sea salt mass in $PM_{2.5}$ total dry mass calculation

As noted in Sect. 5.1 the RAQDPS023 calculated  $PM_{2.5}$  total mass as the sum of seven chemical components (SU, NI, AM, EC, POM, SOM, CM). This quantity corresponds to dry  $PM_{2.5}$  total mass (i.e., without aerosol water) without a contribution from sea salt. The SS contribution had been excluded in earlier versions of the RAQDPS due to large overpredictions that had been observed early in the development of GEM-MACH. However, corrections had been made to the SS emissions scheme (Sect. 3.11.3), and performance evaluation results from Moran et al. (2025) showed that the exclusion of both SS and aerosol water contributed to the RAQDPS023 underprediction of  $PM_{2.5}$  total mass. 1530 Sea salt was thus included in the calculation of forecast  $PM_{2.5}$  total mass in RAQDPS025, although it is known to still have a positive bias (Moran et al., 2025).

### 6.1.9 Updates to solver for gas-phase chemistry

As described in Sects. 3.4 and 3.5 both the gas-phase and aqueous-phase chemistry mechanisms in the RAQDPS023 were solved for a model chemistry time step using the computationally efficient Young and Boris (1977) predictor–corrector algorithm and employing a number of smaller integration time substeps. However, the computer code used 1535 in GEM-MACH for this solver was hardcoded, was challenging to modify and maintain, and was less accurate than some other ordinary-differential-equation (ODE) solvers now available, in particular during the day-to-night and night-to-day transitions. The publicly available Kinetic PreProcessor (KPP) software tool is a symbolic preprocessor that allows chemical mechanisms to be described in a natural and compact way (cf. Table 4), permits the user to choose 1540 from a number of different ODE solvers, and then generates computer code in three high-level computer languages (Fortran, C, Matlab) (Damian et al., 2002; Sandu and Sander, 2006). As a consequence, KPP can deliver more accurate time integrations of chemistry mechanisms, and it also reduces the effort needed to modify and maintain existing chemistry mechanisms and to implement new chemistry mechanisms.

Source code generated by the KPP to use a Rosenbrock solver was introduced in the RAQDPS025 in the gas-phase 1545 chemistry operator in place of the Young-Boris solver. One additional benefit was removal of the need to make the steady-state assumption for short-lived chemical species, which can break down in the upper troposphere due to cold temperatures.

### 6.1.10 Updates to representation of biogenic emissions

The representation of biogenic emissions used in the RAQDPS023 (Sect. 3.11.3) was quite dated and had an overly 1550 simple treatment of the spring and autumn transition seasons. Newer versions of the BEIS scheme were available that both provide more detailed VOC emission speciations and have updates to biomass and emission factors and to the treatment of canopy leaf temperature and soil NO emissions (<https://www.epa.gov/air-emissions-modeling/biogenic->



[emission-inventory-system-beis](#)). Newer versions were also available for the BELD land use and vegetation database that is used in the calculation of biogenic emissions (Zhang and Moran, 2020), and many satellite-based data sets are now available that can provide high-resolution descriptions of temporal and spatial variations in vegetation phenology, including LAI (e.g., Zhang et al., 2021). For example, Campbell et al. (2022) have described the impact of changing from BEIS version 3.14 coupled with the BELD3 vegetation database to BEIS version 3.61 coupled with the BELD5 vegetation database on operational U.S. NAQFC system forecasts.

For the RAQDPS025 the BEIS scheme was updated from version 3.09 to version 3.7, the BELD vegetation database was updated from version 3 to version 4 (Zhang and Moran, 2020), and the satellite-derived, high-spatial resolution LAI monthly climatology described by Zhang et al. (2021) was also adopted, but the crude five-category treatment of phenological season (Sect. 3.9) was not changed. It is also worth noting that considerable uncertainty remains around the treatment of biogenic emissions in general (e.g., Hanna et al., 2005; Warneke et al., 2010; Guenther et al., 2012), so this component of the forecast system is likely to undergo further updates in the future.

#### 6.1.11 Updates to anthropogenic emission inventories and emissions processing methods

The SET4.0.0 emission files used by the RAQDPS023 were based on a 2020 projected Canadian anthropogenic national emissions inventory and 2023 projected U.S. and Mexican anthropogenic national emissions inventories (Sect. 3.11.1). For the RAQDPS025 the SET4.0.0 emission files were replaced by a new set of input emission files called SET5.0.0. The SET5.0.0 emission files are based on the same U.S. and Mexican projected 2023 national inventories (just one year in time before the 2024 implementation of the RAQDPS025) as the SET4.0.0 emission files, but a 2023 projected Canadian national emissions inventory based on the 2019 APEI (ECCC, 2021) was used in place of the 2020 projected Canadian emissions inventory based on the 2015 APEI (ECCC, 2016). As was the case for the national inventories used for SET4.0.0 (Sect. S2), some pre-processing was also required for this new Canadian inventory before the emissions processing step (CMC-RAQDPS-025, 2024). Some improvements were also introduced to the emissions processing methods used by the SMOKE system to prepare the SET5.0.0 emissions files (Sect. S2). These included updates to 15 Canadian gridded spatial surrogates for several important emission sectors, including RWC (CMC-RAQDPS-025, 2024).

#### 6.2 Future work

Work is already underway on the next version of the RAQDPS, including work to migrate to a new upgrade of the ECCC HPC system. Possible future upgrades to GEM-MADH include improvements to the chemistry and dry deposition parameterizations, anthropogenic emissions and BB and other natural emissions, and chemical lateral boundary conditions, and implementation of chemical data assimilation.

Some improvements to the representation of atmospheric chemistry might include the addition of a parameterization of marine halogen chemistry, which can influence surface ozone concentrations in coastal regions (e.g., Sarwar et al., 2015; Li et al., 2019). Newer aqueous-phase chemistry schemes are available that account for the role of individual



base cations and sea salt, and some also include oxidation pathways for SOA formation in cloud droplets (e.g., Gong et al., 2011). Newer versions of ISORROPIA and other inorganic heterogeneous parameterization schemes are also available that treat individual base cations explicitly (e.g., Meng et al., 1995; Fountoukis and Nenes, 2007; Miller et al., 2024). A new solver for the aqueous-phase chemistry mechanism could also be implemented.

1590 It was also noted in Sects. 3.9 and 3.11.3 that the parameterizations for gas-phase dry deposition and biogenic emissions used by the RAQDPS023 rely on a crude description of phenological season with low resolution of associated temporal and spatial variations. Many satellite-based data sets are now available that can provide high-resolution descriptions of temporal and spatial variations in vegetation phenology, including longitudinal and elevation variations (e.g., Zhang and Moran, 2020; Zhang et al., 2021). One such data set was adopted for use by the RAQDPS025 (Sects. 6.1.7 and  
1595 6.1.10), but further use of such data sets could be explored. In addition, two process terms for soil wetness not currently considered by the GEM-MACH gas-phase dry deposition scheme should be included (Sect. 3.9).

Regarding emissions updates, as noted in Sects. 3.11.1 and 6.1.11 there is an ongoing need to make use of the most recent anthropogenic emissions inventories to prepare updated model input emission files. Thus, the SET5.0.0 emission files used by the RAQDPS025, which have a nominal base year of 2023, could be replaced by a newer set of  
1600 input emission files. Also, natural windblown dust emissions were not considered by the RAQDPS023 (Sect. 3.11.3); the addition of an aeolian dust emissions scheme would provide representation of a source of emissions that is currently missing. The estimation of BB emissions by CFFEPS might be improved by updates to fuel- and location-specific emission factors based upon Canada-specific field measurement campaigns, and recent literature (e.g., Hayden et al., 2022, Binte Shahid et al., 2024; Flood et al., 2025). Moran et al. (2025) also found from evaluation of RAQDPS023  
1605 forecasts that the scheme used by the RAQDPS023 to modulate fugitive dust emissions according to current meteorological conditions (Sect. 3.12) should be improved.

While the treatment of CLBCs was updated in the RAQDPS025 (Sect. 6.1.5), this updated treatment is still climatological or static in nature. In principle, CLBCs should be hour- and day-specific (e.g., Giordano et al., 2015; Ma et al., 2021; Tang et al., 2021). For example, Pendlebury et al. (2018) have described an approach whereby time-  
1610 varying O<sub>3</sub> CLBCs can be obtained from a monthly global O<sub>3</sub> climatology combined with GEM model predictions of dynamic tropopause height at each time step. Another possibility to improve the CLBCs used by the RAQDPS would be to run GEM-MACH in a global configuration and then extract regional CLBCs from its forecasts (Chen et al., 2020).

Lastly, the introduction of meteorological data assimilation for the initialization of NWP models resulted in a step change in weather forecasting skill (e.g., Simmons and Hollingsworth, 2002; Bauer et al., 2015). Chemical data  
1615 assimilation (CDA) offers the possibility of similar improvements for chemical weather forecasting. Some global NWP models and CTMs have implemented data assimilation of select chemical fields such as O<sub>3</sub>, CO, NO<sub>2</sub>, HCHO, PM<sub>2.5</sub>, and aerosol optical depth (AOD) to improve their initialization of the chemical state (e.g., Pierce et al., 2007; Benedetti et al., 2009; Saide et al., 2013; Inness et al., 2015, 2019; Chai et al., 2017; Randles et al., 2017; Tang et al., 2017; Kumar et al., 2019; Menut and Bessagnet, 2019; Rochon et al., 2019; CMC-GDPS-8.0.0, 2021a; Ma et al., 2021).



1620 At the same time the number of available AQ measurements for North America, especially from satellite-based sensors but also from surface-based sensors, continues to increase (e.g., Naeger et al., 2021; Jaffe et al., 2023).

An important development goal for the RAQDPS is to implement an operational CDA capability, and some options to do this are available now. These include the assimilation of surface measurements based on the RDAQA system (Sect. 5.2; Robichaud, 2017; Ménard, 2021) and the use of the assimilated O<sub>3</sub> field from GDPS 9.0.0 forecasts  
1625 (Sect. 6.1.2; Rochon et al., 2019; CMC-GDPS-8.0.0, 2021a).

## 7 Summary

Environment and Climate Change Canada (ECCC) has run an operational, continental-scale Regional Air Quality Deterministic Prediction System (RAQDPS) for North America since 2001. The earliest version of the RAQDPS employed an offline chemical transport model called CHRONOS that used the ECCC Global Environmental Multiscale  
1630 (GEM) numerical weather prediction model as a meteorological driver. In 2009 CHRONOS was replaced in the RAQDPS by the online, one-way-coupled GEM-MACH (Global Environmental Multiscale–Modeling Air quality and CHemistry) chemical weather model, which consists of GEM as a meteorological host model and an embedded chemistry module named MACH (Modelling Air quality and CHemistry) that can be activated (or not) by a namelist setting. Since 2009 there have been 24 upgrades of varying magnitude made to the GEM-MACH-based version of the  
1635 RAQDPS to improve forecast skill and to adjust to changes in upstream meteorological systems and ECCC's supercomputers (Table A3). This paper describes version 023 of the RAQDPS, including its dynamics, physics, chemistry, numerics, inputs, outputs, related upstream meteorological systems and downstream AQ systems, and recent and potential future developments. Significantly, it is the first comprehensive publication describing any RAQDPS version. A companion paper (Moran et al., 2025) provides a comprehensive evaluation of RAQDPS023 performance  
1640 for its first forecast year and four hindcast years.

The RAQDPS023 became the ECCC operational regional AQ forecast system on 1 December 2021; it was then migrated without any algorithmic changes to a new ECCC computer system on 28 June 2022 and renamed RAQDPS024. It then continued to run operationally for another two years until it was replaced by an upgraded version, the RAQDPS025, on 11 June 2024. A special wildfire version of the RAQDPS023 called FireWork023 or RAQDPS-  
1645 FW023, which was identical to the RAQDPS023 except for the addition of near-real-time (NRT) biomass burning (BB) emissions as an input, went operational at the same time, was migrated to the new computer system at the same time (RAQDPS-FW024), and was replaced at the same time in 2024. Running this second member of the ECCC regional AQ forecast suite allowed forecasts of the transport and diffusion of wildfire smoke plumes to be calculated in a post-processing step as the difference between the PM<sub>2.5</sub> forecasts from the two model versions.

1650 The RAQDPS023 and RAQDPS-FW023 both used GEM-MACH version 3.1.0.0, which was built on GEM version 5.1.0. Both systems employed a regional configuration with 10 km horizontal grid spacing and a geographic domain covering Canada, the continental U.S. and most of Alaska, and northern Mexico. Both systems were run twice each



day starting at 00 and 12 UTC to produce 72 h forecasts. The RAQDPS-FW023 obtained NRT satellite-detected BB  
emission forecasts for Canada and the U.S. for the next 72 hours from version 4.1 of the Canadian Forest Fire Emissions  
1655 Prediction System (CFFEPS) before each run (Sect. S3).

To obtain the meteorological initial conditions and boundary conditions that were needed, each RAQDPS023 run  
followed a run for the same forecast period by the corresponding ECCC operational regional weather forecast system,  
the 10 km Regional Deterministic Prediction System 8.0.0. The RDPS 8.0.0 was a regional configuration of GEM  
5.1.0 that made 84 h forecasts four times per day. Its horizontal grid was a superset of the RAQDPS023 grid. To  
1660 obtain the meteorological initial conditions and boundary conditions that it needed in turn, each RDPS 8.0.0 run  
followed a run for the same forecast period by the ECCC operational global weather forecast system, the 15 km Global  
Deterministic Prediction System 8.0.0. The GDPS 8.0.0 was a global configuration of GEM 5.1.0 that made 144 h  
forecasts four times per day. For maximum consistency the GDPS 8.0.0, RDPS 8.0.0, and RAQDPS023 all used the  
same rotated latitude-longitude map projection and the same 84 staggered hybrid vertical levels with a top at 0.1 hPa.

1665 All three systems also employed the same GEM dynamical core, including the hydrostatic assumption. Time  
integration was performed using a two-time-level, iterative-implicit, three-dimensional semi-Lagrangian scheme. The  
GDPS 8.0.0 used a 450 s dynamics integration time step while both the RDPS 8.0.0 and RAQDPS023 used a 300 s  
time step. Since semi-Lagrangian advection schemes do not conserve mass, a shape-preserving monotonicity  
correction and a global mass fixer were both used for tracer advection for all three systems. Mass conservation is very  
1670 relevant for a regional AQ model since there can be many sharp chemical concentration gradients in the vicinity of  
strong local emissions sources, and the resulting loss of shape preservation after advection can introduce physically  
unrealistic negative concentrations or positive overshoots. The same physics parameterizations were also used by the  
three systems (Table 1), with only very minor differences in a few parameter settings between the global and regional  
versions to account for their different horizontal grid spacing. And since GEM-MACH is an online model the  
1675 RAQDPS023 could access many meteorological variables predicted by GEM 5.1.0 that were needed by some MACH  
chemistry parameterizations (Table 2).

The RAQDPS023 predicted 41 gas-phase species and 18 particle-phase chemical species, but its three key AQ  
predictands were  $\text{NO}_2$ ,  $\text{O}_3$ , and  $\text{PM}_{2.5}$  total mass, which are needed to calculate the Canadian Air Quality Health Index.  
The AQHI is a health-based, multi-pollutant, additive, no-threshold hourly AQ index that is used to communicate  
1680 current and predicted AQ levels to the Canadian public. Of these three predictands,  $\text{PM}_{2.5}$  mass poses a particular  
challenge because it is a complex pollutant: it has a wide size range; it is composed of many elements and compounds,  
both inorganic and organic; it is subject to many physical and chemical processes; and it has many types of emissions  
sources.

The MACH chemistry module employs a sectional representation to model the PM size distribution, where the number  
1685 of size bins can be specified by the user. For the RAQDPS023 as well as earlier versions, a major simplification made  
to ensure that system execution times would be short enough to fit within its operational 30 minute time slot was to



consider just two PM size bins, one corresponding to particle Stokes diameters in the 0-2.5  $\mu\text{m}$  range (“fine fraction” or  $\text{PM}_{2.5}$ ) and the other to the 2.5-10  $\mu\text{m}$  range (“coarse fraction” or  $\text{PM}_{\text{cf}}$ ). Together these two size bins constitute  $\text{PM}_{10}$ . This is a very coarse representation of the PM size distribution, but it still allowed the model to predict concentrations of  $\text{PM}_{2.5}$  and  $\text{PM}_{10}$ , which are the two PM size ranges considered by most AQ measurement networks and emission inventories. MACH for the RAQDPS023 also represented  $\text{PM}_{2.5}$  chemical composition with a limited number of chemical components, namely sulfate, nitrate, ammonium, elemental carbon, primary organic matter, secondary organic matter, crustal material, sea salt, and aerosol water. However, these nine chemical components align fairly well with the chemical components that are measured by  $\text{PM}_{2.5}$  speciation networks, thus permitting evaluation of  $\text{PM}_{2.5}$  composition predictions. A third simplification in the treatment of PM was that each size bin was assumed to be internally mixed, an assumption that is the least good close to sources of PM but which improves as particles age in the atmosphere.

MACH contains parameterizations to represent a number of physical and chemical processes that influence PM mass concentrations. As described in Sect. 3 these include anthropogenic emissions, smokestack plume rise, sea-salt and biogenic emissions, particle nucleation, condensational growth, coagulation, gravitational settling and dry deposition, hygroscopic growth and aerosol particle activation, vertical diffusion, gas-phase chemistry, secondary organic aerosol formation, gas-particle partitioning, inorganic heterogeneous chemistry, aqueous-phase chemistry, and in-cloud and below-cloud precipitation scavenging.

Chemical tracer initial conditions for the RAQDPS023 were copied from forecast chemical tracer fields corresponding to that initial time from the previous forecast, a so-called perpetual forecast approach. Chemical lateral boundary conditions were obtained from a set of “climatological” seasonal vertical cross-sections of model species mass mixing ratios (MMRs) supplied for each lateral boundary. One other simplification made for the RAQDPS023 to reduce execution time was to call the MACH module every third dynamics time step, that is, to employ a chemistry time step of 900 s. This simplification was possible due to the assumption that there was no feedback of chemistry on meteorology. Even so, activation of the MACH chemistry module increased RAQDPS023 execution time by a factor of 4.4 compared to running only the GEM code.

The pre-processed, hourly, gridded anthropogenic emissions input files used by the RAQDPS023 and RAQDPS-FW023, which are referred to as SET4.0.0 emissions, were new to this version (Table A3). They were based on three national emission inventories: (i) a projected 2020 Canadian Air Pollutant Emissions Inventory; (ii) a projected 2023 U.S. National Emissions Inventory (NEI); and (iii) a projected 2023 Mexican NEI. The SET4.0.0 files were generated during the development of the RAQDPS023 and well before its operational deployment using version 4.7 of the SMOKE emissions processing system. Hourly BB emissions, on the other hand, were forecast for the next 72 h in advance of each RAQDPS-FW023 run by CFFEPS v4.1. Biogenic emissions were treated in a third way; they were estimated every chemistry time step by in-line code in MACH. Sea-salt emissions were also estimated every chemistry time step.



The RAQDPS023 routinely output a large number of hourly gridded fields, including 41 gas-phase chemical MMR fields, eight  $PM_{2.5}$  and eight  $PM_{cf}$  chemical component MMR fields,  $PM_{2.5}$  and  $PM_{10}$  total mass concentration fields, 21 dry deposition flux fields, 12 wet deposition flux fields, and four biogenic emission flux fields. Two downstream operational systems made use of some of these outputs. Point-specific hourly forecasts of  $NO_2$ ,  $O_3$ , and  $PM_{2.5}$  concentrations at Canadian AQ measurement station locations were fed to the Updateable Model Output Statistics for Air Quality (UMOS–AQ) system. UMOS–AQ is a statistical post-processing package for bias correction that can compensate for systematic model errors and account for unresolved SGS phenomena. Its hourly, station-specific regression coefficients are recalculated weekly. A second post-processing system, version 2.0.0 of the Regional Deterministic Air Quality Analysis (RDAQA) system, used RAQDPS023 hourly gridded forecast fields as first-guess fields together with surface AQ measurements to generate objective analyses of hourly North American surface concentration fields for  $O_3$ ,  $NO_2$ ,  $NO$ ,  $PM_{2.5}$ ,  $PM_{10}$ ,  $SO_2$ , and the AQHI. RAQDPS023 forecast performance was also monitored on an ongoing basis, including by a quarterly comparison with AQ forecasts for North America made by four international operational models.

The paper concludes by describing the main innovations made for the RAQDPS025, the successor to the RAQDPS023, which was implemented operationally in June 2024. One key innovation of the RAQDPS025 was to combine the RAQDPS and RAQDPS-FW systems into a single unified system while still identifying wildfire smoke plumes. The RAQDPS025 also has updates to the treatments of vertical diffusion, gas-phase chemistry, gas-phase dry deposition, below-cloud scavenging of size-resolved PM, chemical lateral boundary conditions, and biogenic emissions. As well the meteorological piloting model was changed (to GDPS 9.0.0) and a new set of anthropogenic input emissions files (SET5.0.0) was introduced. Lastly, a short summary of some possible areas of improvements to future RAQDPS versions is provided.



## Appendices

1745

Table A1. List of acronyms and abbreviations.

	ADAGIO	Atmospheric Deposition Analysis Generated by optimal Interpolation from Observations
	ADOM	Acid Deposition and Oxidant Model
	AGL	above ground level
1750	ALKA	See Table 3
	ALKE	See Table 3
	AM	ammonium
	AOD	aerosol optical depth
	APEI	Air Pollutant Emissions Inventory (Canada)
1755	AQ	air quality
	AQHI	Air Quality Health Index (Canada)
	AROM	See Table 3
	AURAMS	A Unified Regional Air quality Modelling System
	BB	biomass burning
1760	BC	black carbon
	BEIS	Biogenic Emission Inventory System
	BELD3	Biogenic Emissions Landuse Database version 3
	CAC	criteria air contaminant
	CAM	Canadian Aerosol Module
1765	CAM-chem	Community Atmosphere Model with chemistry
	CAPE	convective available potential energy
	CCN	cloud condensation nuclei
	CDA	chemical data assimilation
	CF	coarse fraction
1770	CFC	chlorofluorocarbon
	CFFEPS	Canadian Forest Fire Emissions Prediction System
	CFS	Canadian Forest Service
	CHRONOS	Canadian Hemispheric and Regional Ozone and NO <sub>x</sub> System
	CLBC	chemical LBC
1775	CM	crustal material
	CMAQ	Community Multiscale Air Quality model
	CMAS	Community Modeling and Analysis System (University of North Carolina)
	CMC	Canadian Meteorological Centre
	CS	condensable species
1780	CSN	Chemical Speciation Network (U.S.)
	CTM	chemical transport model
	CWFIS	Canadian Wildland Fire Information System
	DDF	dry deposition scaling factor
	DOW	day of the week
1785	EC	elemental carbon
	ECCC	Environment and Climate Change Canada



	EOTH	emissions of “other” VOCs (NAPAP classes 21, 23, 25, 26, 31, and 32)
	EPA	Environmental Protection Agency (U.S.)
	FBP	(Canadian) Forest Fire Behaviour Prediction subsystem
1790	FEPS	Fire Emission Production Simulator (U.S.)
	FW	FireWork
	FWI	(Canadian) Forest Fire Weather Index subsystem
	GAFIS	Global Air quality Forecasting and Information System initiative (WMO)
	GDPS	Global Deterministic Prediction System
1795	GEM	Global Environmental Multiscale (model)
	GEM-MACH	Global Environmental Multiscale–Modelling Air quality and CHEMISTRY (model)
	GMM	gram molar mass
	HETV	HETerogeneous Vectorized scheme
	HPC	high-performance computing
1800	IAU	incremental analysis update
	IAY	instantaneous aerosol yield
	IC	initial condition
	ILMC	iterative locally mass conserving (scheme)
	IMPROVE	Interagency Monitoring of Protected Visual Environments network (U.S.)
1805	ISBA	Interactions between Soil–Biosphere–Atmosphere (land surface model)
	ISOP	isoprene (see Table 3)
	ISORROPIA	“equilibrium” (modern Greek)
	KPP	Kinetic PreProcessor
	LAI	leaf area index
1810	LAM	limited area model
	LBC	lateral boundary condition
	LINOZ	LINearized OZone mechanism
	LST	local standard time
	LWC	liquid water content
1815	MACH	Modelling Air quality and CHEMISTRY (module)
	MLR	multi-variate linear regression
	MMR	mass mixing ratio
	MODIS	Moderate Resolution Imaging Spectroradiometer
	MOZART4	Model for OZone And Related chemical Tracers version 4
1820	MPI	Message Passing Interface
	NAPAP	National Acid Precipitation Assessment Program (U.S.)
	NAPS	National Air Pollution Surveillance system (Canada)
	NAQFC	National Air Quality Forecast Capability (U.S.)
	NASA	National Aeronautics and Space Administration (U.S.)
1825	NEI	National Emissions Inventory (U.S., Mexico)
	NI	nitrate
	NMHC	non-methane hydrocarbon
	NOAA	National Oceanic and Atmospheric Administration (U.S.)
	NRT	near-real time
1830	NWP	numerical weather prediction



	OA	objective analysis
	ODE	ordinary differential equation
	OH	hydroxyl radical
	OI	optimal interpolation
1835	OpenMP	Open Multi-Processing
	OVOC	other VOCs
	PAR	photosynthetic active radiation
	PBL	planetary boundary layer
	PM	particulate matter
1840	PM <sub>coarse</sub>	PM coarse fraction (2.5–10 µm)
	PM <sub>2.5</sub>	PM with aerodynamic diameter of less than 2.5 µm
	PM <sub>10</sub>	PM with aerodynamic diameter of less than 10 µm
	POM	primary organic matter
	QA/QC	quality assurance/quality control
1845	RAQDPS	Regional Air Quality Deterministic Prediction System
	RAQDPS-FW	Regional Air Quality Deterministic Prediction System with FireWork BB emissions
	RDAQA	Regional Deterministic Air Quality Analysis
	RDPS	Regional Deterministic Prediction System
	RH	relative humidity
1850	ROS	rate of spread
	RVFSP-WAC	North American Regional Vegetation Fire and Smoke Pollution Warning and Advisory Centre
	RWC	residential wood combustion
	SCC	source classification code
	SGS	subgrid-scale
1855	SI	Système International d'unités
	SMOKE	Sparse Matrix Operation Kernel Estimation system (CMAS)
	SOA	secondary organic aerosol
	SOM	secondary organic matter
	SS	sea salt
1860	SU	sulfate
	TF	transportable fraction
	TKE	turbulent kinetic energy
	TOLU	See Table 3
	UMOS-AQ	Updateable Model Output Statistics–Air Quality
1865	USFS	U.S. Forest Service
	UTC	Universal Time Coordinated
	VIIRS	Visible Infrared Imaging Radiometer Suite
	VIT	vehicle-induced turbulence
	VOC	volatile organic compound
1870	WA	aerosol water
	WHO	World Health Agency
	WMO	World Meteorological Organization
	4D-IAU	four-dimensional incremental analysis update



1875 Table A2. List of symbols

	$d$	particle diameter (cm)
	$D$	raindrop or frozen hydrometeor diameter (cm)
	$D_i$	gas-phase diffusivity of species $i$ ( $\text{cm}^2 \cdot \text{s}^{-1}$ )
	$D_m$	mean raindrop or frozen hydrometeor diameter (cm)
1880	$\bar{E}(d, l)$	mean snowflake–particle collection efficiency (unitless)
	$E(d, D_m)$	raindrop–particle collection efficiency (unitless)
	$\bar{E}(d, D_m)$	mean raindrop–particle collection efficiency (unitless)
	$f_{\text{cld}}$	total cloud cover fraction by layer (unitless)
	$f_{\text{ctr}}$	precipitation production rate ( $\text{s}^{-1}$ )
1885	$H'$	effective equilibrium constant for gas-liquid partitioning
	$K_{\text{om},1i}$	first partitioning coefficient of the $i$ -th condensable species ( $\mu\text{g} \cdot \text{m}^{-3}$ )
	$K_{\text{om},2i}$	second partitioning coefficient of the $i$ -th condensable species ( $\mu\text{g} \cdot \text{m}^{-3}$ )
	$K_z$	vertical eddy diffusivity for tracers ( $\text{m}^2 \cdot \text{s}^{-1}$ )
	$l$	characteristic collection length scale of frozen hydrometeor (may not be $D$ ) (cm)
1890	$L$	volumetric liquid water fraction in air ( $\text{m}^3 \cdot \text{m}^{-3}$ )
	$n$	number of size bins or sections
	$N_d$	cloud droplet number concentration ( $\text{cm}^{-3}$ )
	$N_p$	particle number density ( $\text{cm}^{-3}$ )
	$p$	(liquid) precipitation rate ( $\text{mm} \cdot \text{hr}^{-1}$ )
1895	$p$	atmospheric pressure (hPa)
	$p_s$	surface pressure (hPa)
	$R$	universal gas constant ( $\text{J} \cdot \text{K}^{-1} \cdot \text{mol}^{-1}$ )
	$R_a$	aerodynamic resistance ( $\text{s} \cdot \text{m}^{-1}$ )
	$R_b$	quasi-laminar sublayer resistance ( $\text{s} \cdot \text{m}^{-1}$ )
1900	$R_c$	surface resistance ( $\text{s} \cdot \text{m}^{-1}$ )
	$Ri$	gradient Richardson number (unitless)
	$Ri_b$	bulk Richardson number (unitless)
	$T$	dry-bulb temperature (K)
	$u^*$	friction velocity ( $\text{m} \cdot \text{s}^{-1}$ )
1905	$V_{\text{rt}}$	raindrop terminal fall speed ( $\text{m} \cdot \text{s}^{-1}$ )
	$V_{\text{st}}$	frozen hydrometeor terminal fall speed ( $\text{m} \cdot \text{s}^{-1}$ )
	$\alpha_{1i}$	mass-based stoichiometric coefficient 1 for SOA formation from $i$ -th CS (unitless)
	$\alpha_{2i}$	mass-based stoichiometric coefficient 2 for SOA formation from $i$ -th CS (unitless)
	$\lambda$	turbulence-regime-specific mixing length (m)
1910	$\lambda_c$	dissipation length scale (m)
	$A_{\text{r}}(d)$	rain scavenging rate coefficient for aerosol particles of diameter $d$ ( $\text{s}^{-1}$ )
	$A_{\text{s}}(d)$	snow scavenging rate coefficient for aerosol particles of diameter $d$ ( $\text{s}^{-1}$ )
	$A_i$	rain scavenging rate coefficient for $i$ -th gas ( $\text{s}^{-1}$ )

1915



1920 Table A3. Chronology of operational RAQDPS and RAQDPS-FW versions. Boldface font indicates a major update to the RAQDPS version and the RAQDPS-FW version (which was introduced operationally in April 2016 as a seasonal forecast system). [See also ECCC changelogs for the RAQDPS ([https://eccc-msc.github.io/open-data/msc-data/nwp\\_raqdps/changelog\\_raqdps\\_en/](https://eccc-msc.github.io/open-data/msc-data/nwp_raqdps/changelog_raqdps_en/)) and RAQDPS-FW ([https://eccc-msc.github.io/open-data/msc-data/nwp\\_raqdps-fw/changelog\\_raqdps-fw\\_en/](https://eccc-msc.github.io/open-data/msc-data/nwp_raqdps-fw/changelog_raqdps-fw_en/)).]

Date	RAQDPS Version	GEM / PHY / GEM-MACH Versions	Change(s)
<b>18 Nov 2009</b>	<b>001</b>	<b>3.3.0 / 4.5 / 1.3.0a</b>	<b>GEM-MACH15 implemented into CMC operational suite</b>
2 Mar 2010	002	3.3.0 / 4.5 / 1.3.0a	New emissions files introduced with modified primary PM <sub>2.5</sub> emissions over some Cdn provinces
20 Oct 2010	003	3.3.0 / 4.5 / 1.3.0a	Meteorological piloting model changed from GEM15-global to GEM-LAM15 regional configuration
<b>25 Oct 2011</b>	<b>004</b>	<b>3.3.3 / 4.7.2 / 1.4.4</b>	<b>New GEM and GEM-MACH versions and new emissions files (SET0)</b>
22 Dec 2011	005	3.3.3 / 4.7.2 / 1.4.5	New GEM-MACH version with correction for radiation calculation at model top
2 May 2012	006	3.3.6 / 4.7.2.1 / 1.4.6	New versions for the new supercomputer used by operations, including bug fixes
<b>3 Oct 2012</b>	<b>007</b>	<b>3.3.8 / 5.0.4.2 / 1.5.0</b>	<b>New GEM and GEM-MACH versions, new grid (15→10 km), new emissions (SET1); RDPS300 piloting</b>
20 Nov 2012	008	3.3.8 / 5.0.4.2 / 1.5.0	Replacement of emissions files introduced in Oct. 2012 (SET1) with Oct. 2011 version (SET0)
<b>26 Feb 2013</b>	<b>009</b>	<b>3.3.8 / 5.0.4.2 / 1.5.1</b>	<b>New GEM-MACH version with 3 bug fixes</b>
10 Apr 2014	010	3.3.8.1 / 5.0.4.3 / 1.5.2	Migration to GEM v3.3.8.1 and PHY v5.0.4.3
18 Nov 2014	011	3.3.8.2 / 5.0.4.4 / 1.5.3	Migration to GEM v3.3.8.2, PHY v5.0.4.4, and RDPS-EnVar
18 Mar 2015	012	3.3.8.2-isba / 5.0.4.4 / 1.5.4	Migration to GEM v3.3.8.2-isba
<b>11 Jun 2015</b>	<b>013</b>	<b>3.3.8.2-isba / 5.0.4.4 / 1.5.4</b>	<b>Replacement of emissions files introduced in Oct. 2011 (SET0) with SET2.1.1 versions</b>
15 Dec 2015	014	3.3.8.4 / 5.0.4.5 / 1.5.5	Migration to GEM v3.3.8.4
22 Feb. 2016	013	3.3.8.2-isba / 5.0.4.4 / 1.5.4	Fallback to RAQDPS013 due to bug found in GEM 3.3.8.4
7 Apr. 2016	015	4.6.2 / 5.6.8 / 2.0.1	Initial migration to GEMv4-based code
<b>13 Apr 2016</b>	<b>FW015</b>	<b>4.6.2 / 5.6.8 / 2.0.1</b>	<b>Initial implementation of RAQDPS-FW with FEPS as a seasonal system (April–October); final run on 7 Sept. 2016</b>
<b>7 Sept. 2016</b>	<b>016</b>	<b>4.8.0 / 5.8.0 / 2.1.1</b>	<b>Harmonization with new RDPSv5 based on GEM4.8.0</b>
<b>7 Sept. 2016</b>	<b>FW016</b>	<b>4.8.0 / 5.8.0 / 2.1.1</b>	<b>New Yin10 horizontal grid, new emissions (SET2.2)</b>
<b>7 Sept. 2016</b>	<b>FW016</b>	<b>4.8.0 / 5.8.0 / 2.1.1</b>	<b>New vertical discretization (non-staggered→staggered)</b>
<b>7 Sept. 2016</b>	<b>FW016</b>	<b>4.8.0 / 5.8.0 / 2.1.1</b>	<b>Clone of RAQDPS016 plus FEPS; final run on 6 Oct. 2016</b>
6 Oct. 2016	017	4.8.3 / 5.8.0 / 2.1.3	GEM update and correction for rare mass-conserving advection error



6 Oct. 2016	FW017	4.8.3 / 5.8.0 / 2.1.3	Clone of RAQDPS017 plus FEPS; final run on 31 Oct. 2016
4 Jan. 2017	018	4.8.3 / 5.8.0 / 2.1.3	Correction to precision of output fields
3 Apr. 2017	FW018	4.8.3 / 5.8.0 / 2.1.3	Clone of RAQDPS017 plus FEPS; final run on 6 Sept. 2017
6 Sep. 2017	019	4.8-LTS.11 / 5.8-LTS.8 / 2.2.0	Migration to ‘science’ network and Cray XC40 backends
6 Sep. 2017	FW019	4.8-LTS.11 / 5.8-LTS.8 / 2.2.0	Clone of RAQDPS019 plus FEPS; final run on 31 Oct. 2017
3 Apr. 2018	FW019	4.8-LTS.11 / 5.8-LTS.8 / 2.2.0	Clone of RAQDPS019 plus FEPS; restarted for 2018 wildfire season
<b>18 Sep. 2018</b>	<b>020</b>	<b>4.8-LTS.13 / 5.8-LTS.9 / 2.3.1</b>	<b>New piloting model (RDPS 6), updated code, new emissions (SET3.1), physics recycling &amp; IAU initialization</b>
<b>18 Sep. 2018</b>	<b>FW020</b>	<b>4.8-LTS.13 / 5.8-LTS.9 / 2.3.1</b>	<b>Clone of RAQDPS020 plus FEPS; final run on 7 Nov. 2018</b>
8 Feb. 2019	020.1	4.8-LTS.16 / 5.8-LTS.16 / 2.3.2	GEM bug fix to ISBA for certain “rain on snow” conditions
12 Apr 2019	020.2	4.8-LTS.16 / 5.8-LTS.16 / 2.3.2	Replacement of SET3.1.0 major-point-source emissions with SET3.1.2 version (reduces number of points by ~75%)
<b>15 Apr 2019</b>	<b>FW020.2</b>	<b>4.8-LTS.16 / 5.8-LTS.16 / 2.3.2</b>	<b>Implementation of CFFEPS v2.04 GEM hourly meteorological fields for all hours now used to estimate wildfire emissions, not just noontime fields GEM update (GEM5.0.0 and PHY6.0.0)</b>
<b>3 July 2019</b>	<b>021</b>	<b>5.0.0 / 6.0.0 / 3.0.0</b>	<b>New vertical discretization (80→84 levels) Update chemistry to GEM-MACH 3.0.0 Extension of forecast length from 48 hours to 72 hours</b>
<b>3 July 2019</b>	<b>FW021</b>	<b>5.0.0 / 6.0.0 / 3.0.0</b>	<b>Implementation of RAQDPS-FW021 with CFFEPS v2.06 (two minor bug fixes); final run for season on 3 Dec. 2019</b>
21 Jan. 2020	022	5.0.2 / 6.0.0 / 3.0.0.2	Computer migration to new Cray XC50 supercomputers
<b>1 Apr. 2020</b>	<b>FW022</b>	<b>5.0.2 / 6.0.0 / 3.0.0.2</b>	<b>Clone of RAQDPS022 plus CFFEPS v2.06; seasonal start for Canadian fire season but runs extended to full year</b>
<b>1 Dec. 2021</b>	<b>023</b>	<b>5.1.0 / 6.1.0 / 3.1.0.0</b>	<b>Update chemistry to GEM-MACH 3.1.0.0 Update meteorology to GEM 5.1.0 and PHY6.1.0 Update anthropogenic emissions (SET3.1.2 to SET4.0.0) New piloting model (RDPS 8.0.0)</b>
<b>1 Dec. 2021</b>	<b>FW023</b>	<b>5.1.0 / 6.1.0 / 3.1.0.0</b>	<b>Implementation of RAQDPS-FW023 with CFFEPS v4.1 Addition of more fuel parameters for wildfire emissions New plume injection height parameterization</b>
28 Jun 2022	024	5.1.2 / 6.1.2 / 3.1.1.2	Migration to new Lenovo ThinkSystem SV650V2 DWC supercomputers
28 Jun 2022	FW024	5.1.2 / 6.1.2 / 3.1.1.2	Migration to new Lenovo ThinkSystem SV650V2 DWC supercomputers
<b>11 Jun 2024</b>	<b>025</b>	<b>5.2.1 / 6.2.1 / 3.2.1.1</b>	<b>Merger of RAQDPS and RAQDPS-FW New piloting model: GDPS-G0 9.0 replaces RDPS 8.0.0 Eight updates to chemistry parameterizations Update anthropogenic emissions (SET4.0.0 to SET5.0.0)</b>



### ***Code and data availability.***

Version 5.1 of the GEM numerical weather prediction model code used by the RAQDPS023 is free software which can be redistributed and/or modified under the terms of version 2.1 of the GNU Lesser General Public License as published by the Free Software Foundation. The GEM source code has been developed by the Meteorological Research Division of ECCC. This code is available for download from <https://zenodo.org/records/17782580> (Environment and Climate Change Canada, 2025).

MACH, the atmospheric chemistry library for the GEM numerical atmospheric model (©2007–2021, Air Quality Research Division and National Prediction Operations Division, Environment and Climate Change Canada) is free software that can be redistributed and/or modified under the terms of the GNU Lesser General Public License as published by the Free Software Foundation – either version 2.1 of the license or any later version. The GEM-MACH version 3.1.0.0 code used by the RAQDPS023 can be downloaded from website <https://doi.org/10.5281/zenodo.15330612> (Savic-Jovicic et al., 2025). Related documentation is also available on that website, including information about key input and configuration files and copies of several reports referenced in this paper. The GEM-MACH v3.1.1.2 source code for the RAQDPS024, an equivalent version to the RAQDPS023 that went into operation after a migration to a new ECCC high-performance computer system in June 2022, is available at <https://zenodo.org/records/13952893>.

The CFFEPS version 4.1 code was used by the RAQDPS-FW023 and RAQDPS-FW024. It is free software that can be redistributed and/or modified under the terms of the GNU Lesser General Public License, either version 2.1 or any later version, as published by the Free Software Foundation. It is available to download from website <https://doi.org/10.5281/zenodo.2579382> (Anderson and Chen, 2021).

### ***Supplement.***

The supplement related to this article is available on-line at <https://doi.org/10.5194/gmd-???>

### ***Author contributions.***

MDM was the science lead for the development of the RAQDPS from the RAQDPS001 up to RAQDPS023 and co-supervisor of all operational deliveries over that period. He conceived and prepared the original and final drafts of this paper. VSJ was the RAQDPS code librarian, lead tester for RAQDPS development, and contributed to the original draft of the manuscript. CAS was the science lead for the development and co-supervisor for the operational deliveries of RAQDPS024 and RAQDPS025. SM was co-supervisor of many operational deliveries of the RAQDPS with assistance from KM and RMA on testing and evaluation. WG, CAS, SM, AA, VSJ, and MDM contributed to the development of different versions of the GEM-MACH code. JZ and QZ were responsible for emissions processing and the preparation of the SET4.0.0 emission input files and contributed to Table 9. JC and AA worked on



RAQDPS-FW and CFFEPS development. AL focused on model performance evaluation and contributed to the original draft of the manuscript. Lastly, VSJ, CAS, WG, JZ, JC, SM, RMA, QZ, and AL reviewed the manuscript.

#### 1955 *Competing interests.*

The authors declare that they have no conflict of interest.

#### *Acknowledgements.*

We are deeply indebted to many colleagues in the Meteorological Research Branch and the Canadian Meteorological Centre of ECCC for their work over many years on the development and operational implementation of the GEM numerical weather prediction model. We would like to thank many people who contributed in some way to the development, evaluation, and implementation of various versions of the RAQDPS and its downstream systems. They include the following current or former ECCC colleagues: David Anselmo, Stavros Antonopoulos, Paul-André Beaulieu, Véronique Bouchet, Elisa Boutzis, Stéphane Chamberland, Shawn Corvec, Sophie Cousineau, Louis-Philippe Crevier, Didier Davignon, Jean de Grandpré, Annie Duhamel, Amin Erfani, Nicolas Gasset, Samuel Gilbert, Sunling Gong, Ping Huang, Irena Ivanova, Alexander Kallaur, Setigui Keita, Dragana Kornic, Hugo Landry, Patrick Manseau, Ron McTaggart-Cowan, Richard Ménard, Thomas Milewski, Richard Moffet, Jacques Montpetit, Heather Morrison, Balbir Pabla, Alain Patoine, Radenko Pavlovic, Diane Pendlebury, Si-Jun Peng, Alain Robichaud, Jacinthe Racine, Matt Reszka, Mourad Sassi, Leo Separovic, Donald Talbot, Kenjiro Toyota, Ayrton Zadra, and Yulia Zaitseva. Many thanks are also due to Kerry Anderson, Peter Englefield, and Dan Thompson of the Canadian Forest Service for their help with the CWFIS and CFFEPS, to Susan O'Neill and Tara Strand of the U.S. Forest Service for their assistance with FEPS, and to Sarah Henderson of the University of British Columbia for collaborating on FireWork analysis. Jérôme Alary, Marc Deslauriers, Francois Lavallée, Anne Monette, David Niemi, Steve Smyth, Brett Taylor, and Shawn Tobin of the ECCC Science Reporting and Assessment Directorate helped us in many ways with accessing, preparing, and processing modelling versions of multiple Canadian national emissions inventories. We very much appreciate the considerable help with modelling versions of various U.S. national emission inventories that we have received over many years from Alison Eyth and George Pouliot of the U.S. EPA. We also acknowledge our continuing access to NRT surface AQ measurements provided by Canada's National Air Pollutant Surveillance network and its provincial, territorial, and regional government partners and by the U.S. EPA AIRNow metanetwork and its state and local, tribal, federal, Canadian, and Mexican partners and to MODIS and VIIRS imagery provided by NOAA and NASA. MDM would also like to thank Paul Makar of ECCC for his many contributions to the development of GEM-MACH, Sylvie Gravel, now retired from ECCC, for her many contributions to the development of GEM-MACH and for reviewing the manuscript, Ron McTaggart-Cowan of ECCC for reviewing the manuscript, and Rosa Wu of ECCC for her unstinting support of this project over multiple years.



## 1985 References

- Akagi, S. K., Yokelson, R. J., Wiedinmyer, C., Alvarado, M. J., Reid, J. S., Karl, T., Crounse, J. D., and Wennberg, P. O.: Emission factors for open and domestic biomass burning for use in atmospheric models, *Atmospheric Chem. Phys.*, 11, 4039–4072, <https://doi.org/10.5194/acp-11-4039-2011>, 2011.
- 1990 Akingunola, A., Makar, P. A., Zhang, J., Darlington, A., Li, S.-M., Gordon, M., Moran, M. D., and Zheng, Q.: A chemical transport model study of plume-rise and particle size distribution for the Athabasca oil sands, *Atmospheric Chem. Phys.*, 18, 8667–8688, <https://doi.org/10.5194/acp-18-8667-2018>, 2018.
- Anderson, K. and Chen, J.: Canadian Fire Emissions Prediction System (CFFEPS) v4.1, Zenodo [software], <https://doi.org/10.5281/zenodo.2579382>, 2021.
- 1995 Anderson, G. K., Sandberg, D. V., and Norhelm, R. A.: Fire Emission Production Simulator (FEPS) User's Guide Version 1., Pacific Northwest Research Station, U.S. Forest Service, Portland, Oregon, January, 97 pp., [http://www.fs.usda.gov/pnw/fera/feps/FEPS\\_users\\_guide.pdf](http://www.fs.usda.gov/pnw/fera/feps/FEPS_users_guide.pdf), 2004.
- Andreae, M. O.: Emission of trace gases and aerosols from biomass burning – an updated assessment, *Atmospheric Chem. Phys.*, 19, 8523–8546, <https://doi.org/10.5194/acp-19-8523-2019>, 2019.
- 2000 Ansari, A. S. and Pandis, S. N.: Response of inorganic PM to precursor concentrations, *Environ. Sci. Technol.*, 32, 2706–2714, <https://doi.org/10.1021/es971130j>, 1998.
- Anselmo, D., Moran, M. D., Ménard, S., Bouchet, V., Makar, P., Gong, W., Kallaur, A., Beaulieu, P.-A., Landry, H., Stroud, C., Huang, P., Gong, S., and Talbot, D.: A new Canadian air quality forecast model: GEM-MACH15, in: *Proc. 12th AMS Conf. on Atmos. Chem.*, Jan. 17-21, Atlanta, Georgia, 6 pp., <https://ams.confex.com/ams/pdfpapers/165388.pdf>, 2010.
- 2005 Antonopoulos, S., Bourgoquin, P., Montpetit, J., and Croteau, G.: Forecasting O<sub>3</sub>, PM<sub>2.5</sub> and NO<sub>2</sub> hourly spot concentrations using an updatable MOS methodology, in: *Air Pollution Modeling and its Application XXI*, edited by: Steyn, D. G. and Trini Castelli, S., Springer Netherlands, Dordrecht, 309–314, [https://doi.org/10.1007/978-94-007-1359-8\\_53](https://doi.org/10.1007/978-94-007-1359-8_53), 2011.
- Aranami, K., Davies, T., and Wood, N.: A mass restoration scheme for limited-area models with semi-Lagrangian advection, *Q. J. R. Meteorol. Soc.*, 141, 1795–1803, <https://doi.org/10.1002/qj.2482>, 2015.
- 2010 Archibald, A. T., Neu, J. L., Elshorbany, Y. F., Cooper, O. R., Young, P. J., Akiyoshi, H., Cox, R. A., Coyle, M., Derwent, R. G., Deushi, M., Finco, A., Frost, G. J., Galbally, I. E., Gerosa, G., Granier, C., Griffiths, P. T., Hossaini, R., Hu, L., Jöckel, P., Josse, B., Lin, M. Y., Mertens, M., Morgenstern, O., Naja, M., Naik, V., Oltmans, S., Plummer, D. A., Revell, L. E., Saiz-Lopez, A., Saxena, P., Shin, Y. M., Shahid, I., Shallcross, D., Tilmes, S., Trickl, T., Wallington, T. J., Wang, T., Worden, H. M., and Zeng, G.: Tropospheric Ozone Assessment Report: A critical review of changes in the tropospheric ozone burden and budget from 1850 to 2100, *Elem. Sci. Anthr.*, 8, 034, <https://doi.org/10.1525/elementa.2020.034>, 2020.
- 2015 Atkinson, R.: Gas-phase tropospheric chemistry of organic compounds: A review, *Atmospheric Environ. Part Gen. Top.*, 24, 1–41, [https://doi.org/10.1016/0960-1686\(90\)90438-S](https://doi.org/10.1016/0960-1686(90)90438-S), 1990.
- Atkinson, R., Baulch, D. L., Cox, R. A., Hampson, R. F., Kerr, J. A., and Troe, J.: Evaluated kinetic and photochemical data for atmospheric chemistry: Supplement IV. IUPAC subcommittee on gas kinetic data evaluation for atmospheric chemistry, *J. Phys. Chem. Ref. Data*, 21, 1125–1568, <https://doi.org/10.1063/1.555918>, 1992.
- 2020 Ault, A. P., Moffet, R. C., Baltrusaitis, J., Collins, D. B., Ruppel, M. J., Cuadra-Rodriguez, L. A., Zhao, D., Guasco, T. L., Ebben, C. J., Geiger, F. M., Bertram, T. H., Prather, K. A., and Grassian, V. H.: Size-dependent changes in sea spray aerosol composition and properties with different seawater conditions, *Environ. Sci. Technol.*, 47, 5603–5612, <https://doi.org/10.1021/es400416g>, 2013.
- 2025 Baklanov, A. and Zhang, Y.: Advances in air quality modeling and forecasting, *Glob. Transit.*, 2, 261–270, <https://doi.org/10.1016/j.glt.2020.11.001>, 2020.
- Barrie, L. A. and Georgii, H. W.: An experimental investigation of the absorption of sulphur dioxide by water drops containing heavy metal ions, *Atmospheric Environ.* 1967, 10, 743–749, [https://doi.org/10.1016/0004-6981\(76\)90075-5](https://doi.org/10.1016/0004-6981(76)90075-5), 1976.



- 2030 Barrie, L. A., Yi, Y., Leaitch, W. R., Lohmann, U., Kasibhatla, P., Roelofs, G.-J., Wilson, J., Mcgovern, F., Benkovitz, C., Mélières, M. A., Law, K., Prospero, J., Kritz, M., Bergmann, D., Bridgeman, C., Chin, M., Christensen, J., Easter, R., Feichter, J., Land, C., Jeuken, A., Kjellström, E., Koch, D., and Rasch, P.: A comparison of large-scale atmospheric sulphate aerosol models (COSAM): overview and highlights, *Tellus B Chem. Phys. Meteorol.*, 53, 615, <https://doi.org/10.3402/tellusb.v53i5.16642>, 2001.
- Barsanti, K. C., Carlton, A. G., and Chung, S. H.: Analyzing experimental data and model parameters: implications for predictions of SOA using chemical transport models, *Atmospheric Chem. Phys.*, 13, 12073–12088, <https://doi.org/10.5194/acp-13-12073-2013>, 2013.
- 2035 Barth, M. C., Rasch, P. J., Kiehl, J. T., Benkovitz, C. M., and Schwartz, S. E.: Sulfur chemistry in the National Center for Atmospheric Research Community Climate Model: Description, evaluation, features, and sensitivity to aqueous chemistry, *J. Geophys. Res. Atmospheres*, 105, 1387–1415, <https://doi.org/10.1029/1999JD900773>, 2000.
- Bauer, P., Thorpe, A., and Brunet, G.: The quiet revolution of numerical weather prediction, *Nature*, 525, 47–55, <https://doi.org/10.1038/nature14956>, 2015.
- 2040 Beard, K. V.: Terminal velocity and shape of cloud and precipitation drops aloft, *J. Atmospheric Sci.*, 33, 851–864, [https://doi.org/10.1175/1520-0469\(1976\)033<0851:TVASOC>2.0.CO;2](https://doi.org/10.1175/1520-0469(1976)033<0851:TVASOC>2.0.CO;2), 1976.
- Beaudoin, A., Bernier, P. Y., Guindon, L., Villemaire, P., Guo, X. J., Stinson, G., Bergeron, T., Magnussen, S., and Hall, R. J.: Mapping attributes of Canada’s forests at moderate resolution through *k*NN and MODIS imagery, *Can. J. For. Res.*, 44, 521–532, <https://doi.org/10.1139/cjfr-2013-0401>, 2014.
- 2045 Bechtold, P., Bazile, E., Guichard, F., Mascart, P., and Richard, E.: A mass-flux convection scheme for regional and global models, *Q. J. R. Meteorol. Soc.*, 127, 869–886, <https://doi.org/10.1002/qj.49712757309>, 2001.
- Bechtold, P., Semane, N., Lopez, P., Chaboureau, J.-P., Beljaars, A., and Bormann, N.: Representing equilibrium and nonequilibrium convection in large-scale models, *J. Atmospheric Sci.*, 71, 734–753, <https://doi.org/10.1175/JAS-D-13-0163.1>, 2014.
- 2050 Bélair, S., Mailhot, J., Strapp, J. W., and MacPherson, J. I.: An examination of local versus nonlocal aspects of a TKE-based boundary layer scheme in clear convective conditions, *J. Appl. Meteorol.*, 38, 1499–1518, [https://doi.org/10.1175/1520-0450\(1999\)038<1499:AEOLVN>2.0.CO;2](https://doi.org/10.1175/1520-0450(1999)038<1499:AEOLVN>2.0.CO;2), 1999.
- 2055 Bélair, S., Crevier, L.-P., Mailhot, J., Bilodeau, B., and Delage, Y.: Operational implementation of the ISBA land surface scheme in the Canadian regional weather forecast model. Part I: Warm season results, *J. Hydrometeorol.*, 4, 352–370, [https://doi.org/10.1175/1525-7541\(2003\)4<352:OIOTIL>2.0.CO;2](https://doi.org/10.1175/1525-7541(2003)4<352:OIOTIL>2.0.CO;2), 2003a.
- Bélair, S., Brown, R., Mailhot, J., Bilodeau, B., and Crevier, L.-P.: Operational implementation of the ISBA land surface scheme in the Canadian regional weather forecast model. Part II: Cold season results, *J. Hydrometeorol.*, 4, 371–386, [https://doi.org/10.1175/1525-7541\(2003\)4<371:OIOTIL>2.0.CO;2](https://doi.org/10.1175/1525-7541(2003)4<371:OIOTIL>2.0.CO;2), 2003b.
- 2060 Bélair, S., Mailhot, J., Girard, C., and Vaillancourt, P.: Boundary layer and shallow cumulus clouds in a medium-range forecast of a large-scale weather system, *Mon. Weather Rev.*, 133, 1938–1960, <https://doi.org/10.1175/MWR2958.1>, 2005.
- Beljaars, A. C. M. and Holtslag, A. A. M.: Flux parameterization over land surfaces for atmospheric models, *J. Appl. Meteorol.*, 30, 327–341, [https://doi.org/10.1175/1520-0450\(1991\)030<0327:FPOLSF>2.0.CO;2](https://doi.org/10.1175/1520-0450(1991)030<0327:FPOLSF>2.0.CO;2), 1991.
- 2065 Benedetti, A., Morcrette, J.-J., Boucher, O., Dethof, A., Engelen, R. J., Fisher, M., Flentje, H., Huneeus, N., Jones, L., Kaiser, J. W., Kinne, S., Mangold, A., Razinger, M., Simmons, A. J., and Suttie, M.: Aerosol analysis and forecast in the European Centre for Medium-Range Weather Forecasts Integrated Forecast System: 2. Data assimilation, *J. Geophys. Res.*, 114, D13205, <https://doi.org/10.1029/2008JD011115>, 2009.
- Benoit, R., Côté, J., and Mailhot, J.: Inclusion of a TKE boundary layer parameterization in the Canadian Regional Finite-Element Model, *Mon. Weather Rev.*, 117, 1726–1750, [https://doi.org/10.1175/1520-0493\(1989\)117<1726:IOATBL>2.0.CO;2](https://doi.org/10.1175/1520-0493(1989)117<1726:IOATBL>2.0.CO;2), 1989.
- 2070 Benoit, R., Desgagné, M., Pellerin, P., Pellerin, S., Chartier, Y., and Desjardins, S.: The Canadian MC2: A semi-Lagrangian, semi-implicit wideband atmospheric model suited for finescale process studies and simulation, *Mon. Weather Rev.*, 125, 2382–2415, [https://doi.org/10.1175/1520-0493\(1997\)125<2382:TCMASL>2.0.CO;2](https://doi.org/10.1175/1520-0493(1997)125<2382:TCMASL>2.0.CO;2), 1997.



- Bermejo, R. and Conde, J.: A conservative quasi-monotone semi-Lagrangian scheme, *Mon. Weather Rev.*, 130, 423–430, [https://doi.org/10.1175/1520-0493\(2002\)130<0423:ACQMSL>2.0.CO;2](https://doi.org/10.1175/1520-0493(2002)130<0423:ACQMSL>2.0.CO;2), 2002.
- 2075 Binkowski, F. S. and Roselle, S. J.: Models-3 Community Multiscale Air Quality (CMAQ) model aerosol component 1. Model description, *J. Geophys. Res. Atmospheres*, 108, 2001JD001409, <https://doi.org/10.1029/2001JD001409>, 2003.
- Binkowski, F. S. and Shankar, U.: The Regional Particulate Matter Model: 1. Model description and preliminary results, *J. Geophys. Res.*, 100, 26191, <https://doi.org/10.1029/95JD02093>, 1995.
- 2080 Binte Shahid, S., Lacey, F. G., Wiedinmyer, C., Yokelson, R. J., and Barsanti, K. C.: NEIVAv1.0: Next-generation Emissions Inventory expansion of Akagi et al. (2011) version 1.0, *Geosci. Model Dev.*, 17, 7679–7711, <https://doi.org/10.5194/gmd-17-7679-2024>, 2024.
- Bloom, S. C., Takacs, L. L., da Silva, A. M., and Ledvina, D.: Data assimilation using incremental analysis updates, *Mon. Weather Rev.*, 124, 1256–1271, [https://doi.org/10.1175/1520-0493\(1996\)124<1256:DAUIAU>2.0.CO;2](https://doi.org/10.1175/1520-0493(1996)124<1256:DAUIAU>2.0.CO;2), 1996.
- Boogaard, H., Walker, K., and Cohen, A. J.: Air pollution: the emergence of a major global health risk factor, *Int. Health*, 11, 417–421, <https://doi.org/10.1093/inthealth/ihz078>, 2019.
- 2085 Boutzis, E. I., Zhang, J., and Moran, M. D.: Expansion of a size disaggregation profile library for particulate matter emissions processing from three generic profiles to 36 source-type-specific profiles, *J. Air Waste Manag. Assoc.*, 70, 1067–1100, <https://doi.org/10.1080/10962247.2020.1743794>, 2020.
- Brasseur, G. P. and Kumar, R.: Chemical weather and chemical climate, *AGU Adv.*, 2, e2021AV000399, <https://doi.org/10.1029/2021AV000399>, 2021.
- 2090 Brasseur, G. P., Xie, Y., Petersen, A. K., Bouarar, I., Flemming, J., Gauss, M., Jiang, F., Kouznetsov, R., Kranenburg, R., Mijling, B., Peuch, V.-H., Pommier, M., Segers, A., Sofiev, M., Timmermans, R., van der A, R., Walters, S., Xu, J., and Zhou, G.: Ensemble forecasts of air quality in eastern China – Part 1: Model description and implementation of the MarcoPolo–Panda prediction system, version 1, *Geosci. Model Dev.*, 12, 33–67, <https://doi.org/10.5194/gmd-12-33-2019>, 2019.
- 2095 Briggs, G. A.: Plume rise and buoyancy effects, in: *Atmospheric Sciences and Power Production, DOE/TIC-27601 (DE84005177)*, edited by D. Randerson, Technical Information Center, U.S. Department of Energy, Oak Ridge, Tennessee, 327–366, 1984.
- Brook, J. R. and Dann, T. F.: Contribution of nitrate and carbonaceous species to PM<sub>2.5</sub> observed in Canadian cities, *J. Air Waste Manag. Assoc.*, 49, 193–199, <https://doi.org/10.1080/10473289.1999.10463794>, 1999.
- 2100 Brook, J. R., Zhang, L., Di-Giovanni, F., and Padro, J.: Description and evaluation of a model of deposition velocities for routine estimates of air pollutant dry deposition over North America., *Atmos. Environ.*, 33, 5037–5051, [https://doi.org/10.1016/S1352-2310\(99\)00250-2](https://doi.org/10.1016/S1352-2310(99)00250-2), 1999a.
- Brook, J. R., Dann, T. F., and Bonvalot, Y.: Observations and interpretations from the Canadian Fine Particle Monitoring Program, *J. Air Waste Manag. Assoc.*, 49, 35–44, <https://doi.org/10.1080/10473289.1999.10463884>, 1999b.
- Brost, R. A.: The sensitivity to input parameters of atmospheric concentrations simulated by a regional chemical model, *J. Geophys. Res.*, 93, 2371, <https://doi.org/10.1029/JD093iD03p02371>, 1988.
- 2105 Buehner, M., McTaggart-Cowan, R., Beaulne, A., Charette, C., Garand, L., Heilliette, S., Lapalme, E., Laroche, S., Macpherson, S. R., Morneau, J., and Zadra, A.: Implementation of deterministic weather forecasting systems based on ensemble–variational data assimilation at Environment Canada. Part I: The global system, *Mon. Weather Rev.*, 143, 2532–2559, <https://doi.org/10.1175/MWR-D-14-00354.1>, 2015.
- 2110 Calvert, J. G., Su, F., Bottenheim, J. W., and Strausz, O. P.: Mechanism of the homogeneous oxidation of sulfur dioxide in the troposphere, *Atmospheric Environ.* 1967, 12, 197–226, [https://doi.org/10.1016/0004-6981\(78\)90201-9](https://doi.org/10.1016/0004-6981(78)90201-9), 1978.
- Campbell, P. C., Tang, Y., Lee, P., Baker, B., Tong, D., Saylor, R., Stein, A., Huang, J., Huang, H.-C., Strobach, E., McQueen, J., Pan, L., Stajner, I., Sims, J., Tirado-Delgado, J., Jung, Y., Yang, F., Spero, T. L., and Gilliam, R. C.: Development and evaluation of an advanced National Air Quality Forecasting Capability using the NOAA Global Forecast System version 16, *Geosci. Model Dev.*, 15, 3281–3313, <https://doi.org/10.5194/gmd-15-3281-2022>, 2022.



- 2115 Caron, J.-F., Milewski, T., Buehner, M., Fillion, L., Reszka, M., Macpherson, S., and St-James, J.: Implementation of deterministic weather forecasting systems based on ensemble–variational data assimilation at Environment Canada. Part II: The regional system, *Mon. Weather Rev.*, 143, 2560–2580, <https://doi.org/10.1175/MWR-D-14-00353.1>, 2015.
- Carter, W. P. L.: A detailed mechanism for the gas-phase atmospheric reactions of organic compounds, *Atmospheric Environ. Part Gen. Top.*, 24, 481–518, [https://doi.org/10.1016/0960-1686\(90\)90005-8](https://doi.org/10.1016/0960-1686(90)90005-8), 1990.
- 2120 Chai, T., Kim, H., Pan, L., Lee, P., and Tong, D.: Impact of Moderate Resolution Imaging Spectroradiometer aerosol optical depth and AirNow PM<sub>2.5</sub> assimilation on Community Multi-scale Air Quality aerosol predictions over the contiguous United States, *J. Geophys. Res. Atmospheres*, 122, 5399–5415, <https://doi.org/10.1002/2016JD026295>, 2017.
- Chang, J. S., Brost, R. A., Isaksen, I. S. A., Madronich, S., Middleton, P., Stockwell, W. R., and Walcek, C. J.: A three-dimensional Eulerian acid deposition model: Physical concepts and formulation, *J. Geophys. Res.*, 92, 14681, <https://doi.org/10.1029/JD092iD12p14681>, 1987.
- 2125 Charron, M., Manzini, E., and Warner, C. D.: Intercomparison of gravity wave parameterizations: Hines Doppler-spread and Warner and McIntyre ultra-simple schemes., *J. Meteorol. Soc. Jpn. Ser II*, 80, 335–345, <https://doi.org/10.2151/jmsj.80.335>, 2002.
- Chen, J. and Menelaou, K.: Regional Air Quality Deterministic Prediction System with near-real-time wildfire emissions (RAQDPSFW): Upgrade to version 023, Technical note, November, Canadian Centre for Meteorological and Environmental Prediction, Montreal, 31 pp., [https://collaboration.cmc.ec.gc.ca/cmc/CMOI/product\\_guide/docs/tech\\_notes/technote\\_raqdpsfw\\_e.pdf](https://collaboration.cmc.ec.gc.ca/cmc/CMOI/product_guide/docs/tech_notes/technote_raqdpsfw_e.pdf), 2021.
- 2130 Chen, J., Moran, M. D., Pavlovic, R., and Munoz-Alpizar, R.: RAQDPS-FireWork v20.2 (RAQDPS020.2FW): Operational version of the Regional Air Quality Deterministic Prediction System with near-real-time wildfire emissions from the Canadian Forest Fire Emission Prediction System (CFFEPS), Technical note, April, Canadian Centre for Meteorological and Environmental Prediction, Montreal, 14 pp., [https://collaboration.cmc.ec.gc.ca/cmc/cmoei/product\\_guide/docs/tech\\_notes/technote\\_raqdps020.2fw\\_20190415\\_e.pdf](https://collaboration.cmc.ec.gc.ca/cmc/cmoei/product_guide/docs/tech_notes/technote_raqdps020.2fw_20190415_e.pdf), 2019a.
- 2135 Chen, J., Anderson, K., Pavlovic, R., Moran, M. D., Englefield, P., Thompson, D. K., Munoz-Alpizar, R., and Landry, H.: The FireWork v2.0 air quality forecast system with biomass burning emissions from the Canadian Forest Fire Emissions Prediction System v2.03, *Geosci. Model Dev.*, 12, 3283–3310, <https://doi.org/10.5194/gmd-12-3283-2019>, 2019b.
- 2140 Chen, J., Pendlebury, D., Gravel, S., Stroud, C., Ivanova, I., de Grandpre, J., and Plummer, D.: Development and current status of the GEM-MACH-Global modelling system at the Environment and Climate Change Canada, in: *Air Pollution Modeling and its Application XXVI*, edited by: Mensink, C., Gong, W., and Hakami, A., Springer International Publishing, Cham, [https://doi.org/10.1007/978-3-030-22055-6\\_18](https://doi.org/10.1007/978-3-030-22055-6_18), 107–112, 2020.
- 2145 Chow, J. C.: Measurement methods to determine compliance with ambient air quality standards for suspended particles, *J. Air Waste Manag. Assoc.*, 45, 320–382, <https://doi.org/10.1080/10473289.1995.10467369>, 1995.
- Chow, J. C., Lowenthal, D. H., Chen, L.-W. A., Wang, X., and Watson, J. G.: Mass reconstruction methods for PM<sub>2.5</sub>: a review, *Air Qual. Atmosphere Health*, 8, 243–263, <https://doi.org/10.1007/s11869-015-0338-3>, 2015.
- Chow, J. C., Watson, J. G., Green, M. C., Wang, X., Chen, L.-W. A., Trimble, D. L., Cropper, P. M., Kohl, S. D., and Gronstal, S. B.: Separation of brown carbon from black carbon for IMPROVE and Chemical Speciation Network PM<sub>2.5</sub> samples, *J Air Waste Manag Assoc*, 68, 494–510, <https://doi.org/10.1080/10962247.2018.1426653>, 2018.
- 2150 Clark, T. L., Voldner, E. C., Dennis, R. L., Seilkop, S. K., Alvo, M., and Olson, M. P.: The evaluation of long-term sulfur deposition models, *Atmospheric Environ.* 1967, 23, 2267–2288, [https://doi.org/10.1016/0004-6981\(89\)90189-3](https://doi.org/10.1016/0004-6981(89)90189-3), 1989.
- Clifton, O. E., Fiore, A. M., Massman, W. J., Baublitz, C. B., Coyle, M., Emberson, L., Fares, S., Farmer, D. K., Gentine, P., Gerosa, G., Guenther, A. B., Helmig, D., Lombardozzi, D. L., Munger, J. W., Patton, E. G., Pusede, S. E., Schwede, D. B., Silva, S. J., Sörgel, M., Steiner, A. L., and Tai, A. P. K.: Dry deposition of ozone over land: Processes, measurement, and modeling, *Rev. Geophys.*, 58, <https://doi.org/10.1029/2019RG000670>, 2020.
- 2155 Clifton, O. E., Schwede, D., Hogrefe, C., Bash, J. O., Bland, S., Cheung, P., Coyle, M., Emberson, L., Flemming, J., Fredj, E., Galmarini, S., Ganzeveld, L., Gazetas, O., Goded, I., Holmes, C. D., Horváth, L., Huijnen, V., Li, Q., Makar, P. A., Mammarella, I., Manca, G., Munger, J. W., Pérez-Camanyo, J. L., Pleim, J., Ran, L., San Jose, R., Silva, S. J., Staebler, R., Sun, S., Tai, A. P.



- 2160 K., Tas, E., Vesala, T., Weidinger, T., Wu, Z., and Zhang, L.: A single-point modeling approach for the intercomparison and evaluation of ozone dry deposition across chemical transport models (Activity 2 of AQMEII4), *Atmospheric Chem. Phys.*, 23, 9911–9961, <https://doi.org/10.5194/acp-23-9911-2023>, 2023.
- CMC-GDPS-8.0.0: Changes to the Global Deterministic Prediction System from version 7.1.0 to version 8.0.0, Technical note, December, Canadian Centre for Meteorological and Environmental Prediction, Montreal, 112 pp., [http://collaboration.cmc.ec.gc.ca/cmc/cmoe/product\\_guide/docs/tech\\_notes/technote\\_gdps-800\\_e.pdf](http://collaboration.cmc.ec.gc.ca/cmc/cmoe/product_guide/docs/tech_notes/technote_gdps-800_e.pdf), 2021a.
- 2165 CMC-GDPS-8.0.0: The Global Deterministic Prediction System (GDPS) version 8.0.0 of the Meteorological Service (MSC) of Canada: Technical specifications document, December, Canadian Centre for Meteorological and Environmental Prediction, Montreal, 14 pp., [https://collaboration.cmc.ec.gc.ca/cmc/cmoe/product\\_guide/docs/tech\\_specifications/tech\\_specifications\\_GDPS\\_8.0.0\\_e.pdf](https://collaboration.cmc.ec.gc.ca/cmc/cmoe/product_guide/docs/tech_specifications/tech_specifications_GDPS_8.0.0_e.pdf), 2021b.
- 2170 CMC-RAQDPS-023: The Regional Air Quality Deterministic Prediction System (RAQDPS) version 023 and the Regional Air Quality Deterministic Prediction System with Near-Real-Time Wildfire Emissions (RAQDPSFW) version 023 of the Meteorological Service of Canada (MSC): Technical Specifications Document, November, Canadian Centre for Meteorological and Environmental Prediction, Montreal, 19 pp., [https://collaboration.cmc.ec.gc.ca/cmc/cmoe/product\\_guide/docs/tech\\_specifications/tech\\_specifications\\_RAQDPS\\_023\\_e.pdf](https://collaboration.cmc.ec.gc.ca/cmc/cmoe/product_guide/docs/tech_specifications/tech_specifications_RAQDPS_023_e.pdf), 2021.
- 2175 CMC-RAQDPS-025: The Regional Air Quality Deterministic Prediction System (RAQDPS): Upgrade from version 024 to version 025, June, Canadian Centre for Meteorological and Environmental Prediction, Montreal, 89 pp., [https://collaboration.cmc.ec.gc.ca/cmc/cmoe/product\\_guide/docs/tech\\_notes/technote\\_raqdps-v25\\_e.pdf](https://collaboration.cmc.ec.gc.ca/cmc/cmoe/product_guide/docs/tech_notes/technote_raqdps-v25_e.pdf), 2024.
- 2180 CMC-RDPS-6.0.0: Regional Deterministic Prediction System (RDPS): Update from version 5.1.0 to version 6.0.0, Technical note, December, Canadian Centre for Meteorological and Environmental Prediction, Montreal, 46 pp., [https://collaboration.cmc.ec.gc.ca/cmc/cmoe/product\\_guide/docs/tech\\_notes/technote\\_rdps-600\\_e.pdf](https://collaboration.cmc.ec.gc.ca/cmc/cmoe/product_guide/docs/tech_notes/technote_rdps-600_e.pdf), 2018.
- CMC-RDPS-8.0.0: Changes to the Regional Deterministic Prediction System (RDPS) from version 7.1.0 to version 8.0.0, Technical note, December, Canadian Centre for Meteorological and Environmental Prediction, Montreal, 36 pp., [https://collaboration.cmc.ec.gc.ca/cmc/cmoe/product\\_guide/docs/tech\\_notes/technote\\_rdps-800\\_e.pdf](https://collaboration.cmc.ec.gc.ca/cmc/cmoe/product_guide/docs/tech_notes/technote_rdps-800_e.pdf), 2021a.
- 2185 CMC-RDPS-8.0.0: The Regional Deterministic Prediction System (RDPS) version 8.0.0 of the Meteorological Service of Canada (MSC): Technical specifications document, December, Canadian Centre for Meteorological and Environmental Prediction, Montreal, 10 pp., [https://collaboration.cmc.ec.gc.ca/cmc/cmoe/product\\_guide/docs/tech\\_specifications/tech\\_specifications\\_RDPS\\_8.0.0\\_e.pdf](https://collaboration.cmc.ec.gc.ca/cmc/cmoe/product_guide/docs/tech_specifications/tech_specifications_RDPS_8.0.0_e.pdf), 2021b.
- 2190 CMC-RDPS-9.0.0: Changes to the Regional Deterministic Prediction System (RDPS) from version 8.0.0 to version 9.0.0, Technical note, June, Canadian Centre for Meteorological and Environmental Prediction, Montreal, 44 pp., [http://collaboration.cmc.ec.gc.ca/cmc/cmoe/product\\_guide/docs/tech\\_notes/technote\\_rdps-900\\_e.pdf](http://collaboration.cmc.ec.gc.ca/cmc/cmoe/product_guide/docs/tech_notes/technote_rdps-900_e.pdf), 2024.
- 2195 Côté, J., Gravel, S., Méthot, A., Patoine, A., Roch, M., and Staniforth, A.: The operational CMC–MRB Global Environmental Multiscale (GEM) model. Part I: Design considerations and formulation, *Mon. Weather Rev.*, 126, 1373–1395, [https://doi.org/10.1175/1520-0493\(1998\)126<1373:TOCMGE>2.0.CO;2](https://doi.org/10.1175/1520-0493(1998)126<1373:TOCMGE>2.0.CO;2), 1998a.
- 2200 Côté, J., Desmarais, J.-G., Gravel, S., Méthot, A., Patoine, A., Roch, M., and Staniforth, A.: The operational CMC–MRB Global Environmental Multiscale (GEM) model. Part II: Results, *Mon. Weather Rev.*, 126, 1397–1418, [https://doi.org/10.1175/1520-0493\(1998\)126<1397:TOCMGE>2.0.CO;2](https://doi.org/10.1175/1520-0493(1998)126<1397:TOCMGE>2.0.CO;2), 1998b.
- 2200 Dabek-Zlotorzynska, E., Dann, T. F., Kalyani Martinelango, P., Celso, V., Brook, J. R., Mathieu, D., Ding, L., and Austin, C. C.: Canadian National Air Pollution Surveillance (NAPS) PM<sub>2.5</sub> speciation program: Methodology and PM<sub>2.5</sub> chemical composition for the years 2003–2008, *Atmos. Environ.*, 45, 673–686, <https://doi.org/10.1016/j.atmosenv.2010.10.024>, 2011.
- Damian, V., Sandu, A., Damian, M., Potra, F., and Carmichael, G. R.: The kinetic preprocessor KPP—a software environment for solving chemical kinetics, *Comput. Chem. Eng.*, 26, 1567–1579, [https://doi.org/10.1016/S0098-1354\(02\)00128-X](https://doi.org/10.1016/S0098-1354(02)00128-X), 2002.
- 2205 Dave, J. V.: Development of programs for computing characteristics of ultraviolet radiation, NASA Report CR-139134, National Aeronautics and Space Administration, Goddard Space Flight Center, Greenbelt, Maryland, 34 pp., 1972.



- Davies, H. C.: A lateral boundary formulation for multi-level prediction models, *Q. J. R. Meteorol. Soc.*, 102, 405–418, <https://doi.org/10.1002/qj.49710243210>, 1976.
- 2210 Day, M., Pouliot, G., Hunt, S., Baker, K. R., Beardsley, M., Frost, G., Mobley, D., Simon, H., Henderson, B. B., Yelverton, T., and Rao, V.: Reflecting on progress since the 2005 NARSTO emissions inventory report, *J. Air Waste Manag. Assoc.*, 69, 1023–1048, <https://doi.org/10.1080/10962247.2019.1629363>, 2019.
- De Leeuw, G., Neele, F. P., Hill, M., Smith, M. H., and Vignati, E.: Production of sea spray aerosol in the surf zone, *J. Geophys. Res. Atmospheres*, 105, 29397–29409, <https://doi.org/10.1029/2000JD900549>, 2000.
- 2215 De Leeuw, G., Andreas, E. L., Anguelova, M. D., Fairall, C. W., Lewis, E. R., O’Dowd, C., Schulz, M., and Schwartz, S. E.: Production flux of sea spray aerosol, *Rev. Geophys.*, 49, 2010RG000349, <https://doi.org/10.1029/2010RG000349>, 2011.
- Delage, Y. and Girard, C.: Stability functions correct at the free convection limit and consistent for both the surface and Ekman layers, *Bound.-Layer Meteorol.*, 58, 19–31, <https://doi.org/10.1007/BF00120749>, 1992.
- 2220 DeMore, W. B., Golden, D. M., Hampson, R. F., Howard, C. J., Kurylo, M. J., Molina, M. J., Ravishankara, A. R., and Sander, S. P.: Chemical Kinetics and Photochemical Data for Use in Stratospheric Modeling: Evaluation Number 8, National Aeronautics and Space Administration, Jet Propulsion Laboratory, California Institute of Technology, 266 pp., 1987.
- Diamantakis, M.: Semi-Lagrangian techniques for atmospheric modelling : current state and future challenges, in: Proc. ECMWF Annual Seminar 2013: Recent developments in numerical methods for atmosphere and ocean modelling, Reading, England, 2–5 September, 183–200, 2013.
- 2225 Diamantakis, M. and Flemming, J.: Global mass fixer algorithms for conservative tracer transport in the ECMWF model, *Geosci. Model Dev.*, 7, 965–979, <https://doi.org/10.5194/gmd-7-965-2014>, 2014.
- Dimov, I., Farago, I., Havasi, A., and Zlatev, Z.: Different splitting techniques with application to air pollution models, *Int. J. Environ. Pollut.*, 32, 174, <https://doi.org/10.1504/IJEP.2008.017102>, 2008.
- Dodge, M.: Chemical oxidant mechanisms for air quality modeling: critical review, *Atmos. Environ.*, 34, 2103–2130, [https://doi.org/10.1016/S1352-2310\(99\)00461-6](https://doi.org/10.1016/S1352-2310(99)00461-6), 2000.
- 2230 Dong, X., Fu, J. S., Huang, K., Tong, D., and Zhuang, G.: Model development of dust emission and heterogeneous chemistry within the Community Multiscale Air Quality modeling system and its application over East Asia, *Atmospheric Chem. Phys.*, 16, 8157–8180, <https://doi.org/10.5194/acp-16-8157-2016>, 2016.
- Duhl, T. R., Helmig, D., and Guenther, A.: Sesquiterpene emissions from vegetation: a review, *Biogeosciences*, 5, 761–777, <https://doi.org/10.5194/bg-5-761-2008>, 2008.
- 2235 Dunker, A. M., Morris, R. E., Pollack, A. K., Schleyer, C. H., and Yarwood, G.: Photochemical modeling of the impact of fuels and vehicles on urban ozone using Auto/Oil Program data, *Environ. Sci. Technol.*, 30, 787–801, <https://doi.org/10.1021/es950175m>, 1996.
- ECCC: 1990–2015 Air Pollutant Emission Inventory Report, Environment and Climate Change Canada, Gatineau, Quebec, 97 pp., [https://publications.gc.ca/collections/collection\\_2017/eccc/En81-26-2015-eng.pdf](https://publications.gc.ca/collections/collection_2017/eccc/En81-26-2015-eng.pdf), 2016.
- 2240 ECCC: Canada’s Air Pollutant Emissions Inventory Report 1990–2019, Environment and Climate Change Canada, Gatineau, Quebec, 99 pp., [https://publications.gc.ca/collections/collection\\_2021/eccc/En81-30-2019-eng.pdf](https://publications.gc.ca/collections/collection_2021/eccc/En81-30-2019-eng.pdf), 2021.
- ECCC: Canada’s Air Pollutant Emissions Inventory Report 1990–2020, Environment and Climate Change Canada, Gatineau, Quebec, 111 pp., [https://publications.gc.ca/collections/collection\\_2022/eccc/En81-30-2020-eng.pdf](https://publications.gc.ca/collections/collection_2022/eccc/En81-30-2020-eng.pdf), 2022a.
- 2245 ECCC: National air pollutant trends, Environment and Climate Change Canada, WWW document, <https://www.canada.ca/en/environment-climate-change/services/environmental-indicators/air-pollutant-emissions.html>, 2022b.
- Eliassen, A. and Saltbones, J.: Decay and transformation rates of SO<sub>2</sub>, as estimated from emission data, trajectories and measured air concentrations, *Atmospheric Environ.* 1967, 9, 425–429, [https://doi.org/10.1016/0004-6981\(75\)90128-6](https://doi.org/10.1016/0004-6981(75)90128-6), 1975.



- 2250 Emmons, L. K., Walters, S., Hess, P. G., Lamarque, J.-F., Pfister, G. G., Fillmore, D., Granier, C., Guenther, A., Kinnison, D., Laepple, T., Orlando, J., Tie, X., Tyndall, G., Wiedinmyer, C., Baughcum, S. L., and Kloster, S.: Description and evaluation of the Model for Ozone and Related chemical Tracers, version 4 (MOZART-4), *Geosci. Model Dev.*, 3, 43–67, <https://doi.org/10.5194/gmd-3-43-2010>, 2010.
- 2255 Emmons, L. K., Schwantes, R. H., Orlando, J. J., Tyndall, G., Kinnison, D., Lamarque, J., Marsh, D., Mills, M. J., Tilmes, S., Bardeen, C., Buchholz, R. R., Conley, A., Gettelman, A., Garcia, R., Simpson, I., Blake, D. R., Meinardi, S., and Pétron, G.: The chemistry mechanism in the Community Earth System Model Version 2 (CESM2), *J. Adv. Model. Earth Syst.*, 12, <https://doi.org/10.1029/2019MS001882>, 2020.
- Environment and Climate Change Canada: Version 5.1 package for the Global Environmental Multiscale (GEM) model (ECCC-ASTD-MRD/gem: 5.1.0), Zenodo [software], <https://doi.org/10.5281/zenodo.17782580>, 2025.
- 2260 Fehsenfeld, F., Calvert, J., Fall, R., Goldan, P., Guenther, A. B., Hewitt, C. N., Lamb, B., Liu, S., Trainer, M., Westberg, H., and Zimmerman, P.: Emissions of volatile organic compounds from vegetation and the implications for atmospheric chemistry, *Glob. Biogeochem. Cycles*, 6, 389–430, <https://doi.org/10.1029/92GB02125>, 1992.
- Fillion, L., Tanguay, M., Lapalme, E., Denis, B., Desgagné, M., Lee, V., Ek, N., Liu, Z., Lajoie, M., Caron, J.-F., and Pagé, C.: The Canadian Regional Data Assimilation and Forecasting System, *Weather Forecast.*, 25, 1645–1669, <https://doi.org/10.1175/2010WAF2222401.1>, 2010.
- 2265 Fitzgerald, J. W., Hoppel, W. A., and Gelbard, F.: A one-dimensional sectional model to simulate multicomponent aerosol dynamics in the marine boundary layer: 1. Model description, *J. Geophys. Res. Atmospheres*, 103, 16085–16102, <https://doi.org/10.1029/98JD01019>, 1998.
- 2270 Flemming, J., Huijnen, V., Arteta, J., Bechtold, P., Beljaars, A., Blechschmidt, A.-M., Diamantakis, M., Engelen, R. J., Gaudel, A., Inness, A., Jones, L., Josse, B., Katragkou, E., Marecal, V., Peuch, V.-H., Richter, A., Schultz, M. G., Stein, O., and Tsikerdekis, A.: Tropospheric chemistry in the Integrated Forecasting System of ECMWF, *Geosci. Model Dev.*, 8, 975–1003, <https://doi.org/10.5194/gmd-8-975-2015>, 2015.
- Flemming, J., Benedetti, A., Inness, A., Engelen, R. J., Jones, L., Huijnen, V., Remy, S., Parrington, M., Suttie, M., Bozzo, A., Peuch, V.-H., Akritidis, D., and Katragkou, E.: The CAMS interim reanalysis of carbon monoxide, ozone and aerosol for 2003–2015, *Atmospheric Chem. Phys.*, 17, 1945–1983, <https://doi.org/10.5194/acp-17-1945-2017>, 2017.
- 2275 Flood, V. A., Strong, K., Whaley, C. H., Chen, J., Wunch, D., Drummond, J. R., Colebatch, O., Gillespie, L., and Mostafavi Pak, N.: The impact of the 2023 Canadian forest fires on air quality in southern Ontario, *J. Geophys. Res. Atmospheres*, 130, e2024JD042254, <https://doi.org/10.1029/2024JD042254>, 2025.
- Foley, K. M., Roselle, S. J., Appel, K. W., Bhave, P. V., Pleim, J. E., Otte, T. L., Mathur, R., Sarwar, G., Young, J. O., Gilliam, R. C., Nolte, C. G., Kelly, J. T., Gilliland, A. B., and Bash, J. O.: Incremental testing of the Community Multiscale Air Quality (CMAQ) modeling system version 4.7, *Geosci. Model Dev.*, 3, 205–226, <https://doi.org/10.5194/gmd-3-205-2010>, 2010.
- 2280 Foley, K. M., Pouliot, G. A., Eyth, A., Aldridge, M. F., Allen, C., Appel, K. W., Bash, J. O., Beardsley, M., Beidler, J., Choi, D., Farkas, C., Gilliam, R. C., Godfrey, J., Henderson, B. H., Hogrefe, C., Koplitz, S. N., Mason, R., Mathur, R., Misenis, C., Possiel, N., Pye, H. O. T., Reynolds, L., Roark, M., Roberts, S., Schwede, D. B., Seltzer, K. M., Sonntag, D., Talgo, K., Toro, C., Vukovich, J., Xing, J., and Adams, E.: 2002–2017 anthropogenic emissions data for air quality modeling over the United States, *Data Brief*, 47, 109022, 33 pp., <https://doi.org/10.1016/j.dib.2023.109022>, 2023.
- 2285 Foroutan, H., Young, J., Napelenok, S., Ran, L., Appel, K. W., Gilliam, R. C., and Pleim, J. E.: Development and evaluation of a physics-based windblown dust emission scheme implemented in the CMAQ modeling system, *J. Adv. Model. Earth Syst.*, 9, 585–608, <https://doi.org/10.1002/2016MS000823>, 2017.
- 2290 Fountoukis, C. and Nenes, A.: ISORROPIA II: a computationally efficient thermodynamic equilibrium model for  $K^+$ – $Ca^{2+}$ – $Mg^{2+}$ – $NH_4^+$ – $Na^+$ – $SO_4^{2-}$ – $NO_3^-$ – $Cl^-$ – $H_2O$  aerosols, *Atmospheric Chem. Phys.*, 7, 4639–4659, <https://doi.org/10.5194/acp-7-4639-2007>, 2007.
- Fu, J. S., Carmichael, G. R., Dentener, F., Aas, W., Andersson, C., Barrie, L. A., Cole, A., Galy-Lacaux, C., Geddes, J., Itahashi, S., Kanakidou, M., Labrador, L., Paulot, F., Schwede, D., Tan, J., and Vet, R.: Improving estimates of sulfur, nitrogen, and ozone total deposition through multi-model and measurement-model fusion approaches, *Environ. Sci. Technol.*, 56, 2134–2142, <https://doi.org/10.1021/acs.est.1c05929>, 2022.



- 2295 Fuchs, N. A. and Sutugin, A. G.: Chapter 3. Properties of high-dispersed aerosols, in: Topics in Current Aerosol Research, G. M. Hidy and J. R. Brock, Eds., Pergamon, Oxford, 29–55, <https://doi.org/10.1016/B978-0-08-016674-2.50006-6>, 1971.
- Fuentes, J. D., Gu, L., Lerdau, M., Atkinson, R., Baldocchi, D., Bottenheim, J. W., Ciccioli, P., Lamb, B., Geron, C., Guenther, A., Sharkey, T. D., and Stockwell, W.: Biogenic hydrocarbons in the atmospheric boundary layer: A review, *Bull. Am. Meteorol. Soc.*, 81, 1537–1575, [https://doi.org/10.1175/1520-0477\(2000\)081<1537:BHITAB>2.3.CO;2](https://doi.org/10.1175/1520-0477(2000)081<1537:BHITAB>2.3.CO;2), 2000.
- 2300 Fung, C. S., Misra, P. K., Bloxam, R., and Wong, S.: A numerical experiment on the relative importance of H<sub>2</sub>O<sub>2</sub> and O<sub>3</sub> in aqueous conversion of SO<sub>2</sub> to SO<sub>4</sub><sup>2-</sup>, *Atmospheric Environ. Part Gen. Top.*, 25, 411–423, [https://doi.org/10.1016/0960-1686\(91\)90312-U](https://doi.org/10.1016/0960-1686(91)90312-U), 1991.
- Fuzzi, S., Baltensperger, U., Carslaw, K., Decesari, S., Denier van der Gon, H., Facchini, M. C., Fowler, D., Koren, I., Langford, B., Lohmann, U., Nemitz, E., Pandis, S., Riipinen, I., Rudich, Y., Schaap, M., Slowik, J. G., Spracklen, D. V., Vignati, E., Wild, M., Williams, M., and Gilardoni, S.: Particulate matter, air quality and climate: lessons learned and future needs, *Atmospheric Chem. Phys.*, 15, 8217–8299, <https://doi.org/10.5194/acp-15-8217-2015>, 2015.
- 2305 Galmarini, S., Makar, P., Clifton, O. E., Hogrefe, C., Bash, J. O., Bellasio, R., Bianconi, R., Bieser, J., Butler, T., Ducker, J., Flemming, J., Hodzic, A., Holmes, C. D., Kioutsioukis, I., Kranenburg, R., Lupascu, A., Perez-Camanyo, J. L., Pleim, J., Ryu, Y.-H., San Jose, R., Schwede, D., Silva, S., and Wolke, R.: Technical note: AQMEII4 Activity I: evaluation of wet and dry deposition schemes as an integral part of regional-scale air quality models, *Atmospheric Chem. Phys.*, 21, 15663–15697, <https://doi.org/10.5194/acp-21-15663-2021>, 2021.
- 2310 Gelbard, F. and Seinfeld, J. H.: Simulation of multicomponent aerosol dynamics, *J. Colloid Interface Sci.*, 78, 485–501, [https://doi.org/10.1016/0021-9797\(80\)90587-1](https://doi.org/10.1016/0021-9797(80)90587-1), 1980.
- Geron, C. D., Guenther, A. B., and Pierce, T. E.: An improved model for estimating emissions of volatile organic compounds from forests in the eastern United States, *J. Geophys. Res.*, 99, 12773–12791, <https://doi.org/10.1029/94JD00246>, 1994.
- 2315 Gery, M. W., Whitten, G. Z., and Killus, J. P.: Development and testing of the CBM-IV (Carbon Bond Mechanism) for urban and regional modeling, Report no. EPA/600/3-88/012, U.S. Environmental Protection Agency, 434 pp., 1988.
- Gery, M. W., Whitten, G. Z., Killus, J. P., and Dodge, M. C.: A photochemical kinetics mechanism for urban and regional scale computer modeling, *J. Geophys. Res. Atmospheres*, 94, 12925–12956, <https://doi.org/10.1029/JD094iD10p12925>, 1989.
- 2320 Ghahreman, R., Gong, W., Beagley, S. R., Akingunola, A., Makar, P. A., and Leitch, W. R.: Modeling aerosol effects on liquid clouds in the summertime Arctic, *J. Geophys. Res. Atmospheres*, 126, e2021JD034962, <https://doi.org/10.1029/2021JD034962>, 2021.
- Ghahreman, R., Gong, W., Makar, P. A., Lupu, A., Cole, A., Banwait, K., Lee, C., and Akingunola, A.: Modeling below-cloud scavenging of size-resolved particles in GEM-MACHv3.1, *Geosci. Model Dev.*, 17, 685–707, <https://doi.org/10.5194/gmd-17-685-2024>, 2024.
- 2325 Giordano, L., Brunner, D., Flemming, J., Hogrefe, C., Im, U., Bianconi, R., Badia, A., Balzarini, A., Baró, R., Chemel, C., Curci, G., Forkel, R., Jiménez-Guerrero, P., Hirtl, M., Hodzic, A., Honzak, L., Jorba, O., Knote, C., Kuenen, J. J. P., Makar, P. A., Manders-Groot, A., Neal, L., Pérez, J. L., Pirovano, G., Pouliot, G., San José, R., Savage, N., Schröder, W., Sokhi, R. S., Syrakov, D., Torian, A., Tuccella, P., Werhahn, J., Wolke, R., Yahya, K., Žabkar, R., Zhang, Y., and Galmarini, S.: Assessment of the MACC reanalysis and its influence as chemical boundary conditions for regional air quality modeling in AQMEII-2, *Atmos. Environ.*, 115, 371–388, <https://doi.org/10.1016/j.atmosenv.2015.02.034>, 2015.
- 2330 Girard, C., Plante, A., Desgagné, M., McTaggart-Cowan, R., Côté, J., Charron, M., Gravel, S., Lee, V., Patoine, A., Qaddouri, A., Roch, M., Spacek, L., Tanguay, M., Vaillancourt, P. A., and Zadra, A.: Staggered vertical discretization of the Canadian Environmental Multiscale (GEM) model using a coordinate of the log-hydrostatic-pressure type, *Mon. Weather Rev.*, 142, 1183–1196, <https://doi.org/10.1175/MWR-D-13-00255.1>, 2014.
- 2335 Gong, S. L.: A parameterization of sea-salt aerosol source function for sub- and super-micron particles, *Glob. Biogeochem. Cycles*, 17, 2003GB002079, <https://doi.org/10.1029/2003GB002079>, 2003.
- Gong, S. L., Barrie, L. A., and Blanchet, J.-P.: Modeling sea-salt aerosols in the atmosphere: 1. Model development, *J. Geophys. Res. Atmospheres*, 102, 3805–3818, <https://doi.org/10.1029/96JD02953>, 1997a.



- 2340 Gong, S. L., Barrie, L. A., Prospero, J. M., Savoie, D. L., Ayers, G. P., Blanchet, J. -P., and Spacek, L.: Modeling sea-salt aerosols in the atmosphere: 2. Atmospheric concentrations and fluxes, *J. Geophys. Res. Atmospheres*, 102, 3819–3830, <https://doi.org/10.1029/96JD03401>, 1997b.
- Gong, S. L., Barrie, L. A., and Lazare, M.: Canadian Aerosol Module (CAM): A size-segregated simulation of atmospheric aerosol processes for climate and air quality models 2. Global sea-salt aerosol and its budgets, *J. Geophys. Res. Atmospheres*, 107, <https://doi.org/10.1029/2001JD002004>, 2002.
- 2345 Gong, S. L., Barrie, L. A., Blanchet, J.-P., von Salzen, K., Lohmann, U., Lesins, G., Spacek, L., Zhang, L., Girard, E., Lin, H., Leaitch, R., Leighton, H., Chylek, P., and Huang, P.: Canadian Aerosol Module: A size-segregated simulation of atmospheric aerosol processes for climate and air quality models 1. Module development, *J. Geophys. Res.*, 108, 4007, <https://doi.org/10.1029/2001JD002002>, 2003.
- 2350 Gong, W., Dastoor, A. P., Bouchet, V. S., Gong, S., Makar, P. A., Moran, M. D., Pabla, B., Ménard, S., Crevier, L.-P., Cousineau, S., and Venkatesh, S.: Cloud processing of gases and aerosols in a regional air quality model (AURAMS), *Atmospheric Res.*, 82, 248–275, <https://doi.org/10.1016/j.atmosres.2005.10.012>, 2006.
- Gong, W., Stroud, C., and Zhang, L.: Cloud processing of gases and aerosols in air quality modeling, *Atmosphere*, 2, 567–616, <https://doi.org/10.3390/atmos2040567>, 2011.
- 2355 Gong, W., Makar, P. A., Zhang, J., Milbrandt, J., Gravel, S., Hayden, K. L., Macdonald, A. M., and Leaitch, W. R.: Modelling aerosol–cloud–meteorology interaction: A case study with a fully coupled air quality model (GEM-MACH), *Atmos. Environ.*, 115, 695–715, <https://doi.org/10.1016/j.atmosenv.2015.05.062>, 2015.
- de Grandpré, J., Tanguay, M., Qaddouri, A., Zerroukat, M., and McLinden, C. A.: Semi-Lagrangian advection of stratospheric ozone on a Yin–Yang grid system, *Mon. Weather Rev.*, 144, 1035–1050, <https://doi.org/10.1175/MWR-D-15-0142.1>, 2016.
- 2360 Grell, G. and Baklanov, A.: Integrated modeling for forecasting weather and air quality: A call for fully coupled approaches, *Atmos. Environ.*, 45, 6845–6851, <https://doi.org/10.1016/j.atmosenv.2011.01.017>, 2011.
- Grell, G. A., Peckham, S. E., Schmitz, R., McKeen, S. A., Frost, G., Skamarock, W. C., and Eder, B.: Fully coupled “online” chemistry within the WRF model, *Atmos. Environ.*, 39, 6957–6975, <https://doi.org/10.1016/j.atmosenv.2005.04.027>, 2005.
- Grewe, V.: A generalized tagging method, *Geosci. Model Dev.*, 6, 247–253, <https://doi.org/10.5194/gmd-6-247-2013>, 2013.
- 2365 Griffin, D., McLinden, C. A., Racine, J., Moran, M. D., Fioletov, V., Pavlovic, R., Mashayekhi, R., Zhao, X., and Eskes, H.: Assessing the impact of Corona-Virus-19 on nitrogen dioxide levels over southern Ontario, Canada, *Remote Sens.*, 12, 4112, <https://doi.org/10.3390/rs12244112>, 2020.
- Griffin, R. J., Cocker, D. R., Flagan, R. C., and Seinfeld, J. H.: Organic aerosol formation from the oxidation of biogenic hydrocarbons, *J. Geophys. Res. Atmospheres*, 104, 3555–3567, <https://doi.org/10.1029/1998JD100049>, 1999.
- 2370 Gross, M., Wan, H., Rasch, P. J., Caldwell, P. M., Williamson, D. L., Klocke, D., Jablonowski, C., Thatcher, D. R., Wood, N., Cullen, M., Beare, B., Willett, M., Lemarié, F., Blayo, E., Malardel, S., Termonia, P., Gassmann, A., Lauritzen, P. H., Johansen, H., Zarzycki, C. M., Sakaguchi, K., and Leung, R.: Physics–dynamics coupling in weather, climate, and Earth system models: Challenges and recent progress, *Mon. Weather Rev.*, 146, 3505–3544, <https://doi.org/10.1175/MWR-D-17-0345.1>, 2018.
- Guenther, A., Zimmerman, P., and Wildermuth, M.: Natural volatile organic compound emission rate estimates for U.S. woodland landscapes, *Atmos. Environ.*, 28, 1197–1210, [https://doi.org/10.1016/1352-2310\(94\)90297-6](https://doi.org/10.1016/1352-2310(94)90297-6), 1994.
- 2375 Guenther, A., Hewitt, C. N., Erickson, D., Fall, R., Geron, C., Graedel, T., Harley, P., Klinger, L., Lerdau, M., McKay, W. A., Pierce, T., Scholes, B., Steinbrecher, R., Tallamraju, R., Taylor, J., and Zimmerman, P.: A global model of natural volatile organic compound emissions, *J. Geophys. Res.*, 100, 8873–8892, <https://doi.org/10.1029/94JD02950>, 1995.
- Guenther, A., Geron, C., Pierce, T., Lamb, B., Harley, P., and Fall, R.: Natural emissions of non-methane volatile organic compounds, carbon monoxide, and oxides of nitrogen from North America, *Atmos. Environ.*, 34, 2205–2230, [https://doi.org/10.1016/S1352-2310\(99\)00465-3](https://doi.org/10.1016/S1352-2310(99)00465-3), 2000.
- 2380



Guenther, A. B., Jiang, X., Heald, C. L., Sakulyanontvittaya, T., Duhl, T., Emmons, L. K., and Wang, X.: The Model of Emissions of Gases and Aerosols from Nature version 2.1 (MEGAN2.1): an extended and updated framework for modeling biogenic emissions, *Geosci. Model Dev.*, 5, 1471–1492, <https://doi.org/10.5194/gmd-5-1471-2012>, 2012.

2385 Hallquist, M., Wenger, J. C., Baltensperger, U., Rudich, Y., Simpson, D., Claeys, M., Dommen, J., Donahue, N. M., George, C., Goldstein, A. H., Hamilton, J. F., Herrmann, H., Hoffmann, T., Iinuma, Y., Jang, M., Jenkin, M. E., Jimenez, J. L., Kiendler-Scharr, A., Maenhaut, W., McFiggans, G., Mentel, Th. F., Monod, A., Prévôt, A. S. H., Seinfeld, J. H., Surratt, J. D., Szmigielski, R., and Wildt, J.: The formation, properties and impact of secondary organic aerosol: current and emerging issues, *Atmospheric Chem. Phys.*, 9, 5155–5236, <https://doi.org/10.5194/acp-9-5155-2009>, 2009.

2390 Hand, J. L., Gill, T. E., and Schichtel, B. A.: Spatial and seasonal variability in fine mineral dust and coarse aerosol mass at remote sites across the United States, *J. Geophys. Res. Atmospheres*, 122, 3080–3097, <https://doi.org/10.1002/2016JD026290>, 2017.

Hänel, G.: The properties of atmospheric aerosol particles as functions of the relative humidity at thermodynamic equilibrium with the surrounding moist air, in: *Advances in Geophysics*, vol. 19, Elsevier, 73–188, [https://doi.org/10.1016/S0065-2687\(08\)60142-9](https://doi.org/10.1016/S0065-2687(08)60142-9), 1976.

2395 Hanna, S. R., Russell, A. G., Wilkinson, J. G., Vukovich, J., and Hansen, D. A.: Monte Carlo estimation of uncertainties in BEIS3 emission outputs and their effects on uncertainties in chemical transport model predictions, *J. Geophys. Res.*, 110, D01302, 15 pp., <https://doi.org/10.1029/2004JD004986>, 2005.

Harrison, R. M., Holman, C. D., McCartney, H. A., and McIlveen, J. F. R.: Nocturnal depletion of photochemical ozone at a rural site, *Atmospheric Environ.* 1967, 12, 2021–2026, [https://doi.org/10.1016/0004-6981\(78\)90140-3](https://doi.org/10.1016/0004-6981(78)90140-3), 1978.

2400 Hayden, K. L., Li, S.-M., Liggio, J., Wheeler, M. J., Wentzell, J. J. B., Leithead, A., Brickell, P., Mittermeier, R. L., Oldham, Z., Mihele, C. M., Staebler, R. M., Moussa, S. G., Darlington, A., Wolde, M., Thompson, D., Chen, J., Griffin, D., Eckert, E., Ditto, J. C., He, M., and Gentner, D. R.: Reconciling the total carbon budget for boreal forest wildfire emissions using airborne observations, *Atmospheric Chem. Phys.*, 22, 12493–12523, <https://doi.org/10.5194/acp-22-12493-2022>, 2022.

2405 Heald, C. L., Jacob, D. J., Fiore, A. M., Emmons, L. K., Gille, J. C., Deeter, M. N., Warner, J., Edwards, D. P., Crawford, J. H., Hamlin, A. J., Sachse, G. W., Browell, E. V., Avery, M. A., Vay, S. A., Westberg, D. J., Blake, D. R., Singh, H. B., Sandholm, S. T., Talbot, R. W., and Fuelberg, H. E.: Asian outflow and trans-Pacific transport of carbon monoxide and ozone pollution: An integrated satellite, aircraft, and model perspective, *J. Geophys. Res. Atmospheres*, 108, 4804, <https://doi.org/10.1029/2003JD003507>, 2003.

2410 Hecht, T. A., Seinfeld, J. H., and Dodge, M. C.: Generalized kinetic mechanism for photochemical smog, *Environ. Sci. Technol.*, 8, 327–339, <https://doi.org/10.1021/es60089a004>, 1974.

Hegg, D. A.: Heterogeneous production of cloud condensation nuclei in the marine atmosphere, *Geophys. Res. Lett.*, 17, 2165–2168, <https://doi.org/10.1029/GL017i012p02165>, 1990.

Heintzenberg, J.: Fine particles in the global troposphere A review, *Tellus B Chem. Phys. Meteorol.*, 41, 149–160, <https://doi.org/10.3402/tellusb.v41i2.15064>, 1989.

2415 Hines, C. O.: Doppler-spread parameterization of gravity-wave momentum deposition in the middle atmosphere. Part 1: Basic formulation, *J. Atmospheric Sol.-Terr. Phys.*, 59, 371–386, [https://doi.org/10.1016/S1364-6826\(96\)00079-X](https://doi.org/10.1016/S1364-6826(96)00079-X), 1997a.

Hines, C. O.: Doppler-spread parameterization of gravity-wave momentum deposition in the middle atmosphere. Part 2: Broad and quasi monochromatic spectra, and implementation, *J. Atmospheric Sol.-Terr. Phys.*, 59, 387–400, [https://doi.org/10.1016/S1364-6826\(96\)00080-6](https://doi.org/10.1016/S1364-6826(96)00080-6), 1997b.

2420 Hogrefe, C., Galmarini, S., Makar, P. A., Kioutsioukis, I., Clifton, O. E., Alyuz, U., Bash, J. O., Bellasio, R., Bianconi, R., Butler, T., Cheung, P., Hodzic, A., Kranenburg, R., Lupascu, A., Momoh, K., Perez-Camanyo, J. L., Pleim, J. E., Ryu, Y.-H., San Jose, R., Schaap, M., Schwede, D. B., and Sokhi, R.: A diagnostic intercomparison of modeled ozone dry deposition over North America and Europe using AQMEII4 regional-scale simulations, <https://doi.org/10.5194/egusphere-2025-225>, 6 February 2025.

2425 Holdaway, D., Thuburn, J., and Wood, N.: Comparison of Lorenz and Charney-Phillips vertical discretisations for dynamics-boundary layer coupling. Part I: Steady states, *Q. J. R. Meteorol. Soc.*, 139, 1073–1086, <https://doi.org/10.1002/qj.2016.2013a>.



- Holdaway, D., Thuburn, J., and Wood, N.: Comparison of Lorenz and Charney-Phillips vertical discretisations for dynamics-boundary layer coupling. Part II: Transients, *Q. J. R. Meteorol. Soc.*, 139, 1087–1098, <https://doi.org/10.1002/qj.2017.2013b>.
- Husain, S. Z. and Girard, C.: Impact of consistent semi-Lagrangian trajectory calculations on numerical weather prediction performance, *Mon. Weather Rev.*, 145, 4127–4150, <https://doi.org/10.1175/MWR-D-17-0138.1>, 2017.
- 2430 Husain, S. Z., Girard, C., Qaddouri, A., and Plante, A.: A new dynamical core of the Global Environmental Multiscale (GEM) model with a height-based terrain-following vertical coordinate, *Mon. Weather Rev.*, 147, 2555–2578, <https://doi.org/10.1175/MWR-D-18-0438.1>, 2019.
- Inness, A., Blechschmidt, A.-M., Bouarar, I., Chabrillat, S., Crepulja, M., Engelen, R. J., Eskes, H., Flemming, J., Gaudel, A., Hendrick, F., Huijnen, V., Jones, L., Kapsomenakis, J., Katragkou, E., Keppens, A., Langerock, B., de Mazière, M., Melas, D., 2435 Parrington, M., Peuch, V. H., Razinger, M., Richter, A., Schultz, M. G., Suttie, M., Thouret, V., Vrekoussis, M., Wagner, A., and Zerefos, C.: Data assimilation of satellite-retrieved ozone, carbon monoxide and nitrogen dioxide with ECMWF's Composition-IFS, *Atmospheric Chem. Phys.*, 15, 5275–5303, <https://doi.org/10.5194/acp-15-5275-2015>, 2015.
- Inness, A., Ades, M., Agustí-Panareda, A., Barré, J., Benedictow, A., Blechschmidt, A.-M., Dominguez, J. J., Engelen, R., Eskes, H., Flemming, J., Huijnen, V., Jones, L., Kipling, Z., Massart, S., Parrington, M., Peuch, V.-H., Razinger, M., Remy, S., Schulz, 2440 M., and Suttie, M.: The CAMS reanalysis of atmospheric composition, *Atmospheric Chem. Phys.*, 19, 3515–3556, <https://doi.org/10.5194/acp-19-3515-2019>, 2019.
- Iversen, T. and Seland, Ø.: A scheme for process-tagged SO<sub>4</sub> and BC aerosols in NCAR CCM3: Validation and sensitivity to cloud processes, *J. Geophys. Res. Atmospheres*, 107, <https://doi.org/10.1029/2001JD000885>, 2002.
- Jacobson, M. Z.: Development and application of a new air pollution modeling system—II. Aerosol module structure and design, 2445 *Atmos. Environ.*, 31, 131–144, [https://doi.org/10.1016/1352-2310\(96\)00202-6](https://doi.org/10.1016/1352-2310(96)00202-6), 1997.
- Jacobson, M. Z.: *Fundamentals of Atmospheric Modeling*, 1st Ed., Cambridge University Press, Cambridge, UK, 656 pp., 1999.
- Jacobson, M. Z.: Strong radiative heating due to the mixing state of black carbon in atmospheric aerosols, *Nature*, 409, 695–697, <https://doi.org/10.1038/35055518>, 2001.
- Jacobson, M. Z., Turco, R. P., Jensen, E. J., and Toon, O. B.: Modeling coagulation among particles of different composition and 2450 size, *Atmos. Environ.*, 28, 1327–1338, [https://doi.org/10.1016/1352-2310\(94\)90280-1](https://doi.org/10.1016/1352-2310(94)90280-1), 1994.
- Jaffe, D., Bertschi, I., Jaegle, L., Novelli, P., Reid, J. S., Tanimoto, H., Vingarzan, R., and Westphal, D. L.: Long-range transport of Siberian biomass burning emissions and impact on surface ozone in western North America, *Geophys. Res. Lett.*, 31, L16106, 4 pp., <https://doi.org/10.1029/2004GL020093>, 2004.
- Jaffe, D. A., Miller, C., Thompson, K., Finley, B., Nelson, M., Ouimette, J., and Andrews, E.: An evaluation of the U.S. EPA's 2455 correction equation for PurpleAir sensor data in smoke, dust, and wintertime urban pollution events, *Atmospheric Meas. Tech.*, 16, 1311–1322, <https://doi.org/10.5194/amt-16-1311-2023>, 2023.
- Jenkin, M. E., Young, J. C., and Rickard, A. R.: The MCM v3.3.1 degradation scheme for isoprene, *Atmospheric Chem. Phys.*, 15, 11433–11459, <https://doi.org/10.5194/acp-15-11433-2015>, 2015.
- Jia, W. and Zhang, X.: Impact of modified turbulent diffusion of PM<sub>2.5</sub> aerosol in WRF-Chem simulations in eastern China, 2460 *Atmospheric Chem. Phys.*, 21, 16827–16841, <https://doi.org/10.5194/acp-21-16827-2021>, 2021.
- Jiang, L., Bessagnet, B., Meleux, F., Couvidat, F., Tognet, F., and Hu, J.: The role of vertical grid resolution and turbulent diffusion uncertainty on chemical transport modeling, *Atmospheric Res.*, 312, 107759, <https://doi.org/10.1016/j.atmosres.2024.107759>, 2024.
- Jiang, W.: Instantaneous secondary organic aerosol yields and their comparison with overall aerosol yields for aromatic and biogenic hydrocarbons, *Atmos. Environ.*, 37, 5439–5444, <https://doi.org/10.1016/j.atmosenv.2003.09.018>, 2003.
- 2465 Jiang, W.: Reply to the “Comment on ‘Instantaneous secondary organic aerosol yields and their comparison with overall aerosol yields for aromatic and biogenic hydrocarbons’”, by Knipping et al. (2004), *Atmos. Environ.*, 38, 2763–2767, <https://doi.org/10.1016/j.atmosenv.2004.02.018>, 2004.



- 2470 Jiang, W.: On the issues regarding instantaneous secondary organic aerosol yields raised by Yu (2005), *Atmos. Environ.*, 39, 7923–7926, <https://doi.org/10.1016/j.atmosenv.2005.07.075>, 2005.
- 2475 Jimenez, J. L., Canagaratna, M. R., Donahue, N. M., Prevot, A. S. H., Zhang, Q., Kroll, J. H., DeCarlo, P. F., Allan, J. D., Coe, H., Ng, N. L., Aiken, A. C., Docherty, K. S., Ulbrich, I. M., Grieshop, A. P., Robinson, A. L., Duplissy, J., Smith, J. D., Wilson, K. R., Lanz, V. A., Hueglin, C., Sun, Y. L., Tian, J., Laaksonen, A., Raatikainen, T., Rautiainen, J., Vaattovaara, P., Ehn, M., Kulmala, M., Tomlinson, J. M., Collins, D. R., Cubison, M. J., E., Dunlea, J., Huffman, J. A., Onasch, T. B., Alfarra, M. R., Williams, P. I., Bower, K., Kondo, Y., Schneider, J., Drewnick, F., Borrmann, S., Weimer, S., Demerjian, K., Salcedo, D., Cottrell, L., Griffin, R., Takami, A., Miyoshi, T., Hatakeyama, S., Shimono, A., Sun, J. Y., Zhang, Y. M., Dzepina, K., Kimmel, J. R., Sueper, D., Jayne, J. T., Herndon, S. C., Trimborn, A. M., Williams, L. R., Wood, E. C., Middlebrook, A. M., Kolb, C. E., Baltensperger, U., and Worsnop, D. R.: Evolution of organic aerosols in the atmosphere, *Science*, 326, 1525–1529, <https://doi.org/10.1126/science.1180353>, 2009.
- 2480 Jin, L., Brown, N. J., Harley, R. A., Bao, J.-W., Michelson, S. A., and Wilczak, J. M.: Seasonal versus episodic performance evaluation for an Eulerian photochemical air quality model, *J. Geophys. Res.*, 115, D09302, <https://doi.org/10.1029/2009JD012680>, 2010.
- Jones, A., Roberts, D. L., and Slingo, A.: A climate model study of indirect radiative forcing by anthropogenic sulphate aerosols, *Nature*, 370, 450–453, <https://doi.org/10.1038/370450a0>, 1994.
- 2485 Kageyama, A. and Sato, T.: The “Yin-Yang grid”: An overset grid in spherical geometry, *Geochem. Geophys. Geosystems*, 5, 15 pp., <https://doi.org/10.1029/2004GC000734>, 2004.
- Kain, J. S. and Fritsch, J. M.: A one-dimensional entraining/detraining plume model and its application in convective parameterization, *J. Atmospheric Sci.*, 47, 2784–2802, [https://doi.org/10.1175/1520-0469\(1990\)047<2784:AODEPM>2.0.CO;2](https://doi.org/10.1175/1520-0469(1990)047<2784:AODEPM>2.0.CO;2), 1990.
- 2490 Kain, J. S. and Fritsch, J. M.: The role of the convective ‘trigger’ function in numerical forecasts of mesoscale convective systems, *Meteorol. Atmospheric Phys.*, 49, 93–106, <https://doi.org/10.1007/BF01025402>, 1992.
- Karamchandani, P. and Venkatram, A.: The role of non-precipitating clouds in producing ambient sulfate during summer: Results from simulations with the Acid Deposition and Oxidant Model (ADOM), *Atmospheric Environ. Part Gen. Top.*, 26, 1041–1052, [https://doi.org/10.1016/0960-1686\(92\)90036-K](https://doi.org/10.1016/0960-1686(92)90036-K), 1992.
- 2495 Karamchandani, P., Lurmann, F., and Venkatram, A.: ADOM/TADAP Model Development Program: Volume 8. Central Operator, ERT Document P-B980-535, May, Environmental Research & Technology, Inc., Newbury Park, California, 136 pp., <https://doi.org/10.5281/zenodo.15330612>, 1985.
- Karamchandani, P., Vijayaraghavan, K., and Yarwood, G.: Sub-grid scale plume modeling, *Atmosphere*, 2, 389–406, <https://doi.org/10.3390/atmos2030389>, 2011.
- 2500 Kelly, J., Makar, P. A., and Plummer, D. A.: Projections of mid-century summer air-quality for North America: effects of changes in climate and precursor emissions, *Atmospheric Chem. Phys.*, 12, 5367–5390, <https://doi.org/10.5194/acp-12-5367-2012>, 2012.
- Kim, D., Chin, M., Cruz, C. A., Tong, D., and Yu, H.: Spring dust in western North America and its interannual variability—Understanding the role of local and transported dust, *J. Geophys. Res. Atmospheres*, 126, <https://doi.org/10.1029/2021JD035383>, 2021.
- 2505 Kim, Y. P., Seinfeld, J. H., and Saxena, P.: Atmospheric gas-aerosol equilibrium I. Thermodynamic model, *Aerosol Sci. Technol.*, 19, 157–181, <https://doi.org/10.1080/02786829308959628>, 1993.
- Kioutsoukis, I., Hogrefe, C., Makar, P. A., Alyuz, U., Bash, J. O., Bellasio, R., Bianconi, R., Buttler, T., Clifton, O. E., Cheung, P., Hodzic, A., Kranenburg, R., Lupascu, A., Momoh, K., Perez-Camaño, J. L., Pleim, J., Ryu, Y.-H., San Jose, R., Schwede, D., Sokhi, R., and Galmarini, S.: Operational and probabilistic evaluation of AQMEII-4 regional scale ozone dry deposition. Time to harmonise our LULC masks, <https://doi.org/10.5194/egusphere-2025-1091>, 19 March 2025.
- Kuhn, M., Builtjes, P. J. H., Poppe, D., Simpson, D., Stockwell, W. R., Andersson-Skold, Y., Baart, A., Das, M., Fiedler, F., Hov, Ø., Kirchner, F., Makar, P. A., Milford, J. B., Roemer, M. G. M., Ruhnke, R., Strand, A., Vogel, B., and Vogel, H.: Intercomparison



- of the gas-phase chemistry in several chemistry and transport models, *Atmos. Environ.*, 32, 693–709, [https://doi.org/10.1016/S1352-2310\(97\)00329-4](https://doi.org/10.1016/S1352-2310(97)00329-4), 1998.
- 2515 Kukkonen, J., Olsson, T., Schultz, D. M., Baklanov, A., Klein, T., Miranda, A. I., Monteiro, A., Hirtl, M., Tarvainen, V., Boy, M., Peuch, V.-H., Poupkou, A., Kioutsioukis, I., Finardi, S., Sofiev, M., Sokhi, R., Lehtinen, K. E. J., Karatzas, K., San José, R., Astitha, M., Kallos, G., Schaap, M., Reimer, E., Jakobs, H., and Eben, K.: A review of operational, regional-scale, chemical weather forecasting models in Europe, *Atmospheric Chem. Phys.*, 12, 1–87, <https://doi.org/10.5194/acp-12-1-2012>, 2012.
- Kulmala, M., Laaksonen, A., and Pirjola, L.: Parameterizations for sulfuric acid/water nucleation rates, *J. Geophys. Res. Atmospheres*, 103, 8301–8307, <https://doi.org/10.1029/97JD03718>, 1998.
- 2520 Kumar, N. and Russell, A. G.: Development of a computationally efficient, reactive subgrid-scale plume model and the impact in the northeastern United States using increasing levels of chemical detail, *J. Geophys. Res. Atmospheres*, 101, 16737–16744, <https://doi.org/10.1029/96JD01372>, 1996.
- Kumar, R., Delle Monache, L., Bresch, J., Saide, P. E., Tang, Y., Liu, Z., da Silva, A. M., Alessandrini, S., Pfister, G., Edwards, D., Lee, P., and Djalalova, I.: Toward improving short-term predictions of fine particulate matter over the United States via assimilation of satellite aerosol optical depth retrievals, *J. Geophys. Res. Atmospheres*, 124, 2753–2773, <https://doi.org/10.1029/2018JD029009>, 2019.
- Kusik, C. L. and Meissner, H. P.: Electrolyte activity coefficients in inorganic processing, in: *AICHE Symposium Series, Fundamental Aspects of Hydrometallurgical Processes*, New York, New York, 74 (173), 14–20, 1978.
- 2530 Larkin, N. K., O'Neill, S. M., Solomon, R., Raffuse, S., Strand, T., Sullivan, D. C., Krull, C., Rorig, M., Peterson, J., and Ferguson, S. A.: The BlueSky smoke modeling framework, *Int. J. Wildland Fire*, 18, 906, <https://doi.org/10.1071/WF07086>, 2009.
- Lauritzen, P. H. and Thuburn, J.: Evaluating advection/transport schemes using interrelated tracers, scatter plots and numerical mixing diagnostics, *Q. J. R. Meteorol. Soc.*, 138, 906–918, <https://doi.org/10.1002/qj.986>, 2012.
- 2535 Lee, B. S., Alexander, M. E., Hawkes, B. C., Lynham, T. J., Stocks, B. J., and Englefield, P.: Information systems in support of wildland fire management decision making in Canada, *Comput. Electron. Agric.*, 37, 185–198, [https://doi.org/10.1016/S0168-1699\(02\)00120-5](https://doi.org/10.1016/S0168-1699(02)00120-5), 2002.
- Lee, P., McQueen, J., Stajner, I., Huang, J., Pan, L., Tong, D., Kim, H., Tang, Y., Kondragunta, S., Ruminski, M., Lu, S., Rogers, E., Saylor, R., Shafran, P., Huang, H.-C., Gorline, J., Upadhayay, S., and Artz, R.: NAQFC developmental forecast guidance for fine particulate matter (PM<sub>2.5</sub>), *Weather Forecast.*, 32, 343–360, <https://doi.org/10.1175/WAF-D-15-0163.1>, 2017.
- 2540 Lei, L. and Whitaker, J. S.: A four-dimensional incremental analysis update for the ensemble Kalman filter, *Mon. Weather Rev.*, 144, 2605–2621, <https://doi.org/10.1175/MWR-D-15-0246.1>, 2016.
- Relievel, J. and Pöschl, U.: Chemists can help to solve the air-pollution health crisis, *Nature*, 551, 291–293, <https://doi.org/10.1038/d41586-017-05906-9>, 2017.
- 2545 Levy, I., Makar, P. A., Sills, D., Zhang, J., Hayden, K. L., Mihele, C., Narayan, J., Moran, M. D., Sjostedt, S., and Brook, J.: Unraveling the complex local-scale flows influencing ozone patterns in the southern Great Lakes of North America, *Atmospheric Chem. Phys.*, 10, 10895–10915, <https://doi.org/10.5194/acp-10-10895-2010>, 2010.
- Li, J. and Barker, H. W.: A radiation algorithm with correlated-k distribution. Part I: Local thermal equilibrium, *J. Atmospheric Sci.*, 62, 286–309, <https://doi.org/10.1175/JAS-3396.1>, 2005.
- 2550 Li, Q., Borge, R., Sarwar, G., de la Paz, D., Gantt, B., Domingo, J., Cuevas, C. A., and Saiz-Lopez, A.: Impact of halogen chemistry on summertime air quality in coastal and continental Europe: application of the CMAQ model and implications for regulation, *Atmospheric Chem. Phys.*, 19, 15321–15337, <https://doi.org/10.5194/acp-19-15321-2019>, 2019.
- Li, S.-M., Anlauf, K. G., Wiebe, H. A., Bottenheim, J. W., and Puckett, K. J.: Evaluation of a comprehensive Eulerian air quality model with multiple chemical species measurements using principal component analysis, *Atmos. Environ.*, 28, 3449–3461, [https://doi.org/10.1016/1352-2310\(94\)90004-3](https://doi.org/10.1016/1352-2310(94)90004-3), 1994.



- 2555 Li, X. and Rappenglueck, B.: A study of model nighttime ozone bias in air quality modeling, *Atmos. Environ.*, 195, 210–228, <https://doi.org/10.1016/j.atmosenv.2018.09.046>, 2018.
- Likens, G. E. and Bormann, F. H.: Acid rain: A serious regional environmental problem, *Science*, 184, 1176–1179, <https://doi.org/10.1126/science.184.4142.1176>, 1974.
- Lorenz, E. N.: Reflections on the conception, birth, and childhood of numerical weather prediction, *Annu. Rev. Earth Planet. Sci.*, 34, 37–45, <https://doi.org/10.1146/annurev.earth.34.083105.102317>, 2006.
- 2560 Lott, F. and Miller, M. J.: A new subgrid-scale orographic drag parametrization: Its formulation and testing, *Q. J. R. Meteorol. Soc.*, 123, 101–127, <https://doi.org/10.1002/qj.49712353704>, 1997.
- Lu, X. and Wang, X.: Improving the four-dimensional incremental analysis update (4DIAU) with the HWRF 4DEnVar Data Assimilation System for rapidly evolving hurricane prediction, *Mon. Weather Rev.*, 149, 4027–4043, <https://doi.org/10.1175/MWR-D-21-0068.1>, 2021.
- 2565 Lurmann, F. W., Lloyd, A. C., and Atkinson, R.: A chemical mechanism for use in long-range transport/acid deposition computer modeling, *J. Geophys. Res.*, 91, 10905, <https://doi.org/10.1029/JD091iD10p10905>, 1986.
- Ma, S., Tong, D., Lamsal, L., Wang, J., Zhang, X., Tang, Y., Saylor, R., Chai, T., Lee, P., Campbell, P., Baker, B., Kondragunta, S., Judd, L., Berkoff, T. A., Janz, S. J., and Stajner, I.: Improving predictability of high-ozone episodes through dynamic boundary conditions, emission refresh and chemical data assimilation during the Long Island Sound Tropospheric Ozone Study (LISTOS) field campaign, *Atmospheric Chem. Phys.*, 21, 16531–16553, <https://doi.org/10.5194/acp-21-16531-2021>, 2021.
- 2570 Macdonald, A. M., Banic, C. M., Leaitch, W. R., and Puckett, K. J.: Evaluation of the Eulerian acid deposition and oxidant model (ADOM) with summer 1988 aircraft data, *Atmospheric Environ. Part Gen. Top.*, 27, 1019–1034, [https://doi.org/10.1016/0960-1686\(93\)90014-P](https://doi.org/10.1016/0960-1686(93)90014-P), 1993.
- 2575 Mailhot, J. and Bélair, S.: An examination of a unified cloudiness-turbulence scheme with various types of cloudy boundary layers, in: *Proc. 14th Symposium on Boundary Layer and Turbulence*, 7-11 August, Aspen, Colorado, American Meteorological Society, 215–218, 2000.
- Mailhot, J., Bélair, S., Benoit, R., Bilodeau, B., Delage, Y., Fillion, L., Garand, L., Girard, C., and Tremblay, A.: Scientific description of RPN physics library - Version 3.6, Technical note, May, Recherche en Prévision Numérique, Environment and Climate Change Canada, Dorval, Quebec, Canada, 197 pp., <https://collaboration.cmc.ec.gc.ca/science/rpn/physics/physic98.pdf>, 1998.
- 2580 Mailhot, J., Bélair, S., Lefaire, L., Bilodeau, B., Desgagné, M., Girard, C., Glazer, A., Leduc, A., Méthot, A., Patoine, A., Plante, A., Rahill, A., Robinson, T., Talbot, D., Tremblay, A., Vaillancourt, P., Zadra, A., and Qaddouri, A.: The 15-km version of the Canadian regional forecast system, *Atmosphere-Ocean*, 44, 133–149, <https://doi.org/10.3137/ao.440202>, 2006.
- 2585 Majdzadeh, M., Stroud, C. A., Sioris, C., Makar, P. A., Akingunola, A., McLinden, C., Zhao, X., Moran, M. D., Abboud, I., and Chen, J.: Development of aerosol optical properties for improving the MESSy photolysis module in the GEM-MACH v2.4 air quality model and application for calculating photolysis rates in a biomass burning plume, *Geosci. Model Dev.*, 15, 219–249, <https://doi.org/10.5194/gmd-15-219-2022>, 2022.
- 2590 Makar, P. A., Wiebe, H. A., Staebler, R. M., Li, S. M., and Anlauf, K.: Measurement and modeling of particle nitrate formation, *J. Geophys. Res. Atmospheres*, 103, 13095–13110, <https://doi.org/10.1029/98JD00978>, 1998.
- Makar, P. A., Bouchet, V. S., and Nenes, A.: Inorganic chemistry calculations using HETV—a vectorized solver for the  $\text{SO}_4^{2-}$ – $\text{NO}_3^-$ – $\text{NH}_4^+$  system based on the ISORROPIA algorithms, *Atmos. Environ.*, 37, 2279–2294, [https://doi.org/10.1016/S1352-2310\(03\)00074-8](https://doi.org/10.1016/S1352-2310(03)00074-8), 2003a.
- 2595 Makar, P. A., Moran, M. D., Scholtz, M. T., and Taylor, A.: Speciation of volatile organic compound emissions for regional air quality modeling of particulate matter and ozone, *J. Geophys. Res.*, 108, 4041, <https://doi.org/10.1029/2001JD000797>, 2003b.
- Makar, P. A., Moran, M. D., Zheng, Q., Cousineau, S., Sassi, M., Duhamel, A., Besner, M., Davignon, D., Crevier, L.-P., and Bouchet, V. S.: Modelling the impacts of ammonia emissions reductions on North American air quality, *Atmospheric Chem. Phys.*, 9, 7183–7212, <https://doi.org/10.5194/acp-9-7183-2009>, 2009.



- 2600 Makar, P. A., Nissen, R., Teakles, A., Zhang, J., Zheng, Q., Moran, M. D., Yau, H., and diCenzo, C.: Turbulent transport, emissions and the role of compensating errors in chemical transport models, *Geosci. Model Dev.*, 7, 1001–1024, <https://doi.org/10.5194/gmd-7-1001-2014>, 2014.
- 2605 Makar, P. A., Gong, W., Milbrandt, J., Hogrefe, C., Zhang, Y., Curci, G., Žabkar, R., Im, U., Balzarini, A., Baró, R., Bianconi, R., Cheung, P., Forkel, R., Gravel, S., Hirtl, M., Honzak, L., Hou, A., Jiménez-Guerrero, P., Langer, M., Moran, M. D., Pabla, B., Pérez, J. L., Pirovano, G., San José, R., Tuccella, P., Werhahn, J., Zhang, J., and Galmarini, S.: Feedbacks between air pollution and weather, Part 1: Effects on weather, *Atmos. Environ.*, 115, 442–469, <https://doi.org/10.1016/j.atmosenv.2014.12.003>, 2015a.
- Makar, P. A., Gong, W., Hogrefe, C., Zhang, Y., Curci, G., Žabkar, R., Milbrandt, J., Im, U., Balzarini, A., Baró, R., Bianconi, R., Cheung, P., Forkel, R., Gravel, S., Hirtl, M., Honzak, L., Hou, A., Jiménez-Guerrero, P., Langer, M., Moran, M. D., Pabla, B., Pérez, J. L., Pirovano, G., San José, R., Tuccella, P., Werhahn, J., Zhang, J., and Galmarini, S.: Feedbacks between air pollution and weather, part 2: Effects on chemistry, *Atmos. Environ.*, 115, 499–526, <https://doi.org/10.1016/j.atmosenv.2014.10.021>, 2015b.
- 2610 Makar, P. A., Akingunola, A., Aherne, J., Cole, A. S., Aklilu, Y., Zhang, J., Wong, I., Hayden, K., Li, S.-M., Kirk, J., Scott, K., Moran, M. D., Robichaud, A., Cathcart, H., Baratzedah, P., Pabla, B., Cheung, P., Zheng, Q., and Jeffries, D. S.: Estimates of exceedances of critical loads for acidifying deposition in Alberta and Saskatchewan, *Atmospheric Chem. Phys.*, 18, 9897–9927, <https://doi.org/10.5194/acp-18-9897-2018>, 2018a.
- 2615 Makar, P. A., Akingunola, A., Aherne, J., Cole, A. S., Aklilu, Y., Zhang, J., Wong, I., Hayden, K., Li, S.-M., Kirk, J., Scott, K., Moran, M. D., Robichaud, A., Cathcart, H., Baratzedah, P., Pabla, B., Cheung, P., Zheng, Q., and Jeffries, D. S.: Supplement to “Estimates of exceedances of critical loads for acidifying deposition in Alberta and Saskatchewan,” *Atmospheric Chem. Phys.*, 18, 16 pp., <https://doi.org/10.5194/acp-18-9897-2018-supplement>, 2018b.
- Makar, P. A., Stroud, C., Akingunola, A., Zhang, J., Ren, S., Cheung, P., and Zheng, Q.: Vehicle-induced turbulence and atmospheric pollution, *Atmospheric Chem. Phys.*, 21, 12291–12316, <https://doi.org/10.5194/acp-21-12291-2021>, 2021.
- 2620 Makar, P. A., Cheung, P., Hogrefe, C., Akingunola, A., Alyuz, U., Bash, J. O., Bell, M. D., Bellasio, R., Bianconi, R., Butler, T., Cathcart, H., Clifton, O. E., Hodzic, A., Kioutsioukis, I., Kranenburg, R., Lupascu, A., Lynch, J. A., Momoh, K., Perez-Camanyo, J. L., Pleim, J., Ryu, Y.-H., San Jose, R., Schwede, D., Scheuschner, T., Shephard, M. W., Sokhi, R. S., and Galmarini, S.: Critical load exceedances for North America and Europe using an ensemble of models and an investigation of causes of environmental impact estimate variability: an AQMEII4 study, *Atmospheric Chem. Phys.*, 25, 3049–3107, <https://doi.org/10.5194/acp-25-3049-2025>, 2025.
- 2625 Malm, W. C. and Hand, J. L.: An examination of the physical and optical properties of aerosols collected in the IMPROVE program, *Atmos. Environ.*, 41, 3407–3427, <https://doi.org/10.1016/j.atmosenv.2006.12.012>, 2007.
- Malm, W. C., Schichtel, B. A., Pitchford, M. L., Ashbaugh, L. L., and Eldred, R. A.: Spatial and monthly trends in speciated fine particle concentration in the United States, *J. Geophys. Res. Atmospheres*, 109, D03306, 22 pp., <https://doi.org/10.1029/2003JD003739>, 2004.
- 2630 Marchuk, G. I.: Splitting and alternating direction methods, in: *Handbook of Numerical Analysis*, vol. 1, Elsevier B.V., 197–462, 1990.
- Mashayekhi, R., Pavlovic, R., Racine, J., Moran, M. D., Manseau, P. M., Duhamel, A., Katal, A., Miville, J., Niemi, D., Peng, S. J., Sassi, M., Griffin, D., and McLinden, C. A.: Isolating the impact of COVID-19 lockdown measures on urban air quality in Canada, *Air Qual. Atmosphere Health*, 14, 1549–1570, <https://doi.org/10.1007/s11869-021-01039-1>, 2021.
- 2635 Mathur, R., Peters, L. K., and Saylor, R. D.: Sub-grid representation of emission source clusters in regional air quality modeling, *Atmos. Environ.*, 26, 3219–3238, [https://doi.org/10.1016/0960-1686\(92\)90478-4](https://doi.org/10.1016/0960-1686(92)90478-4), 1992.
- McFarlane, N. A.: The effect of orographically excited gravity wave drag on the general circulation of the lower stratosphere and troposphere, *J. Atmospheric Sci.*, 44, 1775–1800, [https://doi.org/10.1175/1520-0469\(1987\)044<1775:TEOOEG>2.0.CO;2](https://doi.org/10.1175/1520-0469(1987)044<1775:TEOOEG>2.0.CO;2), 1987.
- 2640 McHenry, J. N., Ryan, W. F., Seaman, N. L., Coats, C. J., Pudykiewicz, J., Arunachalam, S., and Vukovich, J. M.: A real-time Eulerian photochemical model forecast system: Overview and initial ozone forecast performance in the northeast U.S. corridor, *Bull. Am. Meteorol. Soc.*, 85, 525–548, <https://doi.org/10.1175/BAMS-85-4-525>, 2004.



- McKeen, S., Wilczak, J., Grell, G., Djalalova, I., Peckham, S., Hsie, E. -Y., Gong, W., Bouchet, V., Menard, S., Moffet, R., McHenry, J., McQueen, J., Tang, Y., Carmichael, G. R., Pagowski, M., Chan, A., Dye, T., Frost, G., Lee, P., and Mathur, R.: Assessment of an ensemble of seven real-time ozone forecasts over eastern North America during the summer of 2004, *J. Geophys. Res. Atmospheres*, 110, 2005JD005858, <https://doi.org/10.1029/2005JD005858>, 2005.
- 2645
- McKeen, S., Chung, S. H., Wilczak, J., Grell, G., Djalalova, I., Peckham, S., Gong, W., Bouchet, V., Moffet, R., Tang, Y., Carmichael, G. R., Mathur, R., and Yu, S.: Evaluation of several PM<sub>2.5</sub> forecast models using data collected during the ICARTT/NEAQS 2004 field study, *J. Geophys. Res. Atmospheres*, 112, 2006JD007608, <https://doi.org/10.1029/2006JD007608>, 2007.
- 2650
- McKendry, I. G., Macdonald, A. M., Leaitch, W. R., van Donkelaar, A., Zhang, Q., Duck, T., and Martin, R. V.: Trans-Pacific dust events observed at Whistler, British Columbia during INTEX-B, *Atmospheric Chem. Phys.*, 8, 6297–6307, <https://doi.org/10.5194/acp-8-6297-2008>, 2008.
- McLinden, C. A., Olsen, S. C., Hannegan, B., Wild, O., Prather, M. J., and Sundet, J.: Stratospheric ozone in 3-D models: A simple chemistry and the cross-tropopause flux, *J. Geophys. Res. Atmospheres*, 105, 14653–14665, <https://doi.org/10.1029/2000JD900124>, 2000.
- 2655
- McNider, R. T. and Pour-Biazar, A.: Meteorological modeling relevant to mesoscale and regional air quality applications: a review, *J. Air Waste Manag. Assoc.*, 70, 2–43, <https://doi.org/10.1080/10962247.2019.1694602>, 2020.
- McRae, G. J., Goodin, W. R., and Seinfeld, J. H.: Development of a second-generation mathematical model for urban air pollution—I. Model formulation, *Atmospheric Environ.* 1967, 16, 679–696, [https://doi.org/10.1016/0004-6981\(82\)90386-9](https://doi.org/10.1016/0004-6981(82)90386-9), 1982.
- 2660
- McTaggart-Cowan, R. and Zadra, A.: Representing Richardson number hysteresis in the NWP boundary layer, *Mon. Weather Rev.*, 143, 1232–1258, <https://doi.org/10.1175/MWR-D-14-00179.1>, 2015.
- McTaggart-Cowan, R., Vaillancourt, P. A., Zadra, A., Chamberland, S., Charron, M., Corvec, S., Milbrandt, J. A., Paquin-Ricard, D., Patoine, A., Roch, M., Separovic, L., and Yang, J.: Modernization of atmospheric physics parameterization in Canadian NWP, *J. Adv. Model. Earth Syst.*, 11, 3593–3635, <https://doi.org/10.1029/2019MS001781>, 2019a.
- 2665
- McTaggart-Cowan, R., Vaillancourt, P. A., Zadra, A., Separovic, L., Corvec, S., and Kirshbaum, D.: A Lagrangian perspective on parameterizing deep convection, *Mon. Weather Rev.*, 147, 4127–4149, <https://doi.org/10.1175/MWR-D-19-0164.1>, 2019b.
- Ménard, R.: Regional Deterministic Air Quality Analysis (RDAQA): Implementation of version 2.0.0, Technical note, December, Canadian Centre for Meteorological and Environmental Prediction, Montreal, 18 pp., [https://collaboration.cmc.ec.gc.ca/cmc/cmoe/product\\_guide/docs/tech\\_notes/technote\\_rdaqa-200\\_e.pdf](https://collaboration.cmc.ec.gc.ca/cmc/cmoe/product_guide/docs/tech_notes/technote_rdaqa-200_e.pdf), 2021.
- 2670
- Ménard, R. and Robichaud, A.: The chemistry-forecast system at the Meteorological Service of Canada, in: Proc. Annual Seminar on Global Earth-system Monitoring, European Centre for Medium-Range Weather Forecasts, Reading, England, Sept. 5-9, 297–308, <https://www.ecmwf.int/sites/default/files/elibrary/2006/11340-chemistry-forecast-system-meteorological-service-canada.pdf>, 2005.
- 2675
- Ménard, R., Cossette, J.-F., and Deshaies-Jacques, M.: On the complementary role of data assimilation and machine learning: An example derived from air quality analysis, in: Computational Science – ICCS 2020, vol. 12142, edited by: Krzhizhanovskaya, V. V., Závodszy, G., Lees, M. H., Dongarra, J. J., Sloot, P. M. A., Brissos, S., and Teixeira, J., Springer International Publishing, Cham, 212–224, [https://doi.org/10.1007/978-3-030-50433-5\\_17](https://doi.org/10.1007/978-3-030-50433-5_17), 2020.
- Meng, Z., Seinfeld, J. H., Saxena, P., and Kim, Y. P.: Atmospheric gas-aerosol equilibrium: IV. Thermodynamics of carbonates, *Aerosol Sci. Technol.*, 23, 131–154, <https://doi.org/10.1080/02786829508965300>, 1995.
- 2680
- Menut, L. and Bessagnet, B.: What can we expect from data assimilation for air quality forecast? Part I: Quantification with academic test cases, *J. Atmospheric Ocean. Technol.*, 36, 269–279, <https://doi.org/10.1175/JTECH-D-18-0002.1>, 2019.
- Middleton, P.: DAQM-simulated spatial and temporal differences among visibility, PM, and other air quality concerns under realistic emission change scenarios, *J. Air Waste Manag. Assoc.*, 47, 302–316, <https://doi.org/10.1080/10473289.1997.10464446>, 1997.
- 2685



- Middleton, P., Stockwell, W. R., and Carter, W. P. L.: Aggregation and analysis of volatile organic compound emissions for regional modeling, *Atmos. Environ.*, 24, 1107–1133, [https://doi.org/10.1016/0960-1686\(90\)90077-Z](https://doi.org/10.1016/0960-1686(90)90077-Z), 1990.
- Miller, C. A., Hidy, G., Hales, J., Kolb, C. E., Werner, A. S., Haneke, B., Parrish, D., Frey, H. C., Rojas-Bracho, L., Deslauriers, M., Pennell, B., and Mobley, J. D.: Air emission inventories in North America: A critical assessment, *J. Air Waste Manag. Assoc.*, 56, 1115–1129, <https://doi.org/10.1080/10473289.2006.10464540>, 2006.
- 2690
- Miller, S. J., Makar, P. A., and Lee, C. J.: HETerogeneous vectorized or Parallel (HETPv1.0): an updated inorganic heterogeneous chemistry solver for the metastable-state  $\text{NH}_4^+ - \text{Na}^+ - \text{Ca}^{2+} - \text{K}^+ - \text{Mg}^{2+} - \text{SO}_4^{2-} - \text{NO}_3^- - \text{Cl}^- - \text{H}_2\text{O}$  system based on ISORROPIA II, *Geosci. Model Dev.*, 17, 2197–2219, <https://doi.org/10.5194/gmd-17-2197-2024>, 2024.
- Misra, P. K., Bloxam, R., Fung, C., and Wong, S.: Non-linear response of wet deposition to emissions reduction: A model study, *Atmospheric Environ.* 1967, 23, 671–687, [https://doi.org/10.1016/0004-6981\(89\)90015-2](https://doi.org/10.1016/0004-6981(89)90015-2), 1989.
- 2695
- Monson, R. K., Lerdau, M. T., Sharkey, T. D., Schimel, D. S., and Fall, R.: Biological aspects of constructing volatile organic compound emission inventories, *Atmos. Environ.*, 29, 2989–3002, [https://doi.org/10.1016/1352-2310\(94\)00360-W](https://doi.org/10.1016/1352-2310(94)00360-W), 1995.
- Moran, M. D. and Ménard, S.: Regional Air Quality Deterministic Prediction System (RAQDPS): Update from version 020.2 to version 021, Canadian Centre for Meteorological and Environmental Prediction, Montreal, 49 pp., [http://collaboration.cmc.ec.gc.ca/cmc/cmoei/product\\_guide/docs/tech\\_notes/technote\\_raqdps-021\\_20190703\\_e.pdf](http://collaboration.cmc.ec.gc.ca/cmc/cmoei/product_guide/docs/tech_notes/technote_raqdps-021_20190703_e.pdf), 2019.
- 2700
- Moran, M. D., Bouchet, V., Dastoor, A., Gong, S., Gong, W., and Makar, P. A.: Conceptual design for the AES regional particulate-matter model/unified air quality model, *Atmospheric Environment Service*, Toronto, Ontario, October, 102 pp., <https://doi.org/10.5281/zenodo.15330612>, 1998.
- Moran, M. D., Ménard, S., Talbot, D., Huang, P., Makar, P., Gong, W., Landry, H., Gong, S., Gravel, S., Crevier, L.-P., and Kallaur, A.: Particulate-matter forecasting with GEM-MACH15, a new Canadian operational air quality forecast model, in: *Air Pollution Modelling and its Application XX*, Springer, Dordrecht, 289–293, 2010.
- 2705
- Moran, M. D., Chen, J., Ménard, S., Pavlovic, R., Landry, H., Beaulieu, P.-A., Gilbert, S., Makar, P. A., Gong, W., Stroud, C., Kallaur, A., Robichaud, A., Gong, S., and Anselmo, D.: Two years of operational AQ forecasting with GEM-MACH15: A look back and a look ahead, in: *Proc. 10th CMAS Conference*, 24–26 Oct., Chapel Hill, North Carolina, 7 pp., [http://www.cmascenter.org/conference/2011/abstracts/moran\\_two\\_years\\_2011.pdf](http://www.cmascenter.org/conference/2011/abstracts/moran_two_years_2011.pdf), 2011.
- 2710
- Moran, M. D., Dastoor, A., and Morneau, G.: Long-range transport of air pollutants and regional and global AQ modelling, in: *Air Quality Management -- Canadian Perspectives on a Global Issue*, E. Taylor and A. McMillan, Editors, Springer, Dordrecht, [https://link.springer.com/content/pdf/10.1007%2F978-94-007-7557-2\\_4](https://link.springer.com/content/pdf/10.1007%2F978-94-007-7557-2_4), 69–98, 2013.
- Moran, M. D., Ménard, S., Pavlovic, R., Anselmo, D., Antonopoulos, S., Makar, P. A., Gong, W., Gravel, S., Stroud, C., Zhang, J., Zheng, Q., Robichaud, A., Landry, H., Beaulieu, P.-A., Gilbert, S., Chen, J., and Kallaur, A.: Recent advances in Canada's National Operational AQ Forecasting System, in: *Air Pollution Modeling and its Application XXII*, Springer Science + Business Media, Dordrecht, 215–220, 2014.
- 2715
- Moran, M. D., Zheng, Q., Zhang, J., Pavlovic, R., and Sassi, M.: Importance of inventory representativeness for air quality forecasting: a recent North American example, in: *Air Pollution Modeling and its Application XXVI*, Springer, Cham, [https://doi.org/10.1007/978-3-030-22055-6\\_41](https://doi.org/10.1007/978-3-030-22055-6_41), 285–289, 2020a.
- 2720
- Moran, M. D., Manseau, P., Peng, S. J., Stajner, I., Flemming, J., McQueen, J., Lee, P., Razinger, M., and Pavlovic, R.: Ongoing multi-model evaluation of operational air quality forecasts over North America: 2017–2020, 19th CMAS Conference, Virtual, 26–30 Oct., 2020b.
- Moran, M. D., Zhang, J., Pavlovic, R., Savic-Jovicic, V., Ménard, S., Landry, H., Zheng, Q., Lupu, A., Gilbert, S., Peng, S. J., and Manseau, P.: Evolution of the performance of the Canadian operational Regional Air Quality Deterministic Prediction System from 2010 to 2018, in: *Air Pollution Modeling and its Application XXVII*, C. Mensink and V. Matthias (eds.), Springer, Berlin, 157–166, 2021a.
- 2725
- Moran, M. D., Ménard, S., and Kornic, D.: Regional Air Quality Deterministic Prediction System (RAQDPS): Upgrade from version 022 to version 023, Technical note, December, Canadian Centre for Meteorological and Environmental Prediction,



- 2730 Montreal, 48 pp., [https://collaboration.cmc.ec.gc.ca/cmc/cmoin/product\\_guide/docs/lib/technote\\_raqdps023\\_20211130\\_e.pdf](https://collaboration.cmc.ec.gc.ca/cmc/cmoin/product_guide/docs/lib/technote_raqdps023_20211130_e.pdf), 2021b.
- Moran, M. D., Lupu, A., Savic-Jovcic, V., Zhang, J., Zheng, Q., Boutzis, E. I., Mashayekhi, R., Stroud, C., Ménard, S., Chen, J., Menelaou, K., Munoz-Alpizar, R., Kornic, D., and Manseau, P. M.: Operational chemical weather forecasting with the ECCO Regional Air Quality Deterministic Prediction System version 023 (RAQDPS023) - Part 2: Prospective and retrospective performance evaluations, *Geosci. Model Dev.* (under review), 2025.
- 2735 Morawska, L., Thomas, S., Jamriska, M., and Johnson, G.: The modality of particle size distributions of environmental aerosols, *Atmos. Environ.*, 33, 4401–4411, [https://doi.org/10.1016/S1352-2310\(99\)00217-4](https://doi.org/10.1016/S1352-2310(99)00217-4), 1999.
- Munoz-Alpizar, R., Pavlovic, R., Moran, M., Chen, J., Gravel, S., Henderson, S., Ménard, S., Racine, J., Duhamel, A., Gilbert, S., Beaulieu, P.-A., Landry, H., Davignon, D., Cousineau, S., and Bouchet, V.: Multi-year (2013–2016) PM<sub>2.5</sub> wildfire pollution exposure over North America as determined from operational air quality forecasts, *Atmosphere*, 8, 179–202, <https://doi.org/10.3390/atmos8090179>, 2017.
- 2740 Murray, C. J. L., Aravkin, A. Y., Zheng, P., Abbafati, C., Abbas, K. M., Abbasi-Kangevari, M., Abd-Allah, F., Abdelalim, A., et al.: Global burden of 87 risk factors in 204 countries and territories, 1990–2019: a systematic analysis for the Global Burden of Disease Study 2019, *The Lancet*, 396, 1223–1249, [https://doi.org/10.1016/S0140-6736\(20\)30752-2](https://doi.org/10.1016/S0140-6736(20)30752-2), 2020.
- 2745 Naeger, A. R., Newchurch, M. J., Moore, T., Chance, K., Liu, X., Alexander, S., Murphy, K., and Wang, B.: Revolutionary air-pollution applications from future Tropospheric Emissions: Monitoring of Pollution (TEMPO) observations, *Bull. Am. Meteorol. Soc.*, 102, E1735–E1741, <https://doi.org/10.1175/BAMS-D-21-0050.1>, 2021.
- Nenes, A., Pandis, S. N., and Pilinis, C.: ISORROPIA: A new thermodynamic equilibrium model for multiphase multicomponent inorganic aerosols, *Aquat. Geochem.*, 4, 123–152, <https://doi.org/10.1023/A:1009604003981>, 1998.
- 2750 Nenes, A., Pandis, S. N., and Pilinis, C.: Continued development and testing of a new thermodynamic aerosol module for urban and regional air quality models, *Atmos. Environ.*, 33, 1553–1560, [https://doi.org/10.1016/S1352-2310\(98\)00352-5](https://doi.org/10.1016/S1352-2310(98)00352-5), 1999.
- Nguyen, T. K. V., Zhang, Q., Jimenez, J. L., Pike, M., and Carlton, A. G.: Liquid water: ubiquitous contributor to aerosol mass, *Environ. Sci. Technol. Lett.*, 3, 257–263, <https://doi.org/10.1021/acs.estlett.6b00167>, 2016.
- Noilhan, J. and Planton, S.: A simple parameterization of land surface processes for meteorological models, *Mon. Weather Rev.*, 117, 536–549, [https://doi.org/10.1175/1520-0493\(1989\)117<0536:ASPOLS>2.0.CO;2](https://doi.org/10.1175/1520-0493(1989)117<0536:ASPOLS>2.0.CO;2), 1989.
- 2755 NSTC: Air Quality Observation Systems in the United States, November, National Science and Technology Council report, Washington, D.C., 96 pp., <https://csl.noaa.gov/aqrsd/reports/aqmonitoring.pdf>, 2013.
- Odum, J. R., Hoffmann, T., Bowman, F., Collins, D., Flagan, R. C., and Seinfeld, J. H.: Gas/particle partitioning and secondary organic aerosol yields, *Environ. Sci. Technol.*, 30, 2580–2585, <https://doi.org/10.1021/es950943+>, 1996.
- 2760 Odum, J. R., Jungkamp, T. P. W., Griffin, R. J., Forstner, H. J. L., Flagan, R. C., and Seinfeld, J. H.: Aromatics, reformulated gasoline, and atmospheric organic aerosol formation, *Environ. Sci. Technol.*, 31, 1890–1897, <https://doi.org/10.1021/es9605351>, 1997.
- Oran, E. S. and Boris, J. P.: *Numerical Simulation of Reactive Flow*, Second Edition, Cambridge University Press, 550 pp., 2000.
- Orgill, M. M. and Sehmel, G. A.: Frequency and diurnal variation of dust storms in the contiguous U.S.A., *Atmospheric Environ.* 1967, 10, 813–825, [https://doi.org/10.1016/0004-6981\(76\)90136-0](https://doi.org/10.1016/0004-6981(76)90136-0), 1976.
- 2765 Pace, T. G.: Methodology to estimate the transportable fraction (TF) of fugitive dust emissions for regional and urban scale air quality analyses (8/3/2005 Revision), U.S. Environmental Protection Agency, Research Triangle Park, North Carolina, 12 pp., <https://www.nrc.gov/docs/ML1321/ML13213A386.pdf>, 2005.
- 2770 Pan, L., Tong, D., Lee, P., Kim, H.-C., and Chai, T.: Assessment of NO<sub>x</sub> and O<sub>3</sub> forecasting performances in the U.S. National Air Quality Forecasting Capability before and after the 2012 major emissions updates, *Atmos. Environ.*, 95, 610–619, <https://doi.org/10.1016/j.atmosenv.2014.06.020>, 2014.



- Pandis, S. N., Wexler, A. S., and Seinfeld, J. H.: Dynamics of tropospheric aerosols, *J. Phys. Chem.*, 99, 9646–9659, <https://doi.org/10.1021/j100024a003>, 1995.
- Pang, Y., Turpin, B. J., and Gundel, L. A.: On the importance of organic oxygen for understanding organic aerosol particles, *Aerosol Sci. Technol.*, 40, 128–133, <https://doi.org/10.1080/02786820500423790>, 2006.
- Pankow, J. F.: An absorption model of the gas/aerosol partitioning involved in the formation of secondary organic aerosol, *Atmos. Environ.*, 28, 189–193, [https://doi.org/10.1016/1352-2310\(94\)90094-9](https://doi.org/10.1016/1352-2310(94)90094-9), 1994.
- Park, S. H., Gong, S. L., Zhao, T. L., Vet, R. J., Bouchet, V. S., Gong, W., Makar, P. A., Moran, M. D., Stroud, C., and Zhang, J.: Simulation of entrainment and transport of dust particles within North America in April 2001 (“Red Dust Episode”), *J. Geophys. Res.*, 112, D20209, <https://doi.org/10.1029/2007JD008443>, 2007.
- Park, S. H., Gong, S. L., Bouchet, V. S., Gong, W., Makar, P. A., Moran, M. D., Stroud, C. A., and Zhang, J.: Effects of black carbon aging on air quality predictions and direct radiative forcing estimation, *Tellus B Chem. Phys. Meteorol.*, 63, 1026–1039, <https://doi.org/10.1111/j.1600-0889.2011.00558.x>, 2011.
- Pasquill, F. and Smith, F. B.: *Atmospheric Diffusion*, Third Edition, Ellis Horwood, Chichester, 437 pp., 1983.
- Pavlovic, R., Chen, J., Anderson, K., Moran, M. D., Beaulieu, P.-A., Davignon, D., and Cousineau, S.: The FireWork air quality forecast system with near-real-time biomass burning emissions: Recent developments and evaluation of performance for the 2015 North American wildfire season, *J. Air Waste Manag. Assoc.*, 66, 819–841, <https://doi.org/10.1080/10962247.2016.1158214>, 2016.
- Pavlovic, R., Moran, M., Gilbert, S., Davignon, D., Bouchet, V., Stajner, I., McQueen, J., Lee, P., Flemming, J., and Razinger, M.: Multi-model air quality performance analysis over North America for ECCO, NOAA/NWS and CAMS operational forecast systems, 3rd Copernicus Atmosphere Monitoring Service General Assembly, 16-18 October, Lisbon, [https://atmosphere.copernicus.eu/sites/default/files/2018-11/2\\_3rd\\_ECCO\\_NOAA\\_ECMWF\\_v06.pdf](https://atmosphere.copernicus.eu/sites/default/files/2018-11/2_3rd_ECCO_NOAA_ECMWF_v06.pdf), 2018.
- Pendlebury, D., Gravel, S., Moran, M. D., and Lupu, A.: Impact of chemical lateral boundary conditions in a regional air quality forecast model on surface ozone predictions during stratospheric intrusions, *Atmos. Environ.*, 174, 148–170, <https://doi.org/10.1016/j.atmosenv.2017.10.052>, 2018.
- Peterson, J. T.: Calculated actinic fluxes (290–700 nm) for air pollution photochemistry applications, Report EPA-600/4-76-025, U.S. Environmental Protection Agency, Research Triangle Park, North Carolina, 63 pp., 1976.
- Philip, S., Martin, R. V., Pierce, J. R., Jimenez, J. L., Zhang, Q., Canagaratna, M. R., Spracklen, D. V., Nowlan, C. R., Lamsal, L. N., Cooper, M. J., and Krotkov, N. A.: Spatially and seasonally resolved estimate of the ratio of organic mass to organic carbon, *Atmos. Environ.*, 87, 34–40, <https://doi.org/10.1016/j.atmosenv.2013.11.065>, 2014.
- Pierce, R. B., Schaack, T., Al-Saadi, J. A., Fairlie, T. D., Kittaka, C., Lingenfelter, G., Natarajan, M., Olson, J., Soja, A., Zapotocny, T., Lenzen, A., Stobie, J., Johnson, D., Avery, M. A., Sachse, G. W., Thompson, A., Cohen, R., Dibb, J. E., Crawford, J., Rault, D., Martin, R., Szykman, J., and Fishman, J.: Chemical data assimilation estimates of continental U.S. ozone and nitrogen budgets during the Intercontinental Chemical Transport Experiment–North America, *J. Geophys. Res.*, 112, D12S21, <https://doi.org/10.1029/2006JD007722>, 2007.
- Pierce, T., Geron, C., Bender, L., Dennis, R., Tonnesen, G., and Guenther, A.: Influence of increased isoprene emissions on regional ozone modeling, *J. Geophys. Res. Atmospheres*, 103, 25611–25629, <https://doi.org/10.1029/98JD01804>, 1998.
- Pierce, T. E., Kinnee, E. J., and Geron, C. D.: Development of a 1-km vegetation database for modeling biogenic fluxes of hydrocarbons and nitric oxide, Sixth International Conference on Air Surface Exchange of Gases and Particles, 3–7 July, Edinburgh, [https://www.epa.gov/sites/default/files/2015-08/beld3\\_web.pptx](https://www.epa.gov/sites/default/files/2015-08/beld3_web.pptx), Last access: 25 March 2023, 2000.
- Pleim, J. E.: A combined local and nonlocal closure model for the atmospheric boundary layer. Part I: Model description and testing, *J. Appl. Meteorol. Climatol.*, 46, 1383–1395, <https://doi.org/10.1175/JAM2539.1>, 2007.
- Plummer, D., McConnell, J. C., Neary, L., Kaminski, J., Benoit, R., Drummond, J., Narayan, J., Young, V., and Hastie, D. R.: Assessment of emissions data for the Toronto region using aircraft-based measurements and an air quality model, *Atmos. Environ.*, 35, 6453–6463, [https://doi.org/10.1016/S1352-2310\(01\)00450-2](https://doi.org/10.1016/S1352-2310(01)00450-2), 2001.



- Pudykiewicz, J., Benoit, R., and Mailhot, J.: Inclusion and verification of a predictive cloud-water scheme in a regional numerical weather prediction model, *Mon. Weather Rev.*, 120, 612–626, [https://doi.org/10.1175/1520-0493\(1992\)120<0612:IAVOAP>2.0.CO;2](https://doi.org/10.1175/1520-0493(1992)120<0612:IAVOAP>2.0.CO;2), 1992.
- 2820 Pudykiewicz, J. A. and Koziol, A. S.: The application of Eulerian models for air quality prediction and the evaluation of emission control strategies in Canada, *Int. J. Environ. Pollut.*, 16, 425–438, <https://doi.org/10.1504/IJEP.2001.000638>, 2001.
- Pudykiewicz, J. A., Kallaur, A., and Smolarkiewicz, P. K.: Semi-Lagrangian modelling of tropospheric ozone, *Tellus B Chem. Phys. Meteorol.*, 49, 231–248, <https://doi.org/10.3402/tellusb.v49i3.15964>, 1997.
- 2825 Pudykiewicz, J. A., Kallaur, A., Moffet, R., Bouchet, V. S., Jean, M., Makar, P. A., Moran, M. D., Gong, W., and Venkatesh, S.: Operational air quality forecasting in Canada: numerical model guidance for ground-level ozone and particulate matter, in: *Proc. Fifth AMS Conference on Atmospheric Chemistry: Gases, Aerosols, and Clouds*, Long Beach, California, Feb. 9-13, 6 pp., American Meteorological Society, Boston, <https://ams.confex.com/ams/pdfpapers/54490.pdf>, 2003.
- Qaddouri, A. and Lee, V.: The Canadian Global Environmental Multiscale model on the Yin-Yang grid system, *Q. J. R. Meteorol. Soc.*, 137, 1913–1926, <https://doi.org/10.1002/qj.873>, 2011.
- 2830 Randles, C. A., da Silva, A. M., Buchard, V., Colarco, P. R., Darmenov, A., Govindaraju, R., Smirnov, A., Holben, B., Ferrare, R., Hair, J., Shinozuka, Y., and Flynn, C. J.: The MERRA-2 aerosol reanalysis, 1980 onward. Part I: System description and data assimilation evaluation, *J. Clim.*, 30, 6823–6850, <https://doi.org/10.1175/JCLI-D-16-0609.1>, 2017.
- 2835 Ritchie, H., Bélair, S., Bernier, N. B., Buehner, M., Charron, M., Fortin, V., Garand, L., Houtekamer, P., Husain, S., Laroche, S., Lemieux, J.-F., Lin, H., McTaggart-Cowan, R., Milbrandt, J., Mitchell, H., Pellerin, P., Pudykiewicz, J., Separovic, L., Smith, G. C., Tanguay, M., and Vaillancourt, P. A.: Recherche en Prévision Numérique contributions to numerical weather prediction, *Atmosphere-Ocean*, 60, 35–64, <https://doi.org/10.1080/07055900.2022.2038071>, 2022.
- Robichaud, A.: Surface data assimilation of chemical compounds over North America and its impact on air quality and Air Quality Health Index (AQHI) forecasts, *Air Qual. Atmosphere Health*, 10, 955–970, <https://doi.org/10.1007/s11869-017-0485-9>, 2017.
- 2840 Robichaud, A. and Ménard, R.: Multi-year objective analyses of warm season ground-level ozone and PM<sub>2.5</sub> over North America using real-time observations and Canadian operational air quality models, *Atmospheric Chem. Phys.*, 14, 1769–1800, <https://doi.org/10.5194/acp-14-1769-2014>, 2014.
- Robichaud, A., Ménard, R., Zaitseva, Y., and Anselmo, D.: Multi-pollutant surface objective analyses and mapping of air quality health index over North America, *Air Qual. Atmosphere Health*, 9, 743–759, <https://doi.org/10.1007/s11869-015-0385-9>, 2016.
- 2845 Robichaud, A., Cole, A., Moran, M., Lupu, A., Shaw, M., Roy, G., Beauchemin, M., Fortin, V., and Vet, R.: Total deposition maps evaluated from measurement-model fusion in North America (ADAGIO project), in: *Air Pollution Modeling and its Application XXVI*, edited by: Mensink, C., Gong, W., and Hakami, A., Springer International Publishing, Cham, 255–259, [https://doi.org/10.1007/978-3-030-22055-6\\_40](https://doi.org/10.1007/978-3-030-22055-6_40), 2020.
- Rochon, Y. J., Sitwell, M., and Cho, Y.-M.: A study on harmonizing total ozone assimilation with multiple sensors, *Atmospheric Chem. Phys.*, 19, 9431–9451, <https://doi.org/10.5194/acp-19-9431-2019>, 2019.
- 2850 Rood, M. J., Shaw, M. A., Larson, T. V., and Covert, D. S.: Ubiquitous nature of ambient metastable aerosol, *Nature*, 337, 537–539, <https://doi.org/10.1038/337537a0>, 1989.
- Roselle, S. J. and Schere, K. L.: Modeled response of photochemical oxidants to systematic reductions in anthropogenic volatile organic compound and NO<sub>x</sub> emissions, *J. Geophys. Res.*, 100, 22929–22941, <https://doi.org/10.1029/95JD00505>, 1995.
- Roselle, S. J., Pierce, T. E., and Schere, K. L.: The sensitivity of regional ozone modeling to biogenic hydrocarbons, *J. Geophys. Res.*, 96, 7371–7394, <https://doi.org/10.1029/91JD00005>, 1991.
- 2855 Russell, A. and Dennis, R.: NARSTO critical review of photochemical models and modeling, *Atmos. Environ.*, 34, 2283–2324, [https://doi.org/10.1016/S1352-2310\(99\)00468-9](https://doi.org/10.1016/S1352-2310(99)00468-9), 2000.
- Russell, L. M., Pandis, S. N., and Seinfeld, J. H.: Aerosol production and growth in the marine boundary layer, *J. Geophys. Res.*, 99, 20989–21003, <https://doi.org/10.1029/94JD01932>, 1994.



- 2860 Saide, P. E., Carmichael, G. R., Liu, Z., Schwartz, C. S., Lin, H. C., da Silva, A. M., and Hyer, E.: Aerosol optical depth assimilation for a size-resolved sectional model: impacts of observationally constrained, multi-wavelength and fine mode retrievals on regional scale analyses and forecasts, *Atmospheric Chem. Phys.*, 13, 10425–10444, <https://doi.org/10.5194/acp-13-10425-2013>, 2013.
- Samaali, M., Bouchet, V. S., Moran, M. D., and Sassi, M.: Application of a tagged-species method to source apportionment of primary PM<sub>2.5</sub> components in a regional air quality model, *Atmos. Environ.*, 45, 3835–3847, <https://doi.org/10.1016/j.atmosenv.2011.04.007>, 2011.
- 2865 Sandu, A. and Sander, R.: Technical note: Simulating chemical systems in Fortran90 and Matlab with the Kinetic PreProcessor KPP-2.1, *Atmospheric Chem. Phys.*, 6, 187–195, <https://doi.org/10.5194/acp-6-187-2006>, 2006.
- Sarwar, G., Gantt, B., Schwede, D., Foley, K., Mathur, R., and Saiz-Lopez, A.: Impact of enhanced ozone deposition and halogen chemistry on tropospheric ozone over the Northern Hemisphere, *Environ. Sci. Technol.*, 49, 9203–9211, <https://doi.org/10.1021/acs.est.5b01657>, 2015.
- 2870 Sassi, M., Zhang, J., and Moran, M. D.: 2015 SMOKE-ready Canadian Air Pollutant Emission Inventory (APEI) package version 1, [Data set], <http://doi.org/10.5281/zenodo.4883639>, 2021.
- Savic-Jovicic, V., Moran, M. D., and GEM-MACH Development Team: Global Environmental Multiscale model–Modelling Atmospheric CHemistry (GEM-MACH) version 3.1.0.0, Zenodo [software], <https://doi.org/10.5281/zenodo.15330612>, 2025.
- 2875 Saxena, P., Seigneur, C., and Peterson, T. W.: Modeling of multiphase atmospheric aerosols, *Atmospheric Environ.* 1967, 17, 1315–1329, [https://doi.org/10.1016/0004-6981\(83\)90406-7](https://doi.org/10.1016/0004-6981(83)90406-7), 1983.
- Schiermeir, F.: Air monitoring milestones, RAP’s field measurements are in, *Environ. Sci. Technol.*, 12, 644–651, <https://doi.org/10.1021/es60142a608>, 1978.
- Schwartz, S. E. and Warneck, P.: Units for use in atmospheric chemistry (IUPAC Recommendations 1995), *Pure Appl. Chem.*, 67, 1377–1406, <https://doi.org/10.1351/pac199567081377>, 1995.
- 2880 Schwede, D., Cole, A., Vet, R., and Lear, G.: Ongoing US-Canada collaborations on nitrogen and sulfur deposition, EM Pittsburgh Pa, June, 1-5, <https://www.ncbi.nlm.nih.gov/pmc/articles/PMC7923747/pdf/nihms-1655451.pdf>, 2019.
- Schwede, D. B., Pouliot, G., and Pierce, T. E.: Changes to the Biogenic Emission Inventory System Version 3 (BEIS3), 4th Annual CMAS Models-3 User’s Conference, Sept. 26-28, Chapel Hill, North Carolina, 6 pp., [https://www.cmascenter.org/conference/2005/abstracts/2\\_7.pdf](https://www.cmascenter.org/conference/2005/abstracts/2_7.pdf), 2005.
- 2885 Seigneur, C. and Moran, M. D.: Chemical transport models, in: Particulate Matter Science for Policy Makers: A NARSTO Assessment, Cambridge University Press, Cambridge, 283–323, 2004.
- Seigneur, C., Hudischewskyj, A. B., Seinfeld, J. H., Whitby, K. T., Whitby, E. R., Brock, J. R., and Barnes, H. M.: Simulation of aerosol dynamics: A comparative review of mathematical models, *Aerosol Sci. Technol.*, 5, 205–222, <https://doi.org/10.1080/02786828608959088>, 1986.
- 2890 Seinfeld, J. H.: Ozone air quality models: a critical review, *J Air Pollu Contr Assoc*, 38, 616–645, <https://doi.org/10.1080/08940630.1988.10466404>, 1988.
- Seinfeld, J. H. and Pandis, S. N.: *Atmospheric Chemistry and Physics: From Air Pollution to Climate Change*, Third., John Wiley & Sons, Hoboken, New Jersey, 1152 pp., 2016.
- Semeniuk, K. and Dastoor, A.: Current state of aerosol nucleation parameterizations for air-quality and climate modeling, *Atmos. Environ.*, 179, 77–106, <https://doi.org/10.1016/j.atmosenv.2018.01.039>, 2018.
- Sha, T., Ma, X., Zhang, H., Janecek, N., Wang, Y., Wang, Y., Castro García, L., Jenerette, G. D., and Wang, J.: Impacts of soil NO<sub>x</sub> emission on O<sub>3</sub> air quality in rural California, *Environ. Sci. Technol.*, 55, 7113–7122, <https://doi.org/10.1021/acs.est.0c06834>, 2021.
- 2900 Siebesma, A. P. and Cuijpers, J. W. M.: Evaluation of parametric assumptions for shallow cumulus convection, *J. Atmospheric Sci.*, 52, 650–666, [https://doi.org/10.1175/1520-0469\(1995\)052<0650:EOPAFS>2.0.CO;2](https://doi.org/10.1175/1520-0469(1995)052<0650:EOPAFS>2.0.CO;2), 1995.



Siebesma, A. P., Bretherton, C. S., Brown, A., Chlond, A., Cuxart, J., Duynkerke, P. G., Jiang, H., Khairoutdinov, M., Lewellen, D., Moeng, C.-H., Sanchez, E., Stevens, B., and Stevens, D. E.: A large eddy simulation intercomparison study of shallow cumulus convection, *J. Atmospheric Sci.*, 60, 1201–1219, [https://doi.org/10.1175/1520-0469\(2003\)60<1201:ALESIS>2.0.CO;2](https://doi.org/10.1175/1520-0469(2003)60<1201:ALESIS>2.0.CO;2), 2003.

2905 Simmons, A. J. and Hollingsworth, A.: Some aspects of the improvement in skill of numerical weather prediction, *Q. J. R. Meteorol. Soc.*, 128, 647–677, <https://doi.org/10.1256/003590002321042135>, 2002.

Slinn, W. G. N.: Some approximations for the wet and dry removal of particles and gases from the atmosphere, *Water. Air. Soil Pollut.*, 7, <https://doi.org/10.1007/BF00285550>, 1977.

Slinn, W. G. N.: Precipitation scavenging, in: *Atmospheric Science and Power Production*, Chap. 11, edited by: Randerson, D., DOE/TIC-27601, U. S. Dept. of Energy, Technical Information Center, Oak Ridge, Tennessee, 466–532, 1984.

2910 Smith, M. H., Park, P. M., and Consterdine, I. E.: Marine aerosol concentrations and estimated fluxes over the sea, *Q. J. R. Meteorol. Soc.*, 119, 809–824, <https://doi.org/10.1002/qj.49711951211>, 1993.

Sørensen, B., Kaas, E., and Korsholm, U. S.: A mass-conserving and multi-tracer efficient transport scheme in the online integrated Enviro-HIRLAM model, *Geosci. Model Dev.*, 6, 1029–1042, <https://doi.org/10.5194/gmd-6-1029-2013>, 2013.

2915 Stevens, R., Ryjkov, A., Majdzadeh, M., and Dastoor, A.: An improved representation of aerosol mixing state for air quality–weather interactions, *Atmospheric Chem. Phys.*, 22, 13527–13549, <https://doi.org/10.5194/acp-22-13527-2022>, 2022.

Stieb, D. M., Burnett, R. T., Smith-Doiron, M., Brion, O., Shin, H. H., and Economou, V.: A new multipollutant, no-threshold Air Quality Health Index based on short-term associations observed in daily time-series analyses, *J. Air Waste Manag. Assoc.*, 58, 435–450, <https://doi.org/10.3155/1047-3289.58.3.435>, 2008.

2920 Stockwell, W. R. and Lurmann, F. W.: Intercomparison of the ADOM and RADM gas-phase chemical mechanisms, Report prepared for the Electric Power Research Institute, Palo Alto, California, 266 pp., <https://doi.org/10.5281/zenodo.15330612>, 1989.

Stohl, A., Williams, E., Wotawa, G., and Kromp-Kolb, H.: A European inventory of soil nitric oxide emissions and the effect of these emissions on the photochemical formation of ozone, *Atmos. Environ.*, 30, 3741–3755, [https://doi.org/10.1016/1352-2310\(96\)00104-5](https://doi.org/10.1016/1352-2310(96)00104-5), 1996.

2925 Stroud, C. A., Morneau, G., Makar, P. A., Moran, M. D., Gong, W., Pabla, B., Zhang, J., Bouchet, V. S., Fox, D., Venkatesh, S., Wang, D., and Dann, T.: OH-reactivity of volatile organic compounds at urban and rural sites across Canada: Evaluation of air quality model predictions using speciated VOC measurements, *Atmos. Environ.*, 42, 7746–7756, <https://doi.org/10.1016/j.atmosenv.2008.05.054>, 2008.

2930 Stroud, C., Moran, M., Makar, P., Gong, W., Gong, S., Morneau, G., Bouchet, V., Dann, T., Wang, D., and Huang, L.: Impact of updates to BEIS v3 boreal forest emissions on Canadian air quality forecasts, Nov. 16–18, 2nd International Workshop on Air Quality Forecasting Research, Quebec City, <https://doi.org/10.5281/zenodo.15330612>, 2010.

Sundqvist, H., Berge, E., and Kristjánsson, J. E.: Condensation and cloud parameterization studies with a mesoscale numerical weather prediction model, *Mon. Weather Rev.*, 117, 1641–1657, [https://doi.org/10.1175/1520-0493\(1989\)117<1641:CACPSW>2.0.CO;2](https://doi.org/10.1175/1520-0493(1989)117<1641:CACPSW>2.0.CO;2), 1989.

2935 Tang, I. N. and Munkelwitz, H. R.: Water activities, densities, and refractive indices of aqueous sulfates and sodium nitrate droplets of atmospheric importance, *J. Geophys. Res. Atmospheres*, 99, 18801–18808, <https://doi.org/10.1029/94JD01345>, 1994.

Tang, Y., Pagowski, M., Chai, T., Pan, L., Lee, P., Baker, B., Kumar, R., Delle Monache, L., Tong, D., and Kim, H.-C.: A case study of aerosol data assimilation with the Community Multi-scale Air Quality Model over the contiguous United States using 3D-Var and optimal interpolation methods, *Geosci. Model Dev.*, 10, 4743–4758, <https://doi.org/10.5194/gmd-10-4743-2017>, 2017.

2940 Tang, Y., Bian, H., Tao, Z., Oman, L. D., Tong, D., Lee, P., Campbell, P. C., Baker, B., Lu, C.-H., Pan, L., Wang, J., McQueen, J., and Stajner, I.: Comparison of chemical lateral boundary conditions for air quality predictions over the contiguous United States during pollutant intrusion events, *Atmospheric Chem. Phys.*, 21, 2527–2550, <https://doi.org/10.5194/acp-21-2527-2021>, 2021.

Teakles, A. D., So, R., Ainslie, B., Nissen, R., Schiller, C., Vingarzan, R., McKendry, I., Macdonald, A. M., Jaffe, D. A., Bertram, A. K., Strawbridge, K. B., Leaitch, W. R., Hanna, S., Toom, D., Baik, J., and Huang, L.: Impacts of the July 2012 Siberian fire



- 2945 plume on air quality in the Pacific Northwest, *Atmospheric Chem. Phys.*, 17, 2593–2611, <https://doi.org/10.5194/acp-17-2593-2017>, 2017.
- Textor, C., Schulz, M., Guibert, S., Kinne, S., Balkanski, Y., Bauer, S., Berntsen, T., Berglen, T., Boucher, O., Chin, M., Dentener, F., Diehl, T., Easter, R., Feichter, H., Fillmore, D., Ghan, S., Ginoux, P., Gong, S., Grini, A., Hendricks, J., Horowitz, L., Huang, P., Isaksen, I., Iversen, I., Kloster, S., Koch, D., Kirkevåg, A., Kristjansson, J. E., Krol, M., Lauer, A., Lamarque, J. F., Liu, X., Montanaro, V., Myhre, G., Penner, J., Pitari, G., Reddy, S., Seland, Ø., Stier, P., Takemura, T., and Tie, X.: Analysis and quantification of the diversities of aerosol life cycles within AeroCom, *Atmospheric Chem. Phys.*, 6, 1777–1813, <https://doi.org/10.5194/acp-6-1777-2006>, 2006.
- 2950 Thomas, S. J., Girard, C., Benoit, R., Desgagné, M., and Pellerin, P.: A new adiabatic kernel for the MC2 model, *Atmosphere-Ocean*, 36, 241–270, <https://doi.org/10.1080/07055900.1998.9649613>, 1998.
- Tilmes, S., Emmons, L. K., Buchholz, R. R., and The CESM2 Development Team: CESM2.2 CAM-chem as Boundary Conditions, Research Data Archive at the National Center for Atmospheric Research, Computational and Information Systems Laboratory, <https://doi.org/10.5065/XS0R-QE86>, 2022.
- 2955 Tong, D., Feng, I., Gill, T. E., Schepanski, K., and Wang, J.: How many people were killed by windblown dust events in the United States?, *Bull. Am. Meteorol. Soc.*, 104, E1067–E1084, <https://doi.org/10.1175/BAMS-D-22-0186.1>, 2023.
- 2960 Trieu, J., Yao, J., McLean, K. E., Stieb, D. M., and Henderson, S. B.: Evaluating an Air Quality Health Index (AQHI) amendment for communities impacted by residential woodsmoke in British Columbia, Canada, *J. Air Waste Manag. Assoc.*, 70, 1009–1021, <https://doi.org/10.1080/10962247.2020.1797927>, 2020.
- Tsyro, S. G.: To what extent can aerosol water explain the discrepancy between model calculated and gravimetric PM<sub>10</sub> and PM<sub>2.5</sub>?, *Atmospheric Chem. Phys.*, 5, 515–532, <https://doi.org/10.5194/acp-5-515-2005>, 2005.
- 2965 Turpin, B. J. and Lim, H.-J.: Species contributions to PM<sub>2.5</sub> mass concentrations: Revisiting common assumptions for estimating organic mass, *Aerosol Sci. Technol.*, 35, 602–610, <https://doi.org/10.1080/02786820119445>, 2001.
- Urbanski, S.: Wildland fire emissions, carbon, and climate: Emission factors, *For. Ecol. Manag.*, 317, 51–60, <https://doi.org/10.1016/j.foreco.2013.05.045>, 2014.
- U.S. EPA: 2016v1 Platform. U.S. Environmental Protection Agency, WWW Document, <https://www.epa.gov/air-emissions-modeling/2016v1-platform>, 2019.
- 2970 Venkatram, A., Karamchandani, P. K., and Misra, P. K.: Testing a comprehensive acid deposition model, *Atmospheric Environ.* 1967, 22, 737–747, [https://doi.org/10.1016/0004-6981\(88\)90011-X](https://doi.org/10.1016/0004-6981(88)90011-X), 1988.
- Venkatram, A., Karamchandani, P., Kuntasal, G., Misra, P. K., and Davies, D. L.: The development of the acid deposition and oxidant model (ADOM), *Environ. Pollut.*, 75, 189–198, [https://doi.org/10.1016/0269-7491\(92\)90039-D](https://doi.org/10.1016/0269-7491(92)90039-D), 1992.
- 2975 Vet, R. and Ro, C.-U.: Contribution of Canada–United States transboundary transport to wet deposition of sulphur and nitrogen oxides—A mass balance approach, *Atmos. Environ.*, 42, 2518–2529, <https://doi.org/10.1016/j.atmosenv.2007.12.034>, 2008.
- Vukovich, J. M. and Pierce, T.: The implementation of BEIS3 within the SMOKE modeling framework, in: Proc. 11th International Emission Inventory Conference, April 15–18, Atlanta, Georgia, 7 pp., <https://www.epa.gov/sites/default/files/2015-10/documents/vukovich.pdf>, 2002.
- 2980 Wagstrom, K. M., Pandis, S. N., Yarwood, G., Wilson, G. M., and Morris, R. E.: Development and application of a computationally efficient particulate matter apportionment algorithm in a three-dimensional chemical transport model, *Atmos. Environ.*, 42, 5650–5659, <https://doi.org/10.1016/j.atmosenv.2008.03.012>, 2008.
- Wan, H., Rasch, P. J., Zhang, K., Kazil, J., and Leung, L. R.: Numerical issues associated with compensating and competing processes in climate models: an example from ECHAM-HAM, *Geosci. Model Dev.*, 6, 861–874, <https://doi.org/10.5194/gmd-6-861-2013>, 2013.
- 2985 Wang, X., Zhang, L., and Moran, M. D.: Uncertainty assessment of current size-resolved parameterizations for below-cloud particle scavenging by rain, *Atmospheric Chem. Phys.*, 10, 5685–5705, <https://doi.org/10.5194/acp-10-5685-2010>, 2010.



- Wang, X., Zhang, L., and Moran, M. D.: Bulk or modal parameterizations for below-cloud scavenging of fine, coarse, and giant particles by both rain and snow, *J. Adv. Model. Earth Syst.*, 6, 1301–1310, <https://doi.org/10.1002/2014MS000392>, 2014a.
- 2990 Wang, X., Zhang, L., and Moran, M. D.: Development of a new semi-empirical parameterization for below-cloud scavenging of size-resolved aerosol particles by both rain and snow, *Geosci. Model Dev.*, 7, 799–819, <https://doi.org/10.5194/gmd-7-799-2014>, 2014b.
- Wang, Z. S., Chien, C.-J., and Tonnesen, G. S.: Development of a tagged species source apportionment algorithm to characterize three-dimensional transport and transformation of precursors and secondary pollutants, *J. Geophys. Res.*, 114, D21206, <https://doi.org/10.1029/2008JD010846>, 2009.
- 2995 Warneke, C., de Gouw, J. A., Del Negro, L., Brioude, J., McKeen, S., Stark, H., Kuster, W. C., Goldan, P. D., Trainer, M., Fehsenfeld, F. C., Wiedinmyer, C., Guenther, A. B., Hansel, A., Wisthaler, A., Atlas, E., Holloway, J. S., Ryerson, T. B., Peischl, J., Huey, L. G., and Hanks, A. T. C.: Biogenic emission measurement and inventories determination of biogenic emissions in the eastern United States and Texas and comparison with biogenic emission inventories, *J. Geophys. Res.*, 115, D00F18, 21 pp., <https://doi.org/10.1029/2009JD012445>, 2010.
- 3000 Wesely, M. and Hicks, B. B.: A review of the current status of knowledge on dry deposition, *Atmos. Environ.*, 34, 2261–2282, [https://doi.org/10.1016/S1352-2310\(99\)00467-7](https://doi.org/10.1016/S1352-2310(99)00467-7), 2000.
- Wesely, M. L.: Parameterization of surface resistances to gaseous dry deposition in regional-scale numerical models, *Atmospheric Environ.* 1967, 23, 1293–1304, [https://doi.org/10.1016/0004-6981\(89\)90153-4](https://doi.org/10.1016/0004-6981(89)90153-4), 1989.
- 3005 Whitby, K. T.: The physical characteristics of sulfur aerosols, *Atmospheric Environ.* 1967, 12, 135–159, [https://doi.org/10.1016/0004-6981\(78\)90196-8](https://doi.org/10.1016/0004-6981(78)90196-8), 1978.
- Whitby, E. R. and McMurry, P. H.: Modal aerosol dynamics modeling, *Aerosol Sci. Technol.*, 27, 673–688, <https://doi.org/10.1080/02786829708965504>, 1997.
- White, W. H.: Chemical markers for sea salt in IMPROVE aerosol data, *Atmos. Environ.*, 42, 261–274, <https://doi.org/10.1016/j.atmosenv.2007.09.040>, 2008.
- 3010 WHO: WHO global air quality guidelines: particulate matter (PM<sub>2.5</sub> and PM<sub>10</sub>), ozone, nitrogen dioxide, sulfur dioxide and carbon monoxide, World Health Organization, Geneva, <https://apps.who.int/iris/handle/10665/345329>, 300 pp., 2021.
- Widziewicz-Rzońca, K. and Tytła, M.: First systematic review on PM-bound water: exploring the existing knowledge domain using the CiteSpace software, *Scientometrics*, 124, 1945–2008, <https://doi.org/10.1007/s11192-020-03547-w>, 2020.
- 3015 Williams, E. J., Guenther, A., and Fehsenfeld, F. C.: An inventory of nitric oxide emissions from soils in the United States, *J. Geophys. Res.*, 97, 7511, <https://doi.org/10.1029/92JD00412>, 1992a.
- Williams, E. J., Hutchinson, G. L., and Fehsenfeld, F. C.: NO<sub>x</sub> and N<sub>2</sub>O emissions from soil, *Glob. Biogeochem. Cycles*, 6, 351–388, <https://doi.org/10.1029/92GB02124>, 1992b.
- Wilson, L. J. and Vallée, M.: The Canadian Updateable Model Output Statistics (UMOS) system: Design and development tests, *Weather Forecast.*, 17, 206–222, [https://doi.org/10.1175/1520-0434\(2002\)017<0206:TCUMOS>2.0.CO;2](https://doi.org/10.1175/1520-0434(2002)017<0206:TCUMOS>2.0.CO;2), 2002.
- 3020 Wilson, L. J. and Vallée, M.: The Canadian Updateable Model Output Statistics (UMOS) system: Validation against perfect prog, *Weather Forecast.*, 18, 288–302, [https://doi.org/10.1175/1520-0434\(2003\)018<0288:TCUMOS>2.0.CO;2](https://doi.org/10.1175/1520-0434(2003)018<0288:TCUMOS>2.0.CO;2), 2003.
- Winkler, P.: The growth of atmospheric aerosol particles as a function of the relative humidity—II. An improved concept of mixed nuclei, *J. Aerosol Sci.*, 4, 373–387, [https://doi.org/10.1016/0021-8502\(73\)90027-X](https://doi.org/10.1016/0021-8502(73)90027-X), 1973.
- 3025 WMO: Training Materials and Best Practices for Chemical Weather/Air Quality Forecasting, Report no. ETR-26, World Meteorological Organization, Geneva, 576 pp., [https://library.wmo.int/doc\\_num.php?explnum\\_id=10439](https://library.wmo.int/doc_num.php?explnum_id=10439), 2020.
- Yienger, J. J. and Levy II, H.: Empirical model of global soil-biogenic NO<sub>x</sub> emissions, *J. Geophys. Res.*, 100, 11447, <https://doi.org/10.1029/95JD00370>, 1995.



- Young, J. R. and Lurmann, F. W.: ADOM/TADAP Model Development Program: Volume 7. Aqueous-Phase Chemistry, ERT Document P-B980-535, June, Environmental Research & Technology, Inc., Newbury Park, California, 135 pp., <https://doi.org/10.5281/zenodo.15330612>, 1984.
- 3030
- Young, T. R. and Boris, J. P.: A numerical technique for solving stiff ordinary differential equations associated with the chemical kinetics of reactive-flow problems, *J. Phys. Chem.*, 81, 2424–2427, <https://doi.org/10.1021/j100540a018>, 1977.
- Zadra, A., Roch, M., Laroche, S., and Charron, M.: The subgrid-scale orographic blocking parametrization of the GEM Model, *Atmosphere-Ocean*, 41, 155–170, <https://doi.org/10.3137/ao.410204>, 2003.
- 3035 Zhang, J. and Moran, M. D.: U.S.-EPA-BELD4-equivalent landuse database for Canada – Version 2 [Data set], <http://doi.org/10.5281/zenodo.3620734>, 2020.
- Zhang, J., Moran, M. D., Zheng, Q., Makar, P. A., Baratzadeh, P., Marson, G., Liu, P., and Li, S.-M.: Emissions preparation and analysis for multiscale air quality modeling over the Athabasca Oil Sands Region of Alberta, Canada, *Atmospheric Chem. Phys.*, 18, 10459–10481, <https://doi.org/10.5194/acp-18-10459-2018>, 2018.
- 3040 Zhang, J., Makar, P. A., Kharol, S., Moran, M. D., and McLinden, C.: An optimized North America MODIS leaf area index (LAI) dataset for air quality modeling [Data set], <https://doi.org/10.5281/zenodo.5393816>, 2021.
- Zhang, L., Gong, S. L., Padro, J., and Barrie, L. A.: A size-segregated particle dry deposition scheme for an atmospheric aerosol module, *Atmos. Environ.*, 35, 549–560, [https://doi.org/10.1016/S1352-2310\(00\)00326-5](https://doi.org/10.1016/S1352-2310(00)00326-5), 2001.
- 3045 Zhang, L., Moran, M. D., Makar, P. A., Brook, J. R., and Gong, S.: Modelling gaseous dry deposition in AURAMS: a unified regional air-quality modelling system, *Atmos. Environ.*, 36, 537–560, [https://doi.org/10.1016/S1352-2310\(01\)00447-2](https://doi.org/10.1016/S1352-2310(01)00447-2), 2002a.
- Zhang, L., Brook, J. R., and Vet, R.: On ozone dry deposition—with emphasis on non-stomatal uptake and wet canopies, *Atmos. Environ.*, 36, 4787–4799, [https://doi.org/10.1016/S1352-2310\(02\)00567-8](https://doi.org/10.1016/S1352-2310(02)00567-8), 2002b.
- Zhang, L., Wang, X., Moran, M. D., and Feng, J.: Review and uncertainty assessment of size-resolved scavenging coefficient formulations for below-cloud snow scavenging of atmospheric aerosols, *Atmospheric Chem. Phys.*, 13, 10005–10025, <https://doi.org/10.5194/acp-13-10005-2013>, 2013.
- 3050
- Zhang, Y.: Online-coupled meteorology and chemistry models: history, current status, and outlook, *Atmospheric Chem. Phys.*, 8, 2895–2932, <https://doi.org/10.5194/acp-8-2895-2008>, 2008.
- Zhang, Y., Seigneur, C., Seinfeld, J. H., Jacobson, M. Z., and Binkowski, F. S.: Simulation of aerosol dynamics: A comparative review of algorithms used in air quality models, *Aerosol Sci. Technol.*, 31, 487–514, <https://doi.org/10.1080/027868299304039>, 1999.
- 3055
- Zhang, Y., Bocquet, M., Mallet, V., Seigneur, C., and Baklanov, A.: Real-time air quality forecasting, part I: History, techniques, and current status, *Atmos. Environ.*, 60, 632–655, <https://doi.org/10.1016/j.atmosenv.2012.06.031>, 2012a.
- Zhang, Y., Bocquet, M., Mallet, V., Seigneur, C., and Baklanov, A.: Real-time air quality forecasting, part II: State of the science, current research needs, and future prospects, *Atmos. Environ.*, 60, 656–676, <https://doi.org/10.1016/j.atmosenv.2012.02.041>, 2012b.
- 3060
- Zhu, S., Sartelet, K. N., and Seigneur, C.: A size-composition resolved aerosol model for simulating the dynamics of externally mixed particles: SCRAM (v 1.0), *Geosci. Model Dev.*, 8, 1595–1612, <https://doi.org/10.5194/gmd-8-1595-2015>, 2015.



3065 Table 1. RAQDPS023 meteorological configuration and references for GEM host model (see also CMC-RAQDPS-023, 2021).

GEM Attribute or Component	Description	References
Formulation	Hydrostatic primitive equations	Côté et al. (1998a)
Dynamical core	Grid-point model with implicit semi-Lagrangian iterative space-time integration scheme; trapeze-cubic interpolation used for advection trajectory calculations	Côté et al. (1998a) Husain and Girard (2017) Husain et al. (2019)
Grid	Limited-area model (LAM), Arakawa C horizontal grid, Charney-Phillips vertical grid; log-hydrostatic-pressure-type terrain-following vertical coordinate	Girard et al. (2014) Husain et al. (2019)
Map projection / coordinate system	Yin portion of overset Yin–Yang global grid system; rotated lat-long (LAM) grid	Qaddouri and Lee (2011) de Grandpré et al. (2016)
Grid size	772 x 642 horizontal LAM grid, uniform 0.09° grid spacing (~10 km); 84 vertical levels, top at 0.01 hPa	Moran et al. (2021b) CMC-RAQDPS-023 (2021)
Integration time step	300 seconds	CMC-RDPS-8.0.0 (2021b)
Forecast period	72 hours	CMC-RAQDPS-023 (2021)
Horizontal diffusion	Del-4 operator applied to momentum variables (10%) and Del-6 operator (1%) applied for potential temperature	Mailhot et al. (2006) CMC-RDPS-8.0.0 (2021b)
Meteorological tracers	Water vapour, cloud water	Côté et al. (1998a)
Tracer shape preservation	Iterative Locally-Mass-Conserving (ILMC) monotonicity correction in dynamical core	Sørensen et al., 2013)
Tracer mass conservation	Domain mass fixer used to impose mass conservation; a 2-shell estimate of LAM boundary mass flux is employed	Bermejo and Conde (2002) Aranami et al. (2015)
Initialization	4D Incremental Analysis Update (4D-IAU) applied during the 6-hour period from T-3 to T+3 hours; some physics variables from previous forecast are “recycled”	Buehner et al. (2015) CMC-RDPS-8.0.0 (2021a,b)
Lateral boundary conditions	Provided by RDPS 8.0.0 regional NWP system forecasts	CMC-RDPS-8.0.0 (2021a) CMC-RAQDPS-023 (2021)
Land surface scheme	ISBA (Interactions between Soil-Biosphere-Atmosphere) land-surface scheme for land, water, sea ice, and glacier	Noilhan and Planton (1989) Bélaïr et al. (2003a,b)
Surface layer flux scheme	Monin-Obukhov surface-layer similarity theory; unstable stratification (DG1992), stable stratification (BH1991)	Delage and Girard (1992) Beljaars and Holtslag (1991)
Boundary layer vertical diffusion scheme	1.5-order turbulence closure scheme based on a predictive equation for subgrid-scale (SGS) turbulent kinetic energy with statistical representation of SGS clouds and Richardson number hysteresis	Benoit et al. (1989) Bélaïr et al. (1999, 2005) Mailhot and Bélaïr (2000) McTaggart-Cowan & Zadra (2015)
Radiation	Solar and infrared radiation parameterized using a correlated-k distribution technique	Li and Barker (2005) McTaggart-Cowan et al. (2019a)
Grid-scale cloud and precipitation	Condensation scheme with highly parameterized microphysics for non-convective clouds; fractional cloud cover is possible based on grid-scale relative humidity	Sundqvist et al. (1989) Pudykiewicz et al. (1992) McTaggart-Cowan et al. (2019a)
SGS deep convection	Mass-flux scheme that represents vertical transport of heat, moisture, and momentum by SGS deep convective clouds (depths of at least 3 km and roots in PBL); precipitation considered	Kain and Fritsch (1990, 1992) McTaggart-Cowan et al. (2019b)
SGS mid-level convection	Elevated convection (i.e., roots above PBL); based on deep convection scheme; precipitation considered	Kain and Fritsch (1990, 1992) McTaggart-Cowan et al. (2019a)
SGS shallow convection	Mass-flux scheme based on Bechtold et al. (2001); roots in PBL; downdrafts and precipitation not considered	Bechtold et al. (2001, 2014) Siebesma et al., 2003) Siebesma and Cuijpers, 1995)
SGS orographic gravity wave drag	Breaking of mountain-induced gravity waves over SGS orography transports vertical momentum transport	McFarlane (1987) McTaggart-Cowan et al. (2019a)
Non-orographic gravity wave drag	Doppler spread parameterization due to imbalances and geostrophic adjustment	Hines (1997a,b) Charron et al. (2002)
SGS low-level orographic blocking	Exchange of momentum with surface (i.e., drag) due to blocking of low-level winds by mountain barriers	Lott and Miller (1997) Zadra et al. (2003)



Table 2. List of GEM-predicted meteorological fields needed by the MACH module. Two-dimensional fields are associated with the Earth’s surface while three-dimensional fields are associated with the atmospheric column.

<b>GEM Variable</b>			
<b>Name</b>	<b>Description</b>	<b>Dimension</b>	<b>Unit</b>
tplus	dry-bulb temperature at T+DT	3	K
uplus	u-component of wind at T+DT	3	m s <sup>-1</sup>
vplus	v-component of wind at T+DT	3	m s <sup>-1</sup>
huplus	specific humidity at T+DT	3	kg kg <sup>-1</sup>
qcplus	total condensate mixing ratio at T+DT	3	kg kg <sup>-1</sup>
sigm	momentum sigma level ratio (p/ps)	3	–
sigt	thermodynamic sigma level ratio (p/ps)	3	–
wplus	vertical velocity at T+DT	3	Pa s <sup>-1</sup>
ftot	total cloud fraction (within a layer)	3	–
gzmom	geopotential height (momentum level)	3	dam
gztherm	geopotential height (thermal level)	3	dam
kt	vertical diffusion coefficient for heat	3	m <sup>2</sup> s <sup>-1</sup>
mflx	liquid precipitation flux	3	kg m <sup>-2</sup> s <sup>-1</sup>
snoflx	solid precipitation flux	3	kg m <sup>-2</sup> s <sup>-1</sup>
pevp	precipitation evaporation rate	3	s <sup>-1</sup>
ppro	precipitation production rate (auto-conversion and coalescence)	3	s <sup>-1</sup>
lwc	cloud liquid water content	3	kg kg <sup>-1</sup>
cldrad	cloud fraction for radiation calculations	3	–
ncplus	convective cloud fraction at T+DT	3	–
o3lplus	stratospheric ozone mixing ratio at T+DT	3	ug kg <sup>-1</sup>
p0_plus	surface pressure at T+DT	2	hPa
dxdy	horizontal area of each model grid cell	2	m <sup>2</sup>
tsurf	surface dry-bulb temperature	2	K
uddiag	X-component of wind at screen-level height (2 m)	2	m s <sup>-1</sup>
vddiag	Y-component of wind at screen-level height (2 m)	2	m s <sup>-1</sup>
tdiag	screen-level dry-bulb temperature (2 m)	2	K
qdiag	screen-level specific humidity (2 m)	2	kg kg <sup>-1</sup>
glsea	sea-ice fraction	2	–
snodp	snow depth	2	m <sup>2</sup> s <sup>-1</sup>
h	planetary boundary layer height	2	m <sup>2</sup> s <sup>-1</sup>
dlat	latitude (grid-cell centre)	2	degree
dlon	longitude (grid-cell centre)	2	degree
flusolis	total solar flux absorbed at the surface	2	W m <sup>-2</sup>
me_moins	model orography	2	m
ilmo	inverse Monin-Obukhov length	2	m <sup>-1</sup>
wsoil	volumetric water content of liquid water in soil	2	m m <sup>-1</sup>
ue	friction velocity u*	2	m s <sup>-1</sup>
cang	cosine of solar zenith angle	2	–
rainrate	liquid precipitation rate	2	m s <sup>-1</sup>
psn	fraction of grid cell covered by snow	2	–
mg	water/land fraction mask	2	–
alvis	surface solar albedo	2	–



Table 3. List of ADOM-2 gas-phase model chemical species and their physical and model properties. GMM stands for gram molar mass and DDF stands for dry deposition scaling factor (see Sect. 3.9).

Species Name	Description	GMM	VOC Species	Advected	Emitted	Dry Deposited	Wet Deposited	SO2 DDF	O3 DDF
SO2	sulphur dioxide	64.00		✓	✓	✓	✓	1.0	0.0
SO4	sulphuric acid vapour	96.00		✓	✓	✓	✓	1.0	1.0
NO	nitric oxide	30.00		✓	✓	✓		0.0	0.1
NO2	nitrogen dioxide	46.00		✓	✓	✓		0.0	0.8
O3	ozone	48.00		✓		✓		0.0	1.0
H2O2	hydrogen peroxide	34.00		✓		✓	✓	1.0	1.0
HNO3	nitric acid	63.00		✓		✓	✓	10.0	10.0
CO	carbon monoxide	28.00		✓	✓				
PAN	peroxyacetylnitrate and higher PANs	121.00	✓	✓		✓		0.0	0.6
C3H8	propane + others	44.09	✓	✓	✓				
ALKA	>C3 alkanes	93.43	✓	✓	✓				
ETHE	ethene	28.05	✓	✓	✓				
ALKE	>C2 alkenes	57.30	✓	✓	✓				
TOLU	toluene + other mono-substituted aromatics	92.13	✓	✓	✓				
AROM	xylene + other di- and tri-substituted aromatics	117.97	✓	✓	✓				
HCHO	formaldehyde	30.03	✓	✓	✓	✓		0.8	0.2
ALD2	acetaldehyde and higher aldehydes	44.05	✓	✓	✓	✓		0.0	0.05
MEK	methyl ethyl ketone and higher ketones	72.10	✓	✓	✓	✓		0.0	0.05
MGLY	methyl glyoxal	72.00	✓	✓		✓		0.01	0.0
DIAL	general dicarbonyl	84.00	✓	✓		✓		0.0	0.05
ROOH	organic peroxide	62.00	✓	✓		✓		0.1	0.8
CRES	O-cresol	108.13	✓	✓	✓	✓		0.01	0.0
HONO	nitrous acid	47.00		✓	✓	✓		2.0	2.0
RNO3	alkyl nitrate	121.00	✓	✓					
ISOP	isoprene	68.11	✓	✓	✓				
HO2	hydroperoxy radical	33.00		✓					
RO2	total RO2 radicals	61.00	✓	✓					
MCO3	acetyl peroxy radical (CH3CO3)	75.00	✓	✓					
NH3	ammonia	17.03		✓	✓	✓	✓	1.0	0.0
O*SD	oxygen-singlet D	16.00		✓					
O	atomic oxygen (ground state)	16.00		✓					
NO3	nitrogen trioxide	62.00		✓					
N2O5	dinitrogen pentoxide	108.00		✓					
HNO4	pernitric acid	79.01		✓					
OH	hydroxyl radical	17.00		✓					
RO2R	general organic peroxy radical #1	100.00	✓	✓					
R2O2	general organic peroxy radical #2	100.00	✓	✓					
RO2N	alkyl nitrate organic peroxy radical	100.00	✓	✓					
BZO	phenoxy radical	93.00	✓	✓					
CRG1	Criegee biradical #1	46.00	✓	✓					
CRG2	Criegee biradical #2	60.00	✓	✓					
CH4	methane	16.04							
C2H6	ethane	30.07							
H2O	water vapour	18.02							
O2	molecular oxygen	32.00							
M	air	28.97							



Table 4. List of ADOM-2 gas-phase mechanism chemical reactions and reaction rate coefficients in KPP-compliant input format (Damian et al., 2002; Sandu and Sander, 2006). Chemical reactions are listed in the left-hand column, and include first-, second-, and third-order reactions. All of the chemical species are defined in Table 3, except for hv, which indicates a photon of light of frequency  $\nu$ , and DUMMY, which indicates a non-reacting species. The reaction rate coefficients listed in the right-hand column have units of  $s^{-1}$ ,  $cm^3 mol^{-1} s^{-1}$ , and  $cm^6 mol^{-2} s^{-1}$  for first-, second-, and third-order reactions, respectively. SUN is normalized sun intensity and ranges from 0 at night and 1 at noon; TEMP corresponds to ambient atmospheric dry-bulb temperature (K); the ARR2 function describes the reaction rate coefficient in Arrhenius form, where the first argument is the preexponential factor and the second argument provides the E/R value; the TYPE5 function calculates third-order, pressure- and temperature-dependent reaction rate coefficients based on Troe theory (e.g., Seinfeld and Pandis, 2016), where the first argument specifies the F factor, the second and third arguments specify the high-pressure limiting rate coefficient, and the fourth and fifth arguments specify the low-pressure limiting rate coefficient; RCONST(n) is the reaction rate coefficient for the n-th reaction; and CFACTOR is a units conversion factor.

	{ 1.} NO2 + hv = NO + O	: 8.98E-3*SUN ;
	{ 2.} O + O2 + M = O3	: 3.00e-28 / (TEMP ** 2.3) ;
	{ 3.} O + NO2 = NO	: ARR2(6.5E-12, 120.0);
	{ 4.} O + NO2 = NO3	: TYPE5(0.60,8.10e-27,-2.0,2.20e-11,0.0) ;
3095	{ 5.} NO + O3 = NO2	: ARR2(1.8E-12, -1370.0) ;
	{ 6.} NO2 + O3 = NO3	: ARR2(1.2E-13, -2450.0) ;
	{ 7.} NO3 + NO = 2 NO2	: ARR2(1.7E-11, 150.0) ;
	{ 8.} 2 NO + O2 = 2 NO2	: ARR2(3.30E-39, 529.0) ;
	{ 9.} NO3 + NO2 = N2O5	: TYPE5(0.60,9.86e-20,-4.3,2.60e-11,-0.5) ;
3100	{10.} N2O5 = NO3 + NO2	: RCONST(9)*ARR2(9.09e26,-11200.) ;
	{11.} N2O5 + H2O = 2 HNO3	: 1.0E-21 ;
	{12.} NO3 + NO2 = NO + NO2	: ARR2(2.5E-14, -1229.0) ;
	{13.} NO3 + hv = NO	: 1.868e-02*SUN ;
	{14.} NO3 + hv = NO2 + O	: 1.697E-01*SUN ;
3105	{15.} O3 + hv = O	: 4.598E-04*SUN ;
	{16.} O3 + hv = O1D	: 3.394E-05*SUN ;
	{17.} O1D + H2O = 2OH	: 2.2E-10 ;
	{18.} O1D + M = O	: 2.9e-11 ;
	{19.} OH + NO = HONO	: TYPE5(0.60,1.93e-24,-2.6,2.60e-10,-0.5) ;
3110	{20.} HONO + hv = OH + NO	: 1.625e-03*SUN ;
	{21.} NO2 + H2O = HONO + HNO3 - NO2	: 1.0e-24 ;
	{22.} OH + NO2 = HNO3	: TYPE5(0.60,2.20e-22,-3.2,4.00e-8,-1.3) ;
	{23.} HNO3 + hv = NO2 + OH	: 5.828e-07*SUN ;
	{24.} OH + HNO3 = NO3	: ARR2(9.4E-15, 778.0) ;
3115	{25.} OH + CO = HO2	: 2.40e-13 ;
	{26.} O3 + OH = HO2	: ARR2(1.6E-12, -942.0) ;
	{27.} HO2 + NO = OH + NO2	: ARR2(3.7E-12, 240.0) ;
	{28.} NO2 + HO2 = HNO4	: TYPE5(0.60,1.52e-23,-3.2,1.38e-8,-1.4) ;
	{29.} HNO4 = NO2 + HO2	: RCONST(28)*ARR2(4.76e26,-10940.0) ;
3120	{30.} HNO4 + hv = NO2 + HO2	: 8.109e-06*SUN ;
	{31.} HNO4 + OH = NO2	: ARR2(1.30e-12, 380.0) ;
	{32.} O3 + HO2 = OH	: ARR2(1.1E-14, -502.0) ;
	{33.} 2 HO2 = H2O2	: ARR2(2.2E-13, 619.0) ;
	{34.} 2 HO2 + M = H2O2	: ARR2(1.9E-33, 982.0) ;
3125	{35.} 2 HO2 + H2O = H2O2	: ARR2(3.1E-34, 2818.0)+ARR2(2.700e-54, 3137.)*CFACTOR*1.0D6 ;
	{37.} H2O2 + hv = 2 OH	: 7.525E-06*SUN ;
	{38.} OH + H2O2 = HO2	: ARR2(3.3E-12, -200.0) ;
	{39.} NO3 + HO2 = HNO3	: ARR2(2.27e-13, 771.0) ;
	{40.} NO3 + HO2 + M = HNO3	: ARR2(1.9e-33, 982.0) ;
3130	{41.} NO3 + HO2 + H2O = HNO3	: ARR2(3.1e-34, 2818.0)+ARR2(2.700e-54, 3137.)*CFACTOR*1.0D6 ;
	{43.} SO2 + OH = SO4 + HO2	: TYPE5(0.60, 4.48e-23,-3.3,1.50e-12,0.0) ;
	{44.} RO2 + NO = NO	: ARR2(4.20e-12, 180.0) ;
	{45.} RO2 + HO2 = HO2	: ARR2(1.75e-13, 1000.0) ;
	{46.} 2 RO2 = DUMMY	: 1.00e-15 ;
3135	{47.} RO2 + MCO3 = MCO3	: 3.00e-12 ;
	{48.} ROOH + hv = HO2 + OH	: 7.39e-06*SUN ;
	{49.} HCHO + hv {+ 2 O2} = 2 HO2 + CO	: 3.008E-05*SUN ;



3140 {50.} HCHO + hv = CO : 4.301E-05\*SUN ;  
 {51.} HCHO + OH = HO2 + CO : ARR2(1.60e-11, -110.0) ;  
 {52.} HCHO + NO3 = HNO3 + HO2 + CO : ARR2(2.80e-12, -2518.0) ;  
 {53.} HCHO + HO2 = RO2R + RO2 : 1.1E-13\*(1.-20./(20.+ARR2(4.2E-18, 180.0)\*  
 C(ind\_NO)/CFACOR\*1.E6\_dp\*CFACOR));

3145 {54.} ALD2 + OH = MCO3 : ARR2(5.60e-12, 311.0) ;  
 {55.} ALD2 + hv {+ 2 O2} = HCHO + RO2 + RO2R + CO + HO2 : 5.94E-06\*SUN ;  
 {56.} ALD2 + NO3 = MCO3 + HNO3 : ARR2(1.40e-12, -1867.0) ;  
 {57.} MCO3 + NO = HCHO + RO2 + RO2R + NO2 : ARR2(4.20e-12, 180.0) ;  
 {58.} MCO3 + NO2 = PAN : TYPE5(0.19,6.29e-19,-4.1,4.92e-3,-3.6) ;  
 {59.} MCO3 + HO2 = ROOH + HCHO : ARR2(1.75e-13, 1000.0) ;  
 {60.} 2 MCO3 = 2 HCHO + 2 HO2 : 5.30e-12 ;  
 {61.} PAN = MCO3 + NO2 : ARR2(2.00e+16, -13542.0) ;

3150 {62.} MEK + hv = ALD2 + MCO3 + RO2R + RO2 : 1.580e-6\*SUN ;  
 {63.} MEK + OH = 0.5 ALD2 + 0.5 HCHO + 1.5 RO2R + 1.5 RO2 + MCO3 : ARR2(1.20e-11, -745.0) ;  
 {64.} MGLY + hv = MCO3 + CO + HO2 : 1.50e-4\*SUN ;  
 {65.} OH + MGLY = MCO3 + CO : 1.70e-11 ;

3155 {66.} NO3 + MGLY = CO + HNO3 + MCO3 : ARR2(3.00e-13, -1427.0) ;  
 {67.} CH4 + OH = HCHO + RO2R + RO2 : ARR2(2.40e-12, -1710.0) ;  
 {68.} C2H6 + OH = ALD2 + RO2R + RO2 : ARR2(1.70e-11, -1232.0) ;  
 {69.} C3H8 + OH = 0.3 ALD2 + 0.5 MEK + RO2R + RO2 : TEMP\*TEMP\*ARR2(1.27e-17, 14.0) ;  
 {70.} ALKA + OH = 0.111 HCHO + 0.530 ALD2 + 0.640 MEK +  
 0.131 RO2N + 0.869 RO2R + 0.7 R2O2 + 1.7 RO2 : ARR2(1.017e-11,-354.0)\*0.517+ARR2(2.312e-11,-289.0)\*(1.-0.517);

3160 {71.} RNO3 + OH = NO2 + 0.14 MEK + 1.52 ALD2 +  
 0.16 HCHO + 1.39 R2O2 + 1.39 RO2 : ARR2(2.19e-11, -709.0) ;  
 {72.} RO2N + NO = RNO3 : ARR2(4.20e-12, 180.0) ;

3165 {73.} RO2N + HO2 = ROOH + MEK : ARR2(1.75e-13, 1000.0) ;  
 {74.} RO2N + RO2 = RO2 + 0.5 HO2 + MEK : 1.00e-15 ;  
 {75.} RO2N + MCO3 = HCHO + HO2 + MEK : 3.00e-12 ;  
 {76.} R2O2 + NO = NO2 : ARR2(4.20e-12, 180.0) ;  
 {77.} R2O2 + HO2 = ROOH : ARR2(1.75e-13, 1000.0) ;  
 {78.} R2O2 + RO2 = RO2 : 1.00e-15 ;

3170 {79.} R2O2 + MCO3 = HCHO + HO2 : 3.00e-12 ;  
 {80.} RO2R + NO = NO2 + HO2 : ARR2(4.20e-12, 180.0) ;  
 {81.} RO2R + HO2 = ROOH : ARR2(1.75e-13, 1000.0) ;  
 {82.} RO2R + RO2 = 0.5 HO2 + RO2 : 1.00e-13 ;  
 {83.} RO2R + MCO3 = HCHO + HO2 : 3.00e-12 ;

3175 {84.} OH + ETHE = RO2 + 1.56 HCHO + RO2R + 0.22 ALD2 : ARR2(2.15e-12, 411.0) ;  
 {85.} O3 + ETHE = HCHO + 0.42 CO + 0.12 HO2 + 0.4 CRG1 : ARR2(1.20e-14, -2634.0) ;  
 {86.} O + ETHE = HCHO + HO2 + CO + RO2R + RO2 : ARR2(1.04e-11, -792.0) ;  
 {87.} NO3 + ETHE = 2 HCHO + NO2 + R2O2 + RO2 : ARR2(3.70e-12, -2925.0) ;  
 {88.} OH + ALKE = 0.667 HCHO + 1.334 ALD2 +  
 RO2R + RO2 : ARR2(5.323e-12, 504.0)\*0.667 + ARR2(1.074e-11, 549.0)\*(1.-0.667);

3180 {89.} O3 + ALKE = 0.667 ALD2 + 0.427 HCHO + 0.187 CO +  
 0.183 HO2 + 0.177 RO2 + 0.177 RO2R +  
 0.080 OH + 0.133 CRG1 +  
 0.133 CRG2 : ARR2(1.323e-14, -2105.0)\*0.667+ARR2(7.333e-15, -1137.0)\*(1.-0.667);

3185 {90.} O + ALKE = 0.133 ALD2 + 0.267 HO2 + 0.400 RO2 +  
 0.267 CO + 0.267 HCHO +  
 0.400 RO2R + 0.333 MEK : ARR2(1.18e-11, -324.0)\*0.667 + ARR2(2.26e-11, 10.0)\*(1.-0.667);

3190 {91.} NO3 + ALKE = NO2 + 0.667 HCHO + 1.334 ALD2 +  
 R2O2 + RO2 : ARR2(1.143e-11, -1935.0)\*0.667+ARR2(3.23e-11, -975.0)\*(1.-0.667);

3195 {92.} SO2 + CRG1 = SO4 + HCHO : 1.00e-13 ;  
 {93.} SO2 + CRG2 = SO4 + ALD2 : 1.00e-13 ;  
 {94.} CRG1 + H2O = DUMMY : 2.30e-17 ;  
 {95.} CRG2 + H2O = DUMMY : 2.30e-17 ;  
 {96.} CRG1 + HCHO = DUMMY : 2.50e-14 ;  
 {97.} CRG2 + HCHO = DUMMY : 2.50e-14 ;  
 {98.} CRG1 + ALD2 = DUMMY : 2.50e-14 ;  
 {99.} CRG2 + ALD2 = DUMMY : 2.50e-14 ;

3200 {100.} TOLU + OH = 0.16 CRES + 0.16 HO2 + 0.84 RO2R + 0.4 DIAL +  
 0.84 RO2 + 0.13 MGLY + 0.11 HCHO + 0.11 CO : ARR2(2.10e-12, 322.0) ;  
 {101.} AROM + OH = 0.17 CRES + 0.17 HO2 + 0.83 RO2R +  
 0.83 RO2 + 0.590 DIAL + 0.518 MGLY +  
 0.0597 HCHO + 0.0597 CO : ARR2(1.407e-11, 116.0)\*0.628+4.77e-11\*(1.-0.628);

{102.} DIAL + OH = MCO3 : 3.00e-11 ;  
 {103.} DIAL + hv = HO2 + CO + MCO3 : 5.29e-04\*SUN ;



3205	{104.} OH + CRES = 0.2 MGLY + 0.15 RO2N + 0.85 RO2R + RO2 + 0.08 CRES	: 4.00e-11 ;
	{105.} NO3 + CRES = HNO3 + BZO + 0.5 CRES	: 2.20e-11 ;
	{106.} NO2 + BZO = RNO3	: 1.50e-11 ;
	{107.} HO2 + BZO = DUMMY	: ARR2(1.75e-13, 1000.0) ;
3210	{108.} BZO = DUMMY	: 1.00e-3 ;
	{109.} OH + ISOP = HCHO + RO2 + 0.7 HO2 + 0.27 MGLY + 0.2 MCO3 + ETHE + 0.2 ALD2 + 0.1 RO2N + 0.9 R2O2	: ARR2(1.50e-11, 500.0) ;
	{110.} O3 + ISOP = HCHO + 0.4 ALD2 + 0.5 ETHE + 0.2 MGLY + 0.2 CRG2 + 0.4 HO2 + 0.1 OH	: ARR2(7.00e-15, -1900.0) ;
3215	{111.} O + ISOP = 0.6 HO2 + ALD2 + 0.5 RO2 + 0.5 R2O2 + ETHE	: 1.80e-11 ;
	{112.} NO3 + ISOP = NO2 + HCHO + ALD2 + R2O2 + RO2	: 3.20e-13 ;
	{113.} OH + HO2 = DUMMY	: ARR2(4.60e-11, 230.0) ;
	{114.} OH + ROOH = 0.5 RO2R + 0.5 OH + 0.5 RO2	: ARR2(4.00e-12, 180.0) ;
3220		

[Note that reaction 21 represents a two-step heterogeneous reaction on a water surface]



Table 5. List of NAPAP VOC classes and properties and mapping to ADOM-2 lumped VOC species. The “Others” classes include alcohols, ethers, alcohol ethers, esters, etc., while OTH includes all low- and non-reactive species.

NAPAP No.	NAPAP Name (and kOH Range as 10 <sup>4</sup> /[ppm-min])	NAPAP Mean GMM (g mol <sup>-1</sup> )	kOH (1/[ppm-min])	Mapping to ADOM-2 Species	NAPAP Mass Fraction	Reactivity Weight Factor
1	Methane	16.00	1.00E+01	CH4	1	1
2	Ethane	30.00	4.10E+02	C2H6	1	1
3	Propane	44.00	1.80E+03	C3H8	1	1
4	Alkanes (0.25-0.50)	58.57	3.69E+03	ALKA	1	0.5447
5	Alkanes (0.50-1.00)	79.92	6.68E+03	ALKA	1	0.8496
6	Alkanes (1.0-2.0)	113.69	1.32E+04	ALKA	1	1.2482
7	Alkanes (>2.0)	197.06	2.34E+04	ALKA	1	1.5079
8	Alkane/Aromatic Mix	140.57	2.02E+04	ALKA	0.5	1.3242
8	Alkane/Aromatic Mix	140.57	2.02E+04	AROM	0.5	0.09
9	Ethene	28.00	1.24E+04	ETHE	1	1
10	Propene	42.00	3.82E+04	ALKE	1	1
11	Alkenes (Terminal)	71.95	4.71E+04	ALKE	1	1
12	Alkenes (Internal)	69.27	9.88E+04	ALKE	1	1
13	Alkenes (Terminal/Internal Mix)	105.90	5.11E+04	ALKE	1	1
14	Benzene and Halobenzenes	82.57	1.85E+03	C3H8	1	1.03
15	Aromatics (<2)	96.89	9.19E+03	TOLU	1	1
16	Aromatics (>2)	124.50	4.09E+04	AROM	1	1
17	Phenols and Cresols	159.10	5.62E+04	CRES	1	1
18	Styrenes	65.23	9.02E+03	TOLU	0.74032	1
19	Formaldehyde	30.00	1.33E+04	HCHO	1	1
19	Formaldehyde	30.00	1.33E+04	ALKE	0.25968	1
20	Higher Aldehydes	64.40	2.39E+04	ALD2	1	1
21	Acetone	58.00	3.50E+02	OTH	1	1
22	Higher Ketones	89.54	2.68E+03	MEK	1	1
23	Organic Acids	113.75	8.80E+02	OTH	1	1
24	Acetylene	26.00	1.15E+03	C3H8	1	0.66
25	Haloalkenes	149.14	2.50E+02	OTH	1	1
26	Unreactive	0.00	0.00E+00	OTH	1	1
27	Others (<0.25)	48.30	1.37E+03	C3H8	1	0.78
28	Others (0.25-0.50)	47.96	4.96E+03	ALKA	1	0.6865
29	Others (0.50-1.00)	70.08	8.01E+03	ALKA	1	0.9561
30	Others (>1.00)	85.42	1.55E+04	ALKA	1	1.3364
31	Unidentified	0.00	0.00E+00	OTH	1	1
32	Unassigned	0.00	0.00E+00	OTH	1	1
33	Isoprene (anthropogenic)	68.12		ISOP	1	1
34	Alpha-Pinene (anthropogenic)	136.24		ALKE	1	1
35	Other monoterpenes (anthrop.)	136.00		ALKE	1	1

3225

3230



Table 6. List of ADOM aqueous-phase mechanism chemical species and phases (G=gas, P=particle, A=aqueous) .

Species Name	Description	Phase
SO2G	sulfur dioxide gas	G
HPXG	hydrogen peroxide gas	G
RPXG	organic peroxide gas	G
H2SO4 (= SO4P1)	sulfuric acid vapour	G
NH4HSO4 (= SO4P2)	ammonium bisulfate	P
(NH4)2SO4 (= SO4P3)	ammonium sulfate	P
HNO3G	nitric acid vapour	G
NH3G	ammonia gas	G
NH4NO3	ammonium nitrate	P
DUST	soil dust (= crustal material)	P
O3G	ozone gas	G
CO2G (constant)	carbon dioxide gas	G
HSO3-	bisulfite ion	A
H2O2	hydrogen peroxide (aqueous)	A
ROOH	organic peroxide (aqueous)	A
SO4=	sulfate ion	A
NO3-	nitrate ion	A
NH4+	ammonium ion	A
CAT1	total base cations	A
HCO3-	bicarbonate ion	A
H+	hydrogen ion	A
OH-	hydroxide ion	A
FEMN	iron-manganese (aqueous)	A
O3	ozone (aqueous)	A
H2O	cloud water	A

3235



Table 7. List of ADOM aqueous-phase mechanism chemical reactions.

	1.	SO4P1	-->	B1*SO4= + B3*H+ (WITH K= 0)
	2.	SO2G	-->	B1*HSO3- + B1*H+
3240	3.	HSO3- + H+	-->	B2*SO2G
	4.	O3G	-->	B1*O3
	5.	O3	-->	B2*O3G
	6.	HPXG	-->	B1*H2O2
	7.	H2O2	-->	B2*HPXG
3245	8.	HNO3	-->	B1*NO3- + B1*H+
	9.	NO3- + H+	-->	B2*HNO3
	10.	RPXG	-->	B1*ROOH
	11.	ROOH	-->	B2*RPXG
	12.	NH3G	-->	B1*NH4+ + B1*OH-
3250	13.	NH4+ + OH-	-->	B2*NH3G
	14.	DUST	-->	B5*FEMN + B4*HCO3- + B4*CAT1 (+ K = 0)
	15.	CO2G	-->	B1*HCO3- + B1*H+
	16.	HCO3- + H+	-->	B2*CO2G
	17.	H+ + OH-	-->	H2OA
3255	18.	H2OA	-->	H+ + OH-
	19.	HSO3- + O3	-->	SO4= + H+
	20.	HSO3- + H2O2	-->	SO4= + H+
	21.	HSO3- + ROOH	-->	SO4= + H+
	22.	HSO3- (FEMN)	-->	SO4= + H+
3260	23.	SO4P2	-->	B1*SO4= + B1*H+ + B1*NH4+
	24.	SO4P3	-->	B1*SO4= + B3*NH4+
	25.	NH4NO3P	-->	B1*NO3- + B1*NH4+

B1 = LRT, B2 = 1/LRT

B3, B4, and B5 are defined by the emissions data

L = volumetric liquid water fraction in air (m<sup>3</sup> m<sup>-3</sup>)

R = universal gas constant (8.205 x 10<sup>4</sup> ppm L mol<sup>-1</sup> K<sup>-1</sup>)

T = dry-bulb temperature (K)

3265



3270 Table 8. List of IAY parameter values for seven, SOA-forming, ADOM-2 mechanism VOC species.  $\alpha_i$  is the mass-based stoichiometric coefficient (unitless) and  $K_{om,i}$  is the partitioning coefficient ( $m^{-3}\cdot\mu g$ ) of the  $i$ -th condensable species.

Species Name	Description	$\alpha_1$	$K_{om,1}$	$\alpha_2$	$K_{om,2}$	Source
ALKA	>C3 alkanes	0.010	0.020	0.300	0.0005	Griffin et al. (1999)
ALKE	>C2 alkenes	0.010	0.020	0.300	0.0005	Griffin et al. (1999)
TOLU	toluene + other mono-substituted aromatics	0.071	0.053	0.138	0.0019	Odum et al. (1997)
AROM	xylene + other di- and tri-substituted aromatics	0.038	0.042	0.167	0.0014	Jiang (2003)
ISOP	isoprene	0.029	1.620	0.232	0.0086	Barsanti et al. (2013)
$\alpha$ -pinene	$\alpha$ -pinene	0.038	0.171	0.326	0.0040	Jiang (2003)
$\beta$ -pinene	$\beta$ -pinene	0.130	0.044	0.406	0.0049	Jiang (2003)

3275

3280 Table 9. Summary of annual, model-ready Canadian, U.S., and Mexican anthropogenic emissions and ocean shipping emissions (tonnes) for nominal 2021/22 period based on the SET4 emissions input files. Note that (i) inventory emissions from jurisdictions located outside of the model domain (e.g., southern Mexico, Hawaii, Puerto Rico) are not included in these totals, (ii) VOC emissions are calculated as the sum of the emissions of 11 model VOC species (excludes EOTH), (iii) fugitive  $PM_{2.5}$  and  $PM_{10}$  emissions have been reduced by transportable-fraction scaling but not by meteorological modulation, and (iv) in-flight aircraft, biogenic, biomass burning, lightning, volcanic, sea-salt, pollen and other biologicals, and aeolian dust emissions are not included.

3285

Country	$SO_2$	$NO_x$	VOC	CO	$NH_3$	$PM_{2.5}$	$PM_{10}$
Canada	721,123	1,520,279	1,433,913	4,321,607	543,146	418,900	1,447,900
U.S.	1,434,711	6,034,142	8,584,696	29,452,017	3,481,878	2,260,000	9,022,000
Mexico	362,044	1,019,838	715,174	2,227,501	209,016	121,900	210,950
Ocean shipping	165,144	1,184,741	50,636	116,875	493	88,200	145,150
Total	2,683,021	9,759,000	10,784,420	36,118,000	4,234,533	2,889,000	10,826,000

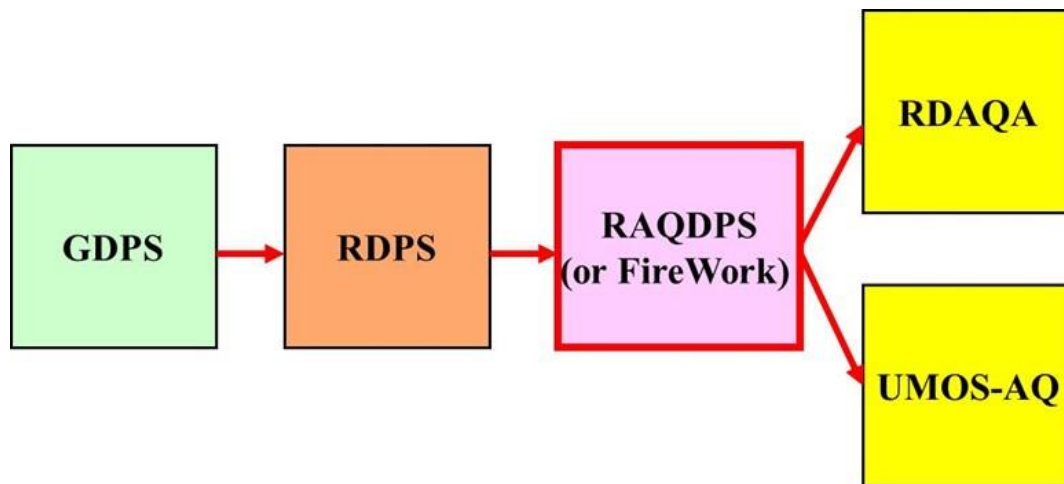
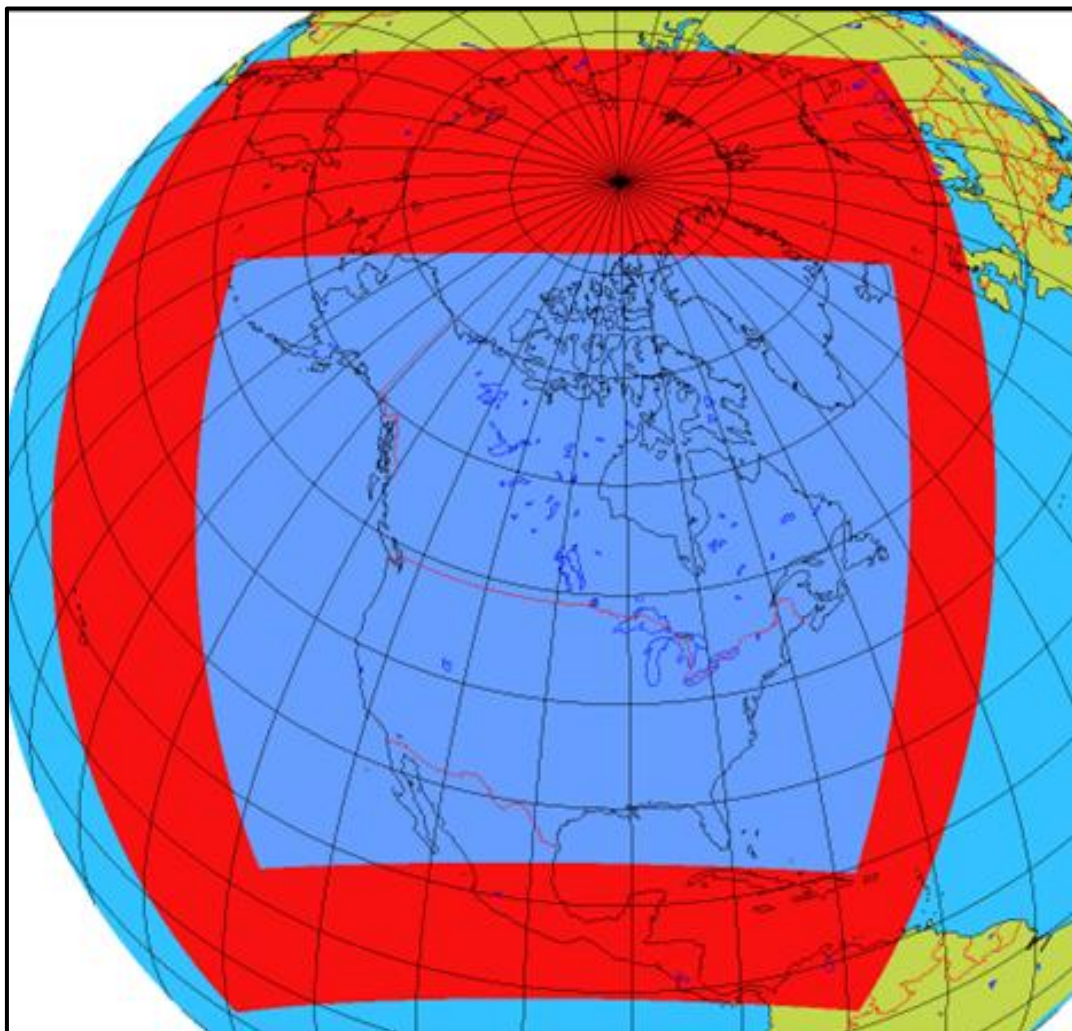


Figure 1. Current RAQDPS “upstream” and “downstream” dependencies on other ECCC operational systems.

3290



3295

Figure 2: Horizontal domains of RAQDPS023 (blue inner area) and RDPS 8.0.0 (surrounding red area plus blue inner area).

3300

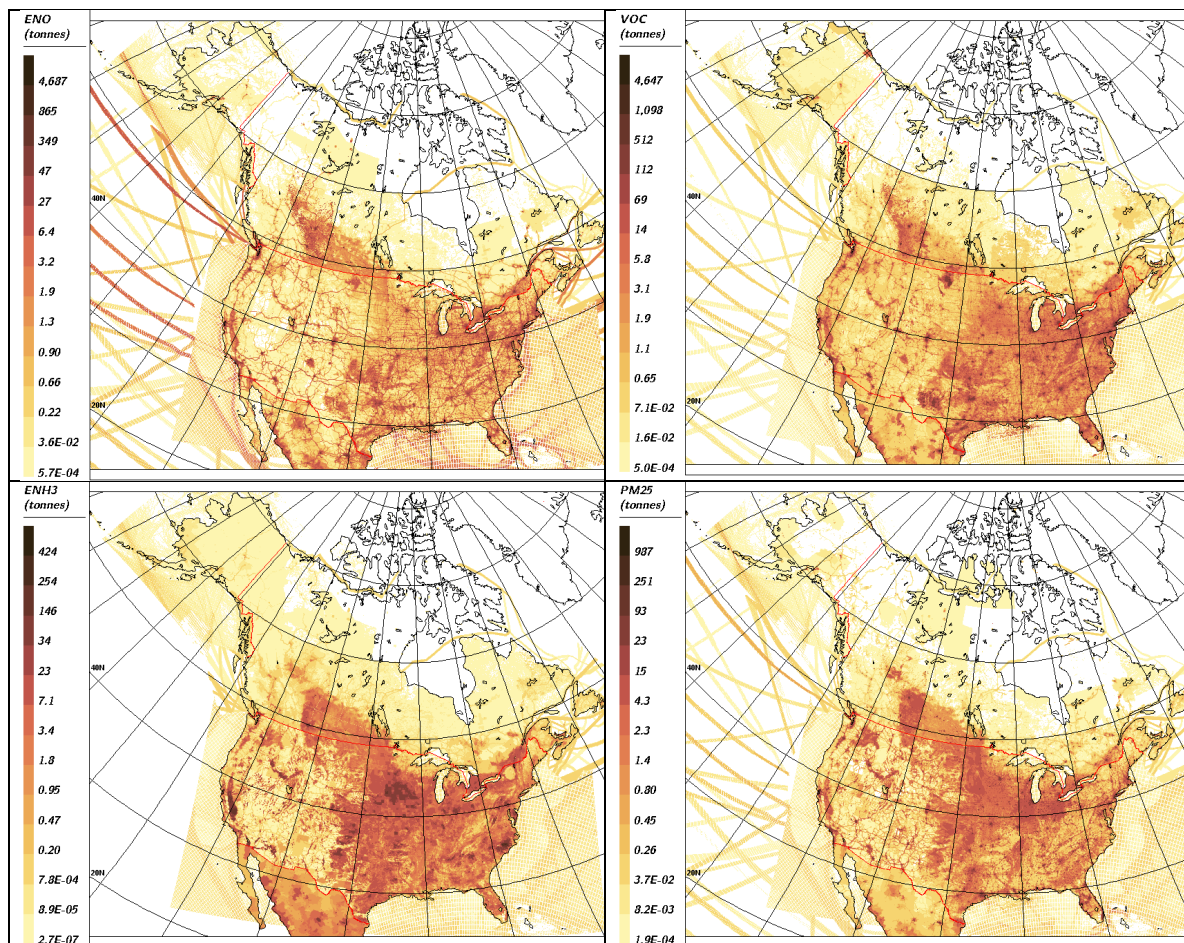


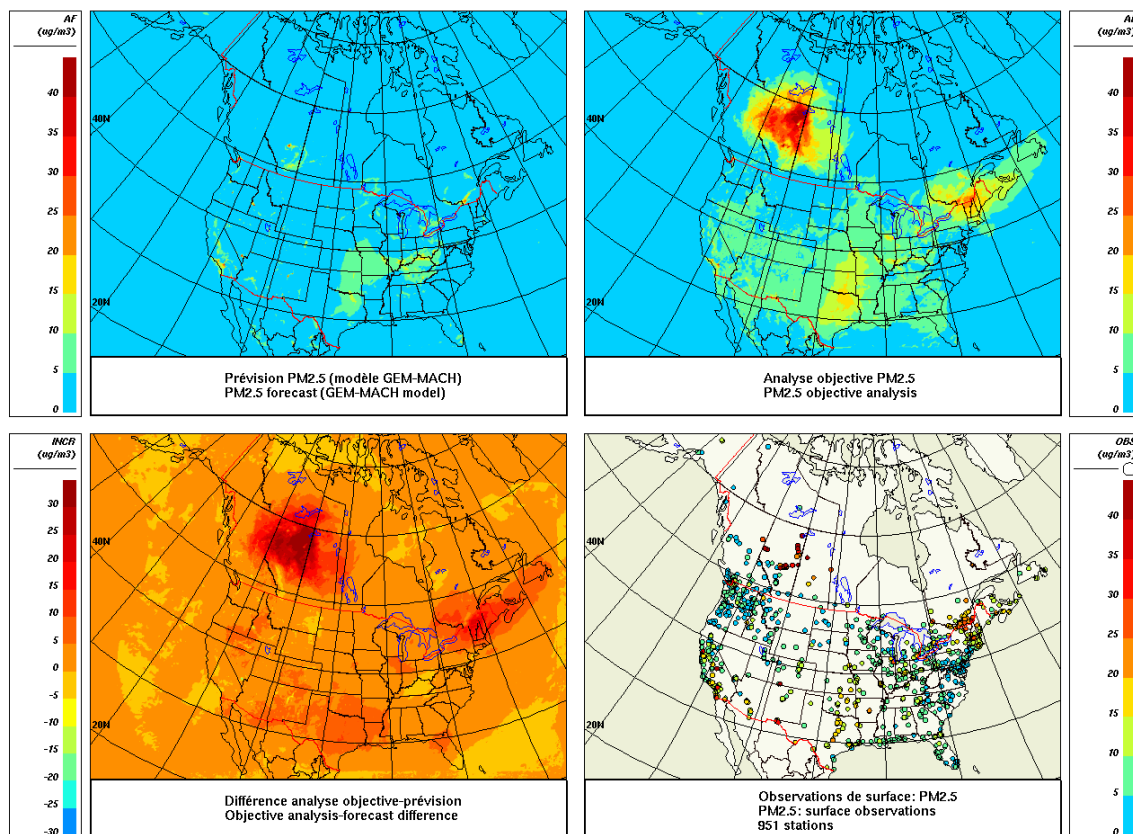
Figure 3. Spatial distribution of SET4.0.0 July anthropogenic emission of four chemical species: (a) NO (tonnes NO/grid cell), (b) VOC (tonnes VOC/grid cell), (c) NH<sub>3</sub> (tonnes NH<sub>3</sub>/grid cell), and (d) PM<sub>2.5</sub> (tonnes PM<sub>2.5</sub>/grid cell). Note that “VOC” here is total model VOC, that is, the sum of the 11 emitted model VOC species (see Table 3), and PM<sub>2.5</sub> emissions are the sum of emissions of the six emitted PM<sub>2.5</sub> chemical components (SU, NI, AM, EC, POM, and CM).

3305

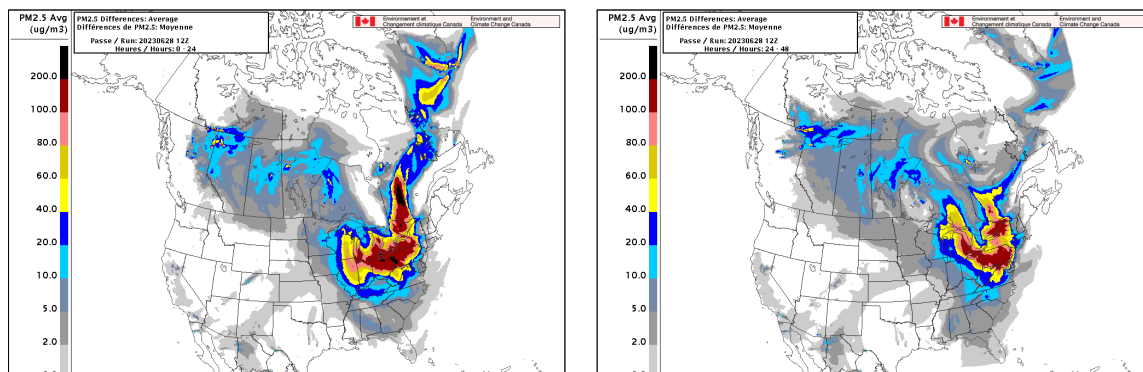
3310



Vendredi 29 septembre 2023 à 16:00Z / Friday September 29 2023 at 16:00Z  
 Late Analysis/Analyse finale



3315 Figure 4. Four-panel presentation of RDAQA 2.0.0 results for  $PM_{2.5}$  surface concentration ( $\mu g m^{-3}$ ) for 28 Sept. 2023 at 16 UTC: (a) RAQDPS023  $PM_{2.5}$  forecast; (b) RDAQA 2.0.0  $PM_{2.5}$  objective analysis; (c)  $PM_{2.5}$  analysis increment (correction to the model forecast); and (d)  $PM_{2.5}$  surface observations.



3320 Figure 5. RAQDPS-FW 12 UTC forecast on 28 June 2023 of contribution of smoke from wildfires to mean surface  $PM_{2.5}$  concentrations ( $\mu g m^{-3}$ ) for hours (a) 00-24 and (b) 24-48.